Distribution Agreement

In presenting this thesis or dissertation as a partial fulfillment of the requirements for an advanced degree from Emory University, I hereby grant to Emory University and its agents the non-exclusive license to archive, make accessible, and display my thesis or dissertation in whole or in part in all forms of media, now or hereafter known, including display on the world wide web. I understand that I may select some access restrictions as part of the online submission of this thesis or dissertation. I retain all ownership rights to the copyright of the thesis or dissertation. I also retain the right to use in future works (such as articles or books) all or part of this thesis or dissertation.

Signature:

Caprichia Jeffers	Date

Statistical Methods for Correlated Count Data

By

Caprichia Jeffers

Doctor of Philosophy

Biostatistics

Howard Chang, Ph.D.
Advisor

Jian Kang, Ph.D.
Advisor

Michael Haber, Ph.D.
Committee Member

Danielle Iuliano, Ph.D.
Committee Member

Accepted:

Lisa A. Tedesco, Ph.D.
Dean of the James T. Laney School of Graduate Studies

Date

Statistical Methods for Correlated Count Data

By

Caprichia Jeffers
M.S., Emory University, 2017
B.A., Agnes Scott College, 2011

Advisors: Howard Chang, Ph.D. and Jian Kang, Ph.D.

An abstract of
A dissertation submitted to the Faculty of the
James T. Laney School of Graduate Studies of Emory University
in partial fulfillment of the requirements for the degree of
Doctor of Philosophy
in Biostatistics
2018

Abstract

Statistical Methods for Correlated Count Data

By

Caprichia Jeffers

Current biomedical research has generated large datasets with complexities requiring new or improved methods of analysis. In this dissertation, I propose various statistical methods for analyzing correlated count datasets motivated by different scientific questions.

Meta-analysis of functional neuroimaging data has become increasingly important. Much attention has been paid to detect consistent activation regions or locations across independently performed studies, while very limited works have focused on co-activation pattern identifications. We propose a Bayesian Poisson-Gamma graphical model for which we introduce a sparsity indicator for the co-activation strength. We develop efficient posterior inference for estimating the co-activation patterns and the associated brain network. We illustrate our methods via simulation studies and a meta-analysis of functional neuroimaging data for emotion state studies. As a results, we are able to create a statistical framework that allows us to make inference about functional co-activation in the brain for coordinate-based meta-analysis data and reproduce general findings in literature.

Influenza, one of the most common transmissible infectious diseases of the respiratory tract, affects populations worldwide. Influenza-associated excess mortality is commonly estimated from time-series of death counts. Presence of temporal autocorrelation in death counts is a well-recognized analytic challenge. We used United States weekly vital records, viral surveillance of 4 influenza subtypes, and population data from 1981 to 2014 to evaluate two methods for addressing temporal autocorrelation. We examined (1) a parametric bootstrap method for generalized linear models that incorporates autocorrelation in the residuals and (2) a Bayesian hierarchical model that incorporates autocorrelation within the mean. Age-specific seasonal influenza-associated excess deaths were estimated from respiratory-coded deaths.

The aforementioned methods, provided unexpected results. The Bayesian method consistently estimated lower influenza-associated mortality compared to the bootstrap method, and often smaller standard error. The smaller estimates may be attributed to better control of temporal residual confounding of viral proxy association. To explore the presence and effect of temporal residual confounding in the model, we examine a methods for adjusting for long-term and seasonal trends using flexible splines. Via simulation study, we evaluate the timescale of the confounding between the outcome and predictors time-series as well as the relationship strength between influenza proxies and trend. As a results, we note how seasonal trend is accounted for and a tightly correlated timescale of confounding have the greatest impact on influenza-related mortality estimation.

Statistical Methods for Correlated Count Data

By

Caprichia Jeffers
M.S., Emory University, 2017
B.A., Agnes Scott College, 2011

Advisors: Howard Chang, Ph.D. and Jian Kang, Ph.D.

A dissertation submitted to the Faculty of the
James T. Laney School of Graduate Studies of Emory University
in partial fulfillment of the requirements for the degree of
Doctor of Philosophy
in Biostatistics
2018

Dedication

I dedicate this dissertation to my beloved grandmother Maude Faye Cline (June 9, 1937 - July 10, 2012) and dear friend Danyel Ieshia Renee Currie (February 2, 1986 - August 21, 2015), and all those who truly believed in me, encouraged me and supported me during this journey.

Contents

List of Figures

List of Tables

Chapter 1

Introduction

1.1 Overview

As new technology expands our ability to collect information, new challenges in data analysis need to be solved. While most basic statistical analysis assumes independence, this research addresses two interesting scientific count data problems when that assumption does not hold. In this dissertation, we propose novel Bayesian methods and analysis techniques for complex count data from various biomedical applications.

1.2 Introduction to Influenza

Influenza is a highly contagious viral infection affecting populations worldwide. Each year, influenza, one of the most common transmissible infectious diseases of the respiratory tract, is estimated to be responsible for 36,000 deaths, 225,000 hospitalization and $87 billion in health care costs in the United States, according to the Centers for Disease Control and Prevention (CDC) (Thompson et al., 2004, 2003). Moreover, the World Health Organization (WHO) reports global impact of influenza is even more disconcerting, with an estimated 3 to 5 million severe cases (World Health Organization, 2004). While, 291,243 to 645,832 seasonal influenza-associated respiratory deaths are estimated annually (Iuliano et al., 2017). A significant portion of these deaths occur among the elderly and those chronically ill, specifically with chronic cardiopulmonary disease. Among children less than five years of age, influenza is responsible for 28,000 to 111,000 deaths (Nair et al., 2011). To alleviate some of the disease burden globally, influenza vaccination has been promoted and expanded in many countries. Countries are working toward a significant reduction in morbidity and mortality caused by the influenza illness. Seasonal epidemics affect 20 to 30% of children and 5 to 10% of adults (Kuster et al., 2011). World Health Organization (2012) recommends influenza vaccination for high risk groups such as

pregnant women, children ages 6 to 59 months, elderly individuals, select chronically-ill individuals and health care professionals. Chronically-ill individuals include those with chronic heart or lung disease, asthma and HIV/AIDS. The elderly are the most likely to be hospitalized or die from influenza illness. The elderly may account for up to 90% of influenza-related deaths per season. Children under two years of age have an estimated 1 to 2 millions cases of influenza-related severe acute respiratory infections and 28,000 to 111,500 deaths annually (Nair et al., 2011).

The measure of disease burden is based on a proxy for influenza incidence because it is impossible to test the entire population for infection. We define the incidence proxy as the proportion of positive specimens for the influenza isolate of interest of patients seeking treatment for influenza-like-illness. While the number of individuals experiencing influenza-like-illness represents the sick population who get specimens tested, the positive result of a specimen test indicates influenza-like-illness that are indeed influenza-related.

Accurate estimation of influenza mortality requires complex mathematical models, since it is impossible to derive such estimates from hospital or death records. Influenza-related mortality estimates themselves are based on an extroplation of estimates whose error is not well understood. The errors (bias and lack of precision) of these estimates have not been investigated fully yet. The methods to be developed in this project will help investigators understand the properties of estimates of mortality due to influenza. Such estimates are crucial for policy-makers to make informed decisions about resource allocation when challenged with public health demands and expand our understanding of the impact of influenza, and aid in better measuring the effectiveness of various influenza interventions. Our proposal is motivated by the gaps in our understanding of estimates of influenza mortality, and by our desire to have a broader impact on vaccination strategy implementation and measures of effectiveness through measurement of influenza mortality (Thompson et al., 2009). In addition,

the methods developed in this project can be applied globally to obtain more precise estimates of the number of cases and deaths prevented by vaccination or resulting patterns of influenza immunity due to changes in vaccination strategies and other interventions. Finally, the estimates of the standard errors surrounding the influenza mortality can be used to determine the sample sizes for future studies.

1.2.1 Motivating Influenza Mortality Dataset

We obtained weekly data on percentages of specimens testing positive for influenza types and subtypes from the Center of Disease Control (CDC), through an active collaboration with committee member Dr. Danielle Iuliano. Respiratory deaths from causes that may be attributed to influenza, positive influenza specimen testing (by influenza type and subtype) data, and population data for each week during influenza season for the United States between 1981 and 2014 are included in the dataset. The proportion of each influenza proxy subtype given the specimen was found to be positive from 1981 to 2014 ranges from 0-50% for Influenza A(H1N1), 0-33% for Influenza A(H3N2), 0-45% for Influenza A(H1N1) pandemic strain, and 0-100% for Influenza B.

1.3 An Introduction to the Human Brain

The human brain is a complex organ with the ability to coordinate all body activities, form perceptions and produce emotions. Billions of nerve cells, known as neurons, are contained in the 3 pound organ. The neuron is a specialized, impulse-conducting cell that is the functional unit of the nervous system (Neuron, 2016). Neurons interact by sending and receiving signals to up to tens of thousands of surrounding neurons. By passing signals via the integration and analysis of information, the neurons allow remote areas of the brain to communicate. At every moment, the

strength and the frequency of the signal changes based on stimulus. Characteristics of the changes indicate brain function.

The blood serves as the indicator of increased neuronal activity; with a corresponding increase in the metabolic demand for glucose. As a result, there is an increase in cerebral blood flow (CBF) to the active region. Therefore, blood flow in the brain is an indirect, slow measure of neural activity. The electricity in the brain can also serve as an indicator of neuronal activity, as the neurons in the brain communicate with each other by sending electrical impulses. Thus, electricity in the brain is a direct measure for neuronal activity.

1.3.1 Functional Neuroimaging

Studies with the focus on functional connectivity determine the association of brain activity between regions by observing the changes in the blood flow and oxygenation levels in the brain or changes in signal over time (Sporns, 2013; Honey et al., 2009). These changes are indicative of functional networks, defined as dynamic patterns of interaction (Sporns, 2013; Honey et al., 2009). There are two main types of data that measure the blood flow in the brain; functional magnetic resonance imaging (fMRI) and positron emission tomography (PET). Observing the blood flow changes in the brain offers the benefit of high spatial resolution, but a limited temporal resolution due to a slower rate of brain hemodynamics. Neuronal activity can change within tens or hundreds of milliseconds (Sporns, 2013). The fMRI and PET scans have a lower temporal resolution due to a slow sampling rate (Sporns, 2013). The undirected statistical dependencies of brain regions are inferred by regional activity correlation (Park and Friston, 2013). Commonly used correlation measurements are cross-correlation, mutual information, spectral coherence or Pearson correlation (Sporns, 2013; Honey et al., 2009). The statistical dependencies, indicating functional connectivity, do not necessarily imply that the regions are physically connected (Park

and Friston, 2013). Determining functional connectivity by inferring the brain network from blood flow and oxygenation data is the focus of the approach introduced in Chapter 2.

Functionally activated points in the brain show on the voxel-level which parts of the brain are engaged in completing a particular function or react to a particular stimuli. Once a parcellation scheme is mapped onto the brain containing the activated voxels; activated regions are indicated. It is of interest to estimate the statistical dependencies between activated regions. The proposed method uses information from the activated regions in the brain (functional activation) to infer the brain functional network (functional connectivity).

1.3.2 Meta Analysis of Functional Neuroimaging

Investigators are increasingly interested in the functionality of the brain. A single functional neuroimaging study is expensive to conduct forcing researchers to limit their sample size. Due to a limited sample size, the findings likely contain false positives. To find true functionally activated brain regions it is beneficial to evaluate multiple studies at a time. In most cases, the meta-analysis data collected are the reported activation points of a study. As a result, functional co-activation, the consistent activation of at the regional or voxel level, is determined during such a study.

1.3.3 Motivating Neuroimaging Dataset

To study the functional co-activation of the brain, we consider a total of 331 functional neuroimaging studies published from 1993 to 2011. Collectively, the data contains information on positive and negative emotions. Resulting in 752 emotional comparisons (positive = 239, negative = 513). The inclusion criteria for the studies in our meta-analysis are as follows: 1. All the subjects included in the study are healthy

adults; 2. All the studies measure regional cerebral blood flow (PET) or blood oxygenation (fMRI); 3. Standard Talairach or Montreal Neurological Institute (MNI) coordinates are provided to ensure the results are spatially normalized standard coordinate systems, thus allowing for comparison of findings across independent studies. In order to make the studies comparable to one another, the data is converted into MNI space. The significant activation locations for each substudy in each study are included. There are a total of 2,345 significant activation coordinates.

1.4 Count Data Analysis

In many cases, the normal distribution can be used to approximate count data, commonly when counts are above zero and the mean is greater than twenty. However when those conditions are not met, modeling count data using a normal distribution can cause inaccurate mean and variance estimation, as well as expected values and confidence intervals less than zero. The distribution of count data assumes a relationship between the mean and variance, and the distribution is truncated on the left at zero. The normal distribution assumes no relationship between the mean and variance. To avoid illogical values below zero, one must choose to use a proper discrete non-negative distribution.

Count response models are a subset of discrete response models used to address non-negative integer responses. Count data models are predominantly based on two distributions: Poisson and negative binomial. The simpler distribution, the Poisson distribution, has a probability mass function of

$$f(y;\lambda) = \frac{e^{\lambda}\lambda^{y}}{y!}, y = 0, 1, 2, \ldots; \lambda > 0, \tag{1.1}$$

where y, the count response, is the random variable and λ, the rate or intensity parameter, is the distribution parameter representing the mean and the variance. An

equivalent mean and variance is a distinct feature of the Poisson distribution. This property is known as *equidispersion*. Equidispersion seldom occurs in real data, thus spurring the creation of other count models that do not have this feature. Usually when this property is violated, the variance is greater than the mean, resulting in *overdispersion*.

To model overdispersed Poisson data, one may employ the negative binomial model. The negative binomial distribution has an additional parameter, known as the heterogeneity parameter. The negative binomial distribution, has a probability mass function of

$$f(y; r, p) = \frac{\Gamma(y+r)}{\Gamma(r)\Gamma(y+1)} p^r (1-p)^y, y = 0, 1, 2, \ldots; 0 < p < 1, \tag{1.2}$$

where y, the count response, is the random variable and p is a positive number. The mean, μ is $\frac{r(1-p)}{p}$ and the variance is $\frac{\mu^2}{r} + \mu$. The distribution counts the number of failures before the rth success. The advantage of this parameterization of the negative binomial is the range of the outcome, number of failures, is restricted to non-negative integers.

1.5 Correlated Response Data

Correlation is the measure of dependence between two random variables that takes a value between -1 and 1. A correlation of the value zero indicates the two random variables are linearly unrelated, while a correlation value of one indicates that one random variable exactly predicts the other.

Correlated (dependent) data is indicated by a predictive relationship between covariates. Two covariates are considered correlated when one covariate can predict the value of the other covariate. Observations are often correlated by subject, time, or location. While correlated data is common in public health research, most statisti-

cal analysis make the basic assumption that each observation is independent. The improper analysis of correlated data is a common error. The dependence among observations must be accounted for when conducting statistical analysis. Ignoring correlation leads to erroneous statistical inference (i.e. statistical tests, confidence intervals, p-values).

Statistical analysis of correlated data requires methods that properly account for the correlation in the response variable. In the following chapters, correlated data is accounted for in the use of multivariate distribution and autocorrelation modeling. Multivariate distributions are a way to parametrically account for correlation in the data. It is a multi-dimensional joint distribution that includes correlation. Autocorrelation, often referred to as serial correlation, uses time-series methodology to account for correlation over time. This method is a relationship in which closer time points have a stronger correlation than time points further apart.

1.6 Bayesian Methods

Bayesian inference assumes parameters, p, that govern the data generating process are considered unknown and have their own distribution. Researchers begin by specifying a probability model for stochastic parameter values, that may include useful prior information about the parameter. Bayesian Statistics are based on Bayes Theorem, i.e. $P(A|B) = \frac{P(B|A)P(A)}{P(B)}$. More specifically, it is $h(p|data) \propto f(data|p)g(p)$, where $h(p|data)$ is the posterior distribution of p, $f(data|p)$ is the likelihood of p, and $g(p)$ is the prior distribution of p.

Bayesians induce the posterior distribution of the parameter, p, from $h(p|data)$, starting with a prior, prior distribution of the parameter before seeing the data, $g(p)$. The result is a description of the posterior distribution (for example, means, quantiles). The posterior is proportional to the numerator of Bayes Theorem. $h(p|data) \propto$

$f(data|p)g(p)$. The region of the highest posterior probability is indicated by the highest posterior density intervals. The interpretation of results differ from the frequentist approach. Based on the analysis of the Bayesian approach, a Bayesian can interpret their 95% confidence interval as a 95% probability that the true parameter (for example, population mean) is in the said interval. Basically, the interval describes the variability in the parameter for fixed data.

1.6.1 Impact of Bayesian Method on Biomedical Research

The Bayesian approach's flexibility and interpretability has made it a prominent in research. The approach can incorporate prior knowledge by informing prior distributions in the model. It is important to note that the selection of the prior distribution of the parameter of interest may determine the type of results concluded. The fact that two researchers both using the Bayesian approach can reach two different results is a reason for criticism from frequentist statisticians. Bayesian statisticians may find it difficult to quantify their prior beliefs into a probability distribution, or even come to a consensus about the prior distribution among researchers in the field. It is important to select an accurate prior or when no information is known, a noninfomative prior.

1.6.2 Bayesian Tools

While the theory and the interpretation of the Bayesian approach may be preferred, the computation required for a Bayesian analysis may be difficult. Finding the posterior distribution using Bayes Theorem may be more complex than we can do in closed form; however, computational tools can be used. Often computationally intensive algorithms are utilized - most commonly, Markov Chain Monte Carlo Gibbs or Metropolis-Hastings algorithms.

1.7 Contributions

In Chapter 2, the objective is to develop a Bayesian method to determine functional activation pattern over multiple studies, and provide a convenient framework to conduct statistical inference about the brain network. Our proposed model extends existing methods' ability when determining the brain network from coordinate-based meta-analysis of neuroimaging data. Our proposed model in Chapter 3, employs a hierarchical Bayesian framework and a parametric bootstrap method to control for autocorrelation in estimating influenza-associated mortality. The proposed method extents existing methods by addressing temporal autocorrelation. Finally, Chapter 4 extends the research in Chapter 3 by employing natural cubic splines to account for long-term and seasonal trends in the data.

Chapter 2

Bayesian analysis of multivariate sparse count data with application to meta-analysis of functional neuroimaging data

This chapter is joint work with Dr. Jian Kang.

2.1 Introduction

2.1.1 Neuroimaging

The science of the brain provides insight into how one of the body's most complex organs operates. The brain enables action and cognition among a limitless number of other functions, despite having a fixed anatomy (Park and Friston, 2013). These networks of neurons interact, allowing non-invasive imaging techniques to map the brain and providing the ability to infer some diagnosis status and treatment responses related to the brain. Neuroimaging visually summarizes the activity arising from a population of neurons in the brain. Analysis of the brain is made possible through neuroimaging and tools from graph theory and dynamic systems (Honey et al., 2009; Sporns, 2013). Neuroimaging studies mainly study two types of connectivity: structural and functional. Structural connectivity in the brain is the physical connection between brain regions (Honey et al., 2009), also referred to as anatomical links (Park and Friston, 2013) or the human connectome (Sporns, 2013).

Functional Connectivity

Studies of functional connectivity explores the association of brain activity between regions by observing the differences in the blood flow and oxygenation levels between regions of the brain or the changes within regions over time (Sporns, 2013; Honey et al., 2009). These changes are indicative of functional networks, defined by dynamic patterns of interaction (Sporns, 2013; Honey et al., 2009). The collection of functional data usually comes from one of two techniques: the study of the electrical and magnetic activity in the brain, or the study of the blood flow and oxygenation changes that take place when neurons are active (Park and Friston, 2013; Sporns,

2013). Inferring functional connectivity is the focus of the approach introduced here.

Functional Co-activation

Neuroscience has established functional activation as a fundamental indicator of brain organization in humans. It shows us on the voxel-level which parts of the brain are engaged in completing a particular function. Once a parcellation scheme is mapped onto the brain containing the activated voxels, activated regions are indicated. It is of interest to estimate the statistical dependencies between activated regions. The proposed method uses information from the activated regions in the brain (functional activation) to infer brain functional co-activation. Torta and Cauda (2011) defines co-activation as when a group of regions is reported together across studies as evidence of their functional connection. Functional co-activation is significant because the resulting networks can provide information on the functional relationships within the human brain (Torta and Cauda, 2011).

2.1.2 Preprocessing Pipeline

Before functional neuroimaging data can be analyzed, it must be preprocessed. The described preprocessing pipeline ensures that the functional neuroimaging data does not contribute any unnecessary noise and is prepared for analysis. Because a complete scan of the brain cannot be completed at once, different parts of the brain are scanned at different times (Bowman et al., 2007). Slice timing correction allows images of the brain from different time points that complete one scan, to correspond to a single time point. This allows us to view the brain image as if a complete scan could be completed in a single moment (Lindquist et al., 2008). Next, spatial alignment (also known as motion correction) ensures that collected time-series images can be mapped to a single image if the subject moves in the scanner. In order to make comparisons across subjects, one spatially normalizes the data during preprocessing.

By spatially normalizing (also known as co-registering) the data, each subject's brain scan is scaled to a standard template brain. Finally, spatial smoothing is completed to provide better continuity between anatomical difference and to meet assumptions essential to random field theory (Lindquist et al., 2008). The preprocessing pipeline is required to correctly analyze functional neuroimaging data.

2.1.3 fMRI from single-subject studies

Understanding the interactions in neural activity between brain regions is an expanding research area of interest. It is essential to elucidating brain function. Neuroimaging, a visual summary of neural activity, paired with tools from graph theory and dynamic systems allows analysis of the brain and enables inference of it's connectivity (Sporns, 2013; Honey et al., 2009). The typical functional neuroimaging modalities include functional magnetic resonance imaging (fMRI) and positron emission tomography (PET).

Functional brain images are acquired over a period of time while the subject experiences a stimuli. During the experience, the changes in signal measurements between images are used to make inference about stimuli-related activation. Information about the stimuli's effect can be used to localize regions in the brain based on the type of stimuli, determine existing networks that explain brain function, and also predict psychological or diseased states.

A typical fMRI experiment acquires between 100 to 2,000 images and each image has about 100,000 voxels (Lindquist et al., 2008). The experiment may be repeated many times on each subject. It is not possible to get a full spatiotemporal model. As a result, some analysis shortcuts can be made. It is up to the researcher to select which shortcuts are deemed appropriate and necessary based on how they affect the power and validity of the results (Lindquist et al., 2008).

Understanding the interactions in neural activity between brain regions is an ex-

panding research area of interest. It is intrinsic in elucidating brain function. Neuroimaging, a visual summary of neural activity, paired with tools from graph theory and dynamic systems allows analysis of the brain and enables inference of it's connectivity (Sporns, 2013; Honey et al., 2009). The typical functional neuroimaging modalities include functional magnetic resonance imaging (fMRI) and positron emission tomography (PET).

Typically a single fMRI or PET study collects data from 20 - 40 subjects due to a relatively high cost of MRI scanner time (Kang et al., 2011). Thus, single studies may produce unreliable results. fMRI scans can capture irrelevant features because a large dataset is obtained from each subject and the brain is a complex organ. A single fMRI study must have adequate power to detect real effects and reject misleading noise. Cremers et al. (2017) reports weakly diffuse effects are generally inflated compared to strong localized effects when sample size is small. Meta-analysis data mitigates the limitations of single functional neuroimaging studies by estimating the consistent activation patterns across studies making inference on the population-level. In this work, we focus on identifying the co-activation patterns using meta-analysis data. We propose a Bayesian Poisson-Gamma graphical model with a parameter and prior specification to account for sparse data. We develop an efficient posterior inference for estimating the co-activation patterns which was influenced by Xue et al. (2014a) method.

There is limited research on determining functional co-activation patterns from foci collected over different studies. To date, methods have aimed to identify the co-activation patterns between region pairs in meta-analysis and full image data (Postuma and Dagher, 2006; Kober et al., 2008; Cauda et al., 2011; Torta and Cauda, 2011; Robinson et al., 2012; Patel et al., 2013) or to employ component-driven approaches (Kober et al., 2008). In particular, Nielsen et al. (2004) proposed a matrix factorization algorithm, in which a matrix that represents the activation associated

with particular tasks is decomposed. Kober et al. (2008) uses very different steps to determine co-activation. Kober et al. (2008) proposed a functional grouping approach, which analyzes the spatial density of reported foci using multilevel kernel density analysis (MKDA) and then combines non-metric multidimensional scaling and cluster analysis to group regions based on their co-activation patterns. MKDA identifies brain voxels with more reported peaks than would be expected near by randomly. Neumann et al. (2010) have developed a structural learning approach in a Bayesian framework for constructing a directed functional network, which yields probabilistic dependency between brain regions. The above methods are intended to identify co-activated regions, but they do not permit likelihood-based statistical inference for co-activation patterns of multiple foci. More recently, Xue et al. (2014a) proposed a Poisson graphical model for estimating the co-activation patterns based on the meta-analysis data.

In Xue et al. (2014a), a graphical model was developed for the region-wise observed foci counts based on the multivariate Poisson distribution. A penalized likelihood approach was used to estimate the sparse covariance matrix. It imposes sparsity on regions with little association to shrink the strength of co-activation toward zero. The EM algorithm was used to find the penalized maximum likelihood estimates (PMLE). Specifically, in the expectation step, Xue et al. (2014a) found the expectation of the unobserved number of co-activation foci given the number of foci in each region separately. In the maximization step, the maximum penalized complete data log-likelihood was determined.

The limitations of this previous work include the penalty term cannot guarantee sparsity, and the known limitations of the EM algorithm. The EM algorithm is known to have the solutions converges to a local optimum, have the maximization step slow down as the number of parameters increase, and the EM algorithm does not directly produce the standard error of estimation with which to perform inference.

2.1.4 Meta-Analysis

Functional co-activation is the measurement of the consistent co-activation of brain regions across different functional neuroimaging studies. The following approach specifically identifies co-activation in a coordinate-based meta-analysis. Unlike a single fMRI study exploring functional connectivity using time-series of brain signal activity as data, multiple fMRI studies exploring functional co-activation uses active voxels as data, also known as foci.

The typical collection of fMRI data from a single study can be seen on the left side of Figure 2.1. A single study begins with the collection of fMRI time-series data, then preprocessing of the data. Next the statistical analysis is used to fit the time-series; followed by a resulting Statistical Parametric Map, often referred to as a T-map. The T-map maps the voxels of brain activation onto a template. Generally studies report the foci. These reported foci summarize the active voxels in significant regions of the brain. The reported coordinate locations of the foci are collected and used for analysis for meta-analysis studies.

An example of meta-analysis data collections for a study can be seen in Figure 2.2. A study may include multiple substudies that compare emotional states. The meta-analysis data collected combines includes information about the regional level foci counts from each substudy. The number of foci (peak activation points) indicates brain activity.

Our work is the first to incorporate a Bayesian framework for functional co-activation pattern identification to determine brain networks based on region-level activation counts using a Poisson-Gamma graphical model. Our proposed method has the following features: (a) it is based on a graphical model to represent sparse brain networks, (b) it provides more interpretable results than many existing methods by explicitly modeling the strength of functional co-activations and it's probability, and (c) it utilizes fast computational algorithms for parameter estimation.

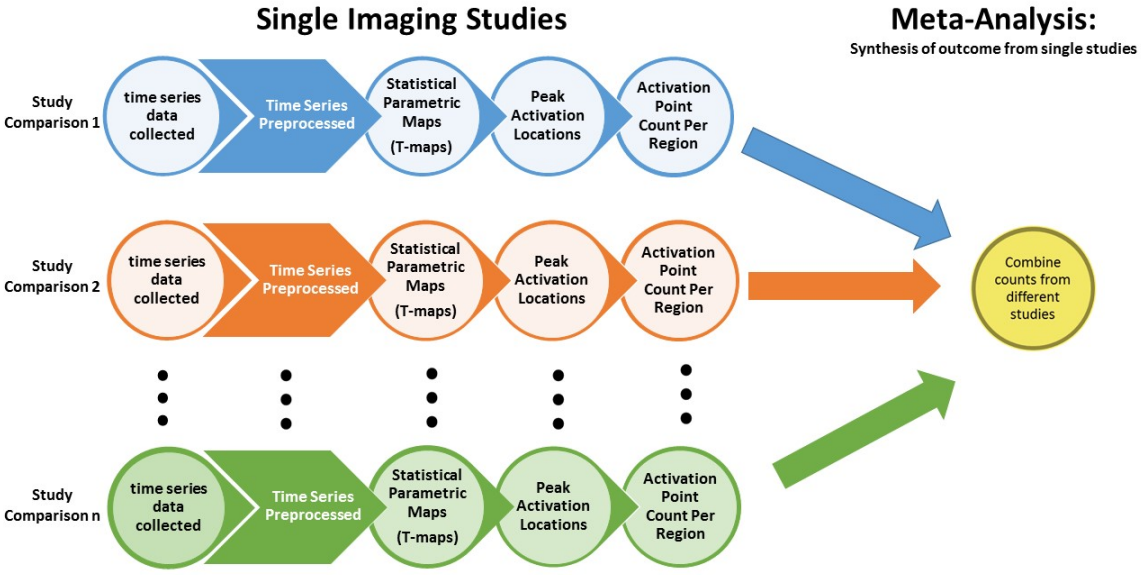

Figure 2.1: Pipeline of analyzing the time series data of k single functional neuroimaging studies funneled into one dataset. The activation points are combined from different studies and then summarized into the regional activation point counts which are the observed data, $\boldsymbol{X}^{\boldsymbol{k}}$, in the model.

Study	fron	temp	occi	pari
s_Aalto2002	0	7	2	0
s_Aalto2002	0	4	2	0
s_Aalto2002	0	0	2	0
s_Aalto2002	0	2	0	0
s_Aalto2005	0	2	2	0
s_Aalto2005	1	5	2	0
s_Adams2003	0	0	0	0
s_Beauregard2001	0	1	3	2
s_Blair1999	0	3	1	0
s_Blair1999	1	0	0	0
s_Blair1999	1	0	0	0
s_Blair1999	1	1	0	0
s_Breiter1996	0	2	1	0
s_Breiter1996	0	2	0	0
s_Buchanan2000	1	0	0	0

Figure 2.2: Example of meta-analysis data collection

2.2 Methods

We propose a Bayesian Poisson-Gamma graphical model. We also propose a prior specification to introduce sparsity in the model. Our proposed method can identify the consistent co-activation locations across studies and provides a convenient framework for statistical inference on the dependence structure of the sparse count data. Our Bayesian approach parameterization allows indication of where co-activation exist and a prior distribution for the strength of co-activation between two regions. The standard Markov chain Monte Carlo (MCMC) algorithm can be straightforwardly applied for posterior computation.

Compared to classical statistics approaches, the proposed Bayesian method enjoys the following advantages. First, it is natural to incorporate the prior knowledge of brain functional connectivity and structural connectivity into the model. Second, it provides an appropriate uncertainty measure (i.e.posterior inclusion probability and posterior credible interval) for the sparse Poisson graph learning based on the posterior inference. Third, the regional activation can be more flexibly decomposed using expected values. Fourth, it can generate results to address a variety of scientific questions of interests with formal probabilistic statements. In addition, the MCMC method for posterior inference is straightforward to implement and the computational cost is moderate in contrast to the optimization procedures.

In our sparse hierarchical Bayesian model, at the top-level, the marginal Poisson distribution is used to model the foci count for each region. On second-level, we decompose parameters of the top-level into components introducing dependence. We model the distributions of number of foci over multiple regions, where the covariance matrix characterizes the region-level (top-level) co-activation patterns. We impose sparsity on the covariance matrix by assigning a parameter, δ, as an indicator for co-activation with a prior reflecting sparsity. The proposed model defines a sparse brain co-activation network. To facilitate the model inference, we introduce a set of

variables $\boldsymbol{\lambda}$ which are parameters in the function of the expectation represent the expected number of co-activation foci between regions per observation. The posterior computational algorithms are then developed.

2.2.1 Notation

Suppose we have p brain regions of interest, the brain network has $\binom{p}{2}$ possible co-activation relationships, given we are only interested in two-way interactions. Denote by i, j two region indices ($1 \leq i, j \leq p$). For emotion study k ($k = 1, \ldots, n$), we observe the number of foci in each region $\mathbf{X^k} = (X_1^k, \ldots, X_p^k)$, where $\mathbf{X^k}$ is a vector of foci counts in different regions for study k, X_i^k represents the number of foci in region i for a given study k. $X_i^k \in \{0, 1, 2, \ldots\}$, where the value zero is frequently observed.

2.2.1.1 Poisson-Gamma Model

Different from the multivariate Poisson graphical model (Xue et al., 2014a), we propose a new model to project the co-activation structure in the brain and infer functional co-activation. For any two regions, i and j, in our model, k indexes the observations of each of the studies included in the dataset. k can range from 1 to n, the total number of included observations. The total number of activation points found in region i and region j is X_i^k and X_j^k, respectively. The number of total activation points in a region, marginally, can be modeled as a Poisson distribution where $X_i^k \mid \mu_i^k \sim \text{Poisson}(\mu_i^k)$. We directly decompose μ_i^k, the mean of regional co-activation count, to substudy-specific co-activation intensity parameters. We used the term "activation" to refer the activation for a single region. We use "co-activation" to refer the activations between two regions.

$$E(X_i^k) = \mu_i^k = \sum_{j=1}^{p} \theta_{ij}^k$$

For the Bayesian Poisson-Gamma model, $\theta_{i,j}^k$ represents the unobserved number of co-activations in the two regions, say i and j, for study k. $\boldsymbol{\theta}_{p\times p}^k = (\theta_{i,j}^k)_{1\leq i,j\leq p}$ can also be interpreted as representations of the separate foci into groups without any joint activation ($\theta_{i,i}^k$) and by activation with other regions ($\theta_{i,j}^k$). $\theta_{i,i}^k$ and $\theta_{j,j}^k$ (diagonal elements of the co-activation matrix for the k^{th} study) both represent the expected number of localized foci in regions i and j without joint activation. Each random variable, $\theta_{i,j}^k$, has an independent Gamma distribution with parameters $\lambda_{i,j}$ and $\beta_0 = 1$ using Gamma shape and rate notation.

$$\theta_{ij}^k \sim \text{Gamma}\,(\lambda_{ij}, \beta_0)$$

The strength of the co-activation between regions is parameterized by each element of the intensity matrix, $\boldsymbol{\lambda}$.

$$\lambda_{ij} \sim \text{Gamma}\,(a_0, b_0)$$

Note that for potentially co-activated regions ($i \neq j$), the covariance of regional activation representing the strength of co-activation can be defined as:

$$\text{Cov}(X_i^k, X_j^k) = \text{E}\{\text{Cov}(X_i^k, X_j^k \mid \mu_i^k, \mu_j^k)\} + \text{Cov}\{\text{E}(X_i^k \mid \mu_i^k), \text{E}(X_j^k \mid \mu_j^k)\} = \frac{\lambda_{ij}}{\beta_0^2}$$

where $\text{E}\{\text{Cov}(X_i^k, X_j^k \mid \mu_i^k, \mu_j^k)\} = 0$, $\text{Cov}\{\text{E}(X_i^k \mid \mu_i^k), \text{E}(X_j^k \mid \mu_j^k)\} = \text{Var}(\theta_{i,j}^k) = \frac{\lambda_{ij}}{\beta_0^2}$ and $\text{Var}(X_i^k) = \text{E}\{\text{Var}(X_i^k \mid \boldsymbol{\theta})\} + \text{Var}\{\text{E}(X_i^k \mid \boldsymbol{\theta})\} = \sum_{j=1}^p \frac{1+\beta_0}{\beta_0^2}\lambda_{ij}$.

2.2.1.2 Sparse Poisson-Gamma Model

To account for sparse activation within the data (X_i^k) is frequently observed as zero, we extent the aforementioned model to better account for sparsity. We define the parameter $\mu_{i,j}^k$ with an co-activation indicator function, $\delta_{i,j}$. The co-activation indicator function signifies a region pair has contribution. The expected value of regional

activation count (X_i^k) is now defined as $\mu_i^k = \sum_{j=1}^{p} \theta_{ij}^k \delta_{ij}$ and $\delta_{ij} \sim$ Bernoulli(π_0). The prior of θ_{ij}^k remains the same. Then for potentially co-activated regions ($i \neq j$), we define covariance conditional on the presence of co-activation. When two regions are assumed to be co-activated, then $\text{Cov}(X_i^k, X_j^k \mid \delta_{ij} = 1) = \frac{\lambda_{ij}}{\beta_0^2}$. On the other hand, when two regions are deemed not to be co-activated $\text{Cov}(X_i^k, X_j^k \mid \delta_{ij} = 0) = 0$. The variance of a single region can be derived as $\text{Var}(X_i^k \mid \boldsymbol{\delta}) = \sum_{j=1}^{p} \frac{1+\beta_0}{\beta_0^2} \lambda_{ij} \delta_{ij}$.

This type of model allows sparsity to be modeled in the parameter $\boldsymbol{\delta}$, where the Bernoulli probability of obtaining a positive (nonzero) value is π_0. The model was developed to address the high occurrence of zeros in the observed data and to analyze and interpret zero counts.

Consider our data application to a meta-analysis study of emotional-state peak activation voxels in which the latent variable is the number of co-activation voxels across studies, θ_{ij}^k. In this case, it is assumed that only where no co-activation is found, $\delta_{ij} = 0$, will there be zero co-activation voxels ($\lambda_{i,j} = 0$) and where there exists co-activation between regions, $\delta_{ij} = 1$, some positive (nonzero) number of co-activation voxels will be found ($\lambda_{i,j} > 0$). If the relationship between two brain regions is considered co-activated, the value of co-activation voxels must be positive.

Our proposed sparsity model aims to achieve convergence of the full conditional distributions in order to correctly infer the posterior distribution. Our results help us estimate our predictive error (i.e. mean squared error), with a goal of minimizing it.

All analysis was conducted using R (R Core Team, n.d.).

2.3 Simulation Study

We conducted a simulation study to compare the performance of our non-sparse methods (EM-PG and Poisson Gamma omitting the indicator function) to our proposed sparse method using generated data. First, the data was generated by defining

a sparsely co-activated intensity matrix, $\boldsymbol{\lambda}_{p\times p}$, where p is the total number of the regions of interest. Second, from the set intensity parameters, a dataset of 300 or 600 observations, θ_{ij}^k, co-activation values, are generated by Poisson(λ_{ij}). The regional activation, X_i^k, was calculated from the generated $\boldsymbol{\theta}$ and considered to be our observed data. The simulated data were modeled using the previously mentioned graphical models. The performance of each model on each dataset is summarized by the estimated $\hat{\boldsymbol{\lambda}}$ MSE. In MCMC techniques, the choice of initial values is important as it may influence the posterior distribution. Our initial values are randomly choosen for each chain. By setting reasonable initial values, we are confident in our results.

The following are the default values on the simulations, unless otherwise stated. There are 3 or 5 regions in the networks, with a proportion of co-activation between any two regions being $\frac{1}{3}$. Each dataset contains 300 or 600 observations and was run for 20,000 iterations with a burn-in of 15,000 with 5 chains.

To evaluate the ability of our proposed sparse method in determining the correct co-activation and functional network, we assess the accuracy of determining a sparse network's intensity matrix $\boldsymbol{\lambda} = (\lambda_{ij})$ and co-activations $\boldsymbol{\delta} = (\delta_{ij})$. Specifically, a mean square error (MSE), an average of the squares of the difference between the estimated intensity conditioned on the presence of co-activation and the true value over all possible co-activations was used to assess performance of the model. The correct regional connections in the functional network are measured using sensitivity (true connection rate given there is a true connection), specificity (true disconnection rate given there is no true connection), and false discovery rate (FDR). These quantities indicate the accuracy of the network solution.

2.3.0.1 Simulation Results

Number of Studies

In order to evaluate the asymptotic properties of the proposed method, we observe

Regions	Studies		Methods Nonsparse	Sparse
3	**300**	**MSE**	0.010	0.004
		Sensitivity	1	1
		Specificity	0	1
		FDR	0.667	0
	600	**MSE**	0.021	0.008
		Sensitivity	1	1
		Specificity	0	1
		FDR	0.667	0
5	**300**	**MSE**	0.021	0.002
		Sensitivity	1	1
		Specificity	0	1
		FDR	0.7	0
	600	**MSE**	0.023	0.006
		Sensitivity	0.143	1
		Specificity	1	1
		FDR	0	0

Table 2.1: Estimation summary of each method as number of studies vary

the results as the number of studies increases. As the sample size increases, the intensity estimations do not necessarily improve. The MSE is able to stabilize early. Our method is able to estimate the network with a small sample size. The nominal increase in the MSE is believed to be due to randomness. It can also be observed that the number of regions does not effect the MSE results. The proposed sparse method can determine co-activation well as seen the sensitivity, specificity and false discovery rate measures. Thus, true region co-activations in the network are correctly identified as existing by our proposed sparse method, and all region pairs with no co-activation are correctly identified as not existing by our proposed sparse method. Results are summarized in Table 2.1.

Proportion of Co-activated Region Pairs

How the estimation methods perform when the proportion of co-activated regions within network is sparse is important, as sparsity motivated the proposed method. To observe the estimation ability of the proposed sparse method, the density of the network is varied in the model. There are two generated datasets: sparse and non-sparse. The sparse dataset allows approximately $\frac{1}{3}$ of co-activations to exist, while in the non-sparse dataset approximately $\frac{3}{4}$ co-activations have a signal. From Table 2.2, we see as sparsity of the network decreases, the average MSE increases when employing the proposed sparse method. This result indicates that our method performs better with sparse functional data that often occurs in real datasets. When data is not sparse the ability to estimate the intensity matrix is weakened, but our method maintains its ability to correctly determine co-activation as seen from the specificity, sensitivity and false discovery rate.

The utility of the proposed sparse Poisson-Gamma method as opposed to the nonsparse methods is exhibited through its ability to estimate the strength of co-activation as well as infer the functional co-activation network.

2.4 Data Analysis

To study the functional co-activation of the brain, we consider a total of 331 functional neuroimaging studies published from 1993 to 2011. Collectively, the data contains information on induced positive (n = 239) and negative (n = 513) emotions. Resulting in 752 emotional comparisons (substudies). There are a total of 2,345 significant activation coordinates.The inclusion criteria for the studies in our meta-analysis are as follows:

1. All the subjects included in the study are healthy adults;

2. All the studies measure regional cerebral blood flow (PET) or blood oxygenation

Regions	Proportion Co-activated		Methods: Nonsparse	Methods: Sparse
3	**Sparse**	**MSE**	0.010	0.004
		Sensitivity	1	1
		Specificity	0	1
		FDR	0.667	0
	Dense	**MSE**	0.068	0.036
		Sensitivity	1	1
		Specificity	0	1
		FDR	0.333	0
5	**Sparse**	**MSE**	0.021	0.002
		Sensitivity	1	1
		Specificity	0	1
		FDR	0.7	0
	Dense	**MSE**	0.032	0.888
		Sensitivity	1	1
		Specificity	0	0.429
		FDR	0.3	0.571

Table 2.2: Estimation summary of each method as proportion of co-activated region pairs vary

(fMRI);

3. Standard Talairach space (Talairach and Tournoux, 1988) or Montreal Neurological Institute and International Consortium for Brain Mapping (MNI) coordinates (Mazziotta et al., 2001) are provided to ensure the results are spatially normalized standard coordinate systems, thus allowing for comparison of findings across independent studies.

Studies assessing learning and memory were excluded along with those exploring the anticipation of the stimulus. In addition, studies with motivational states that the affective states were not clear (e.g. thirst) were excluded. Once the data was mapped to the template, Automated Anatomical Labeling (AAL) (Tzourio-Mazoyer et al., 2002) was applied to calculate the number of activation points in each of the 116 anatomical volumes of interest (AVOI). Of the 116 AVOI, 42 regions distributed of the frontal, temporal, occipital and parietal lobes were chosen as the focus.

The selected 42 regions are analyzed on two levels. The first level is between lobes in the brain and the second level is within each lobe of the brain.

Level 1 Lobes

The brain is composed of four lobes: frontal, temporal, parietal and occipital. Memories with sensations of taste, sound, sight and touch are all processed in the temporal lobe. The occipital lobe is processes what you see, while the frontal lobe processes cognitive functions and physical activity. Finally, temperature, taste and touch are processed by the parietal lobe (Mayo Clinic, 2018). The results of our meta-analysis data are summarized in Tables 2.3, 2.4, and 2.5. Overall, positive and negative emotions, have caused a signal between the frontal lobe and occipital lobe, the frontal lobe and temporal lobe, and the temporal lobe and occipital lobe. When comparing the co-activation found between positive and negative emotion, the co-activation frontal-parietal, temporal-occipital, and frontal-temporal differ. The positive emotion data finds a signal between the previously mentioned regions compared

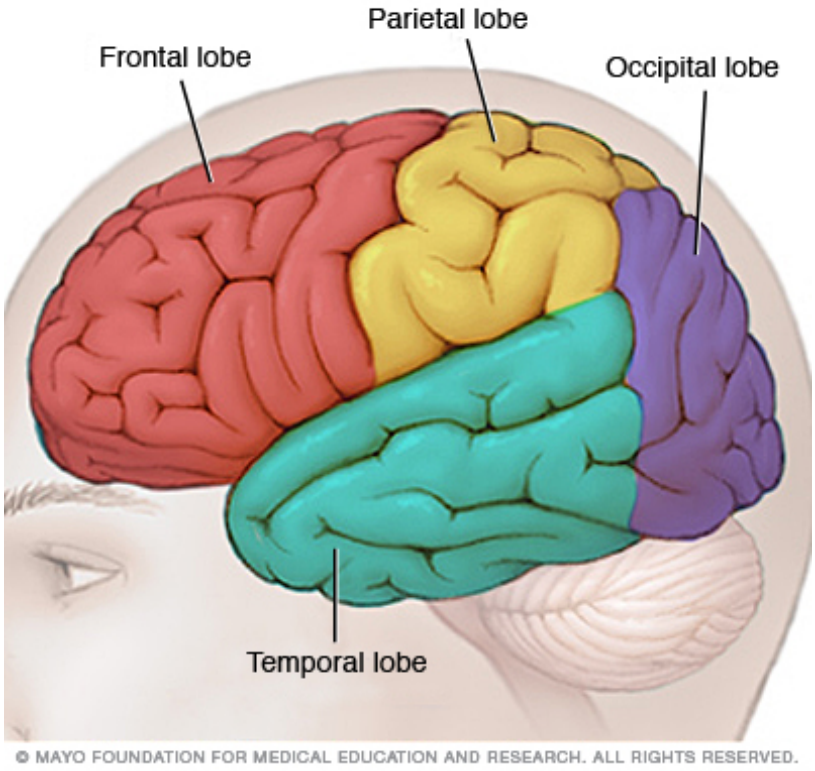

Figure 2.3: Level 1 - Brain Lobes: There are four primary lobes on the brain the frontal, temporal, parietal and occipital. (Mayo Clinic, 2018)

	Parietal	Occipital	Temporal
Frontal	0.00	0.03 (0.02, 0.06)	0.24 (0.07, 0.46)
Parietal		0.00	0.00
Occipital			1.08 (0.08, 4.71)

Table 2.3: Overall emotion data of Lobe Matrix using proposed spare method

to what is found during the stimulus of negative emotion.

Level 2 Occipital

Within the occipital lobe, five weak signals were found in the overall data. When the data is split to compare the effects of positive and negative emotion, more co-activations are found in the positive emotions data (14 compared to 6 in the negative dataset). The signal differences seen the positive emotion dataset are between the Superior left and right sides, the Superior left with the Middle (left and right), and the multiple co-activations with the Inferior region. The Inferior left with the Superior

	Parietal	Occipital	Temporal
Frontal	0.00	0.05 (0.03, 0.08)	0.16 (0.06, 0.74)
Parietal		0.00	0.52 (0.11, 2.14)
Occipital			0.00

Table 2.4: Negative emotion data of Lobe Matrix using proposed spare method

	Parietal	Occipital	Temporal
Frontal	0.38 (0.08, 2.03)	0.02 (0.02, 0.03)	0.00
Parietal		0.00	2.92 (0.04, 8.98)
Occipital			1.00 (0.17, 6.25)

Table 2.5: Positive emotion data of Lobe Matrix using proposed spare method

right and Middle left, as well as the Inferior right with the left Superior, Middle and Inferior. The results are shown in Figure 2.4 and Tables 2.6, and 2.7.

Level 2 Parietal

Within the parietal lobe, 13 weak signals were found in the overall data. When the effects of positive and negative emotion are compared, both emotions generate similar proportions of co-activation. Differences in co-activation by emotion type are found in the following regions: Superior left and right, Superior left and Precuneus right, Superior right and Inferior left, Cingulum Post Left and Inferior left, and Cingulum Post left and Precuneus left. Parietal results are shown in Tables 2.8, and 2.9.

Level 2 Frontal

The analysis of negative and positive emotions within the frontal lobe found some difference in co-activation. The differences in results, albeit most are rather weak, are co-activation between the frontal middle left and right for the negative emotion and

	Occipital Sup R	Occipital Mid L	Occipital Mid R	Occipital Inf L	Occipital Inf R
Occipital Sup L	0.00	0.00	0.00	0.27 (0.03, 2.04)	0.00
Occipital Sup R		0.05 (0.03, 0.10)	0.02 (0.02, 0.03)	0.00	0.10 (0.03, 0.45)
Occipital Mid L			0.00	0.00	0.00
Occipital Mid R				0.06 (0.04, 0.10)	0.17 (0.04, 0.74)
Occipital Inf L					0.00

Table 2.6: Negative emotion data of Occipital Region Matrix from the Proposed Sparse Method

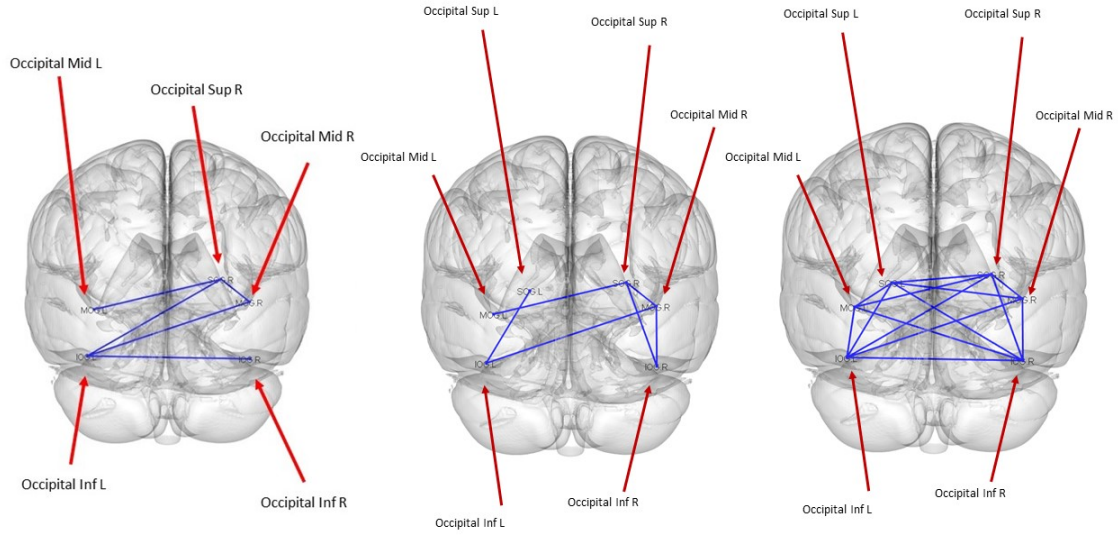

Figure 2.4: Occipital Region: The displayed results from the overall data, negative emotions studies and positive emotion studies (left to right).

	Occipital Sup R	Occipital Mid L	Occipital Mid R	Occipital Inf L	Occipital Inf R
Occipital Sup L	0.02 (0.02, 0.03)	0.37 (0.02, 3.38)	0.06 (0.02, 0.15)	0.30 (0.02, 2.81)	0.05 (0.03, 0.10)
Occipital Sup R		0.04 (0.03, 0.05)	0.19 (0.02, 1.66)	0.48 (0.06, 1.91)	0.03 (0.02, 0.05)
Occipital Mid L			0.00	0.42 (0.04, 2.57)	0.12 (0.05, 0.30)
Occipital Mid R				0.11 (0.04, 0.36)	0.06 (0.03, 0.11)
Occipital Inf L					0.15 (0.05, 0.52)

Table 2.7: Positive emotion data of Occipital Region Matrix from the Proposed Sparse Method

	Parietal Sup R	Parietal Inf L	Parietal Inf R	Precuneus L	Precuneus R	Cingulum Post L	Cingulum Post R
Parietal Sup L	0.00	0.06 (0.04, 0.08)	0.03 (0.02, 0.04)	0.03 (0.02, 0.05)	0.00	0.03 (0.02, 0.05)	0.04 (0.03, 0.09)
Parietal Sup R		0.00	0.13 (0.03, 0.61)	0.03 (0.02, 0.08)	0.05 (0.02, 0.11)	0.03 (0.02, 0.07)	0.02 (0.02, 0.03)
Parietal Inf L			0.06 (0.03, 0.16)	0.02 (0.02, 0.03)	0.03 (0.03, 0.04)	0.00	0.06 (0.02, 0.20)
Parietal Inf R				0.03 (0.02, 0.08)	0.04 (0.02, 0.11)	0.04 (0.03, 0.06)	0.03 (0.03, 0.04)
Precuneus L					0.06 (0.02, 0.16)	0.00	0.04 (0.03, 0.06)
Precuneus R						0.04 (0.03, 0.06)	0.08 (0.02, 0.28)
Cingulum Post L							0.10 (0.04, 0.24)

Table 2.8: Negative emotion data of Parietal Region Matrix from the Proposed Sparse Method

	Parietal Sup R	Parietal Inf L	Parietal Inf R	Precuneus L	Precuneus R	Cingulum Post L	Cingulum Post R
Parietal Sup L	0.24 (0.03, 1.53)	0.21 (0.04, 1.41)	0.07 (0.03, 0.28)	0.04 (0.02, 0.08)	0.03 (0.02, 0.08)	0.27 (0.02, 3.04)	0.05 (0.02, 0.22)
Parietal Sup R		0.02 (0.01, 0.04)	0.03 (0.02, 0.04)	0.57 (0.04, 3.11)	0.03 (0.02, 0.04)	0.02 (0.02, 0.04)	0.02 (0.01, 0.04)
Parietal Inf L			0.16 (0.02, 0.98)	0.03 (0.02, 0.04)	0.28 (0.02, 1.82)	0.03 (0.03, 0.06)	0.12 (0.02, 0.74)
Parietal Inf R				0.10 (0.03, 0.37)	0.02 (0.02, 0.02)	0.02 (0.02, 0.02)	0.04 (.03, 0.06)
Precuneus L					0.07 (0.03, 0.15)	0.06 (0.04, 0.11)	0.15 (0.02, 0.75)
Precuneus R						0.17 (0.02, 0.88)	0.03 (0.02, 0.04)
Cingulum Post L							0.09 (0.03, 0.41)

Table 2.9: Positive emotion data of Parietal Region Matrix from the Proposed Sparse Method

positive emotion resulted in the following co-activations: the frontal superior left and right, the frontal superior left and superior medial right, the frontal superior right and frontal med orb right, the rectus left and frontal superior medial right, the rectus right and frontal superior medial right, the rectus right and frontal superior medial left, and the frontal superior left and cingulum anterior right. Frontal results are shown in Tables 2.10, and 2.11.

	Frontal Sup R	Frontal Mid L	Frontal Mid R	Frontal Sup Medial L	Frontal Sup Medial R	Frontal Med Orb L	Frontal Med Orb R	Rectus L	Rectus R	Cingulum Ant L	Cingulum Ant R
Frontal Sup L	0.00	0.00	0.04 (0.02, 0.07)	0.04 (0.03, 0.06)	0.00	0.03 (0.03, 0.05)	0.03 (0.03, 0.04)	0.04 (0.02, 0.11)	0.00	0.05 (0.03, 0.08)	0.00
Frontal Sup R		0.05 (0.03, 0.08)	0.13 (0.02, 0.67)	0.00	0.07 (0.03, 0.18)	0.04 (0.03, 0.05)	0.00	0.00	0.04 (0.02, 0.07)	0.06 (0.03, 0.19)	0.04 (0.03, 0.05)
Frontal Mid L			0.10 (0.03, 0.42)	0.04 (0.03, 0.08)	0.02 (0.02, 0.03)	0.03 (0.02, 0.05)	0.02 (0.02, 0.03)	0.02 (0.02, 0.03)	0.00	0.00	0.00
Frontal Mid R				0.04 (0.03, 0.07)	0.08 (0.03, 0.28)	0.07 (0.02, 0.25)	0.03 (0.02, 0.04)	0.04 (0.02, 0.08)	0.00	0.05 (0.03, 0.08)	0.00
Frontal Sup Medial L					0.00	0.02 (0.02, 0.04)	0.02 (0.01, 0.03)	0.02 (0.02, 0.03)	0.04 (0.02, 0.14)	0.10 (0.03, 0.36)	0.00
Frontal Sup Medial R						0.03 (0.02, 0.04)	0.00	0.00	0.00	0.06 (0.02, 0.22)	0.05 (0.03, 0.07)
Frontal Med Orb L							0.03 (0.02, 0.03)	0.00	0.00	0.07 (0.03, 0.26)	0.05 (0.03, 0.15)
Frontal Med Orb R								0.00	0.04 (0.02, 0.11)	0.04 (0.02, 0.08)	0.04 (0.02, 0.10)
Rectus L									0.00	0.00	0.04 (0.03, 0.05)
Rectus R										0.03 (0.03, 0.04)	0.03 (0.02, 0.05)
Cingulum Ant L											0.24 (0.03, 0.94)

Table 2.10: Negative emotion data of Frontal Region Matrix from the Proposed Sparse Method

Level 2 Temporal

	Frontal Sup R	Frontal Mid L	Frontal Mid R	Frontal Sup Medial L	Frontal Sup Medial R	Frontal Med Orb L	Frontal Med Orb R	Rectus L	Rectus R	Cingulum Ant L	Cingulum Ant R
Frontal Sup L	0.11 (0.05, 0.33)	0.00	0.02 (0.02, 0.02)	0.21 (0.04, 0.91)	0.63 (0.04, 4.12)	0.31 (0.04, 1.46)	0.17 (0.03, 1.00)	0.05 (0.03, 0.09)	0.05 (0.02, 0.17)	0.27 (0.03, 1.48)	0.12 (0.03, 0.52)
Frontal Sup R		0.04 (0.02, 0.09)	0.12 (0.03, 0.60)	0.04 (0.02, 0.11)	0.03 (0.02, 0.05)	0.03 (0.02, 0.06)	0.17 (0.03, 1.21)	0.04 (0.03, 0.08)	0.02 (0.02, 0.04)	0.11 (0.03, 0.88)	0.08 (0.03, 0.21)
Frontal Mid L			0.00	0.05 (0.02, 0.18)	0.02 (0.02, 0.03)	0.47 (0.04, 3.02)	0.46 (0.02, 4.57)	0.03 (0.02, 0.04)	0.02 (0.02, 0.04)	0.05 (0.03, 0.07)	0.08 (0.03, 0.14)
Frontal Mid R				0.03 (0.02, 0.04)	0.14 (0.03, 1.29)	0.04 (0.02, 0.11)	0.06 (0.03, 0.07)	0.03 (0.02, 0.06)	0.03 (0.02, 0.04)	0.02 (0.02, 0.03)	0.04 (0.03, 0.05)
Frontal Sup Medial L					0.00	0.57 (0.03, 3.39)	0.04 (0.02, 0.10)	0.13 (0.04, 0.37)	0.04 (0.02, 0.07)	1.15 (0.04, 9.98)	0.00
Frontal Sup Medial R						0.00	0.02 (0.02, 0.03)	0.20 (0.03, 1.24)	0.23 (0.02, 2.15)	0.09 (0.04, 0.28)	0.06 (0.03, 0.10)
Frontal Med Orb L							0.71 (0.03, 7.23)	0.02 (0.02, 0.03)	0.10 (0.03, 0.41)	0.02 (0.02, 0.03)	0.00
Frontal Med Orb R								0.03 (0.02, 0.05)	0.05 (0.02, 0.15)	0.06 (0.03, 0.22)	0.21 (0.03, 0.77)
Rectus L									0.05 (0.03, 0.10)	0.08 (0.04, 0.13)	0.02 (0.02, 0.03)
Rectus R										0.05 (0.03, 0.09)	0.25 (0.03, 2.00)
Cingulum Ant L											0.07 (0.03, 0.11)

Table 2.11: Positive emotion data of Frontal Region Matrix from the Proposed Sparse Method

Although the overall dataset showed very few co-activtions within the temporal region, the positive emotion data found 10 strong signals of co-activation, as shown in Tables 2.13 and 2.12.

	Temporal_Sup.R	Temporal_Pole_Sup.L	Temporal_Pole_Sup.R	Temporal_Mid.L	Temporal_Mid.R	Temporal_Pole_Mid.L	Temporal_Pole_Mid.R	Temporal_Inf.L	Temporal_Inf.R	Fusiform.L	Fusiform.R	Hippocampus.L	Hippocampus.R	ParaHippocampal.L	ParaHippocampal.R
Temporal_Sup.L	0.00	0.47 (0.03, 2.18)	0.02 (0.02, 0.03)	0.14 (0.04, 0.44)	0.03 (0.02, 0.05)	0.04 (0.02, 0.07)	1.21 (0.02, 9.82)	0.09 (0.02, 0.50)	0.05 (0.03, 0.11)	0.52 (0.05, 1.86)	0.04 (0.03, 0.06)	0.03 (0.02, 0.07)	0.03 (0.02, 0.04)	0.05 (0.03, 0.09)	0.04 (0.02, 0.08)
Temporal_Sup.R		0.16 (0.03, 0.93)	0.07 (0.03, 0.20)	0.05 (0.03, 0.08)	0.06 (0.03, 0.12)	0.02 (0.02, 0.03)	0.02 (0.02, 0.04)	0.07 (0.03, 0.16)	0.06 (0.03, 0.15)	0.15 (0.02, 1.01)	0.05 (0.02, 0.07)	0.02 (0.01, 0.03)	0.02 (0.02, 0.03)	0.05 (0.02, 0.19)	0.07 (0.03, 4.69)
Temporal_Pole_Sup.L			0.40 (0.06, 1.56)	0.00	0.19 (0.06, 0.89)	0.04 (0.02, 0.06)	0.07 (0.03, 0.20)	0.00	0.02 (0.02, 0.03)	3.69 (0.04, 30.43)	0.00	0.06 (0.04, 0.08)	0.10 (0.03, 0.29)	1.55 (0.02, 9.10)	0.09 (0.02, 0.56)
Temporal_Pole_Sup.R				0.03 (0.02, 0.05)	0.87 (0.06, 4.77)	0.05 (0.03, 0.08)	0.05 (0.02, 0.10)	0.03 (0.02, 0.05)	0.03 (0.02, 0.06)	0.04 (0.03, 0.08)	0.11 (0.03, 0.82)	0.04 (0.02, 0.15)	0.04 (0.02, 0.07)	0.02 (0.01, 0.03)	0.04 (0.03, 0.07)
Temporal_Mid.L					0.09 (0.03, 0.29)	0.02 (0.02, 0.03)	0.03 (0.01, 0.04)	0.06 (0.03, 0.14)	0.00	0.04 (0.03, 0.06)	0.05 (0.03, 0.09)	0.02 (0.01, 0.03)	0.04 (0.03, 0.08)	0.65 (0.03, 4.41)	0.04 (0.02, 0.07)
Temporal_Mid_R						0.03 (0.02, 0.05)	0.07 (0.03, 0.16)	0.06 (0.03, 0.12)	0.34 (0.03, 1.52)	0.95 (0.03, 6.02)	1.67 (0.05, 8.15)	0.06 (0.02, 0.16)	0.05 (0.03, 0.09)	0.06 (0.04, 0.08)	0.06 (0.02, 0.25)
Temporal_Pole_Mid.L							0.00	0.08 (0.02, 0.42)	0.02 (0.02, 0.03)	0.07 (0.03, 0.20)	0.04 (0.03, 0.07)	0.02 (0.02, 0.03)	0.03 (0.02, 0.04)	0.02 (0.02, 0.04)	0.03 (0.02, 0.06)
Temporal_Pole_Mid_R							0.06 (0.02, 0.21)	0.02 (0.02, 0.03)	0.05 (0.03, 0.11)	0.03 (0.02, 0.05)	0.02 (0.02, 0.03)	0.03 (0.02, 0.04)	0.02 (0.02, 0.03)	0.04 (0.02, 0.07)
Temporal_Inf.L								0.04 (0.03, 0.07)	0.04 (0.02, 0.06)	0.06 (0.03, 0.12)	0.02 (0.01, 0.04)	0.04 (0.02, 0.07)	0.03 (0.02, 0.06)	0.05 (0.02, 0.15)	
Temporal_Inf_R									0.03 (0.02, 0.04)	0.03 (0.02, 0.04)	0.06 (0.02, 0.23)	0.00	0.03 (0.02, 0.07)	0.69 (0.03, 6.78)	
Fusiform.L										0.00	0.02 (0.01, 0.03)	0.17 (0.02, 1.16)	0.00	0.03 (0.02, 0.05)	
Fusiform_R											0.03 (0.02, 0.04)	0.29 (0.02, 1.68)	0.43 (0.03, 3.75)	0.02 (0.02, 0.03)	
Hippocampus.L												0.00	0.18 (0.03, 1.47)	0.05 (0.02, 0.09)	
Hippocampus.R													0.10 (0.03, 0.42)	0.44 (0.03, 2.26)	
ParaHippocampal.L														0.03 (0.02, 0.06)	

Table 2.12: Positive emotion data of Temporal Region Matrix from the Proposed Sparse Method

2.5 Discussion

In this paper, we present a Bayesian Poisson-Gamma graphical model, to specify the probability of observing zero foci in a region. These novel coordinate-based neuroimaging meta-analysis approaches allow us to determine functional co-activation between regions in the brain and infer functional dependencies. We see the successful

	Temporal_Sup_R	Temporal_Pole_Sup_L	Temporal_Pole_Sup_R	Temporal_Mid_L	Temporal_Mid_R	Temporal_Pole_Mid_L	Temporal_Pole_Mid_R	Temporal_Inf_L	Temporal_Inf_R	Fusiform_L	Fusiform_R	Hippocampus_L	Hippocampus_R	ParaHippocampal_L	ParaHippocampal_R
Temporal_Sup_L	0.00	0.06 (0.03, 0.12)	0.00	0.05 (0.03, 0.07)	0.00	0.04 (0.02, 0.08)	0.03 (0.02, 0.05)	0.05 (0.02, 0.19)	0.03 (0.02, 0.04)	0.04 (0.02, 0.09)	0.03 (0.02, 0.04)	0.04 (0.02, 0.11)	0.02 (0.02, 0.03)	0.04 (0.02, 0.12)	0.03 (0.02, 0.04)
Temporal_Sup_R		0.05 (0.03, 0.07)	0.05 (0.03, 0.08)	0.00	0.04 (0.03, 0.06)	0.00	0.00	0.02 (0.02, 0.03)	0.03 (0.02, 0.05)	0.08 (0.03, 0.21)	0.03 (0.02, 0.04)	0.04 (0.02, 0.08)	0.06 (0.03, 0.18)	0.02 (0.02, 0.03)	0.03 (0.02, 0.06)
Temporal_Pole_Sup_L			0.06 (0.04, 0.11)	0.04 (0.03, 0.07)	0.18 (0.03, 1.08)	0.19 (0.03, 0.98)	0.00	0.05 (0.03, 0.15)	0.08 (0.03, 0.23)	0.00	0.03 (0.02, 0.03)	0.04 (0.03, 0.07)	0.11 (0.02, 0.55)	0.04 (0.03, 0.06)	0.05 (0.03, 0.13)
Temporal_Pole_Sup_R				0.00	0.00	0.03 (0.02, 0.03)	0.03 (0.03, 0.05)	0.02 (0.02, 0.02)	0.96 (0.03, 6.77)	0.05 (0.03, 0.10)	0.05 (0.03, 0.07)	0.03 (0.03, 0.04)	0.04 (0.02, 0.07)	0.02 (0.02, 0.03)	0.04 (0.03, 0.05)
Temporal_Mid_L					0.00	0.03 (0.02, 0.05)	0.00	0.04 (0.03, 0.06)	0.04 (0.03, 0.07)	0.05 (0.02, 0.09)	0.09 (0.03, 0.43)	0.25 (0.03, 1.69)	0.03 (0.02, 0.07)	0.02 (0.02, 0.03)	0.04 (0.02, 0.09)
Temporal_Mid_R						0.09 (0.03, 0.33)	0.04 (0.03, 0.05)	0.02 (0.02, 0.03)	0.04 (0.03, 0.06)	0.06 (0.03, 0.12)	0.07 (0.03, 0.16)	0.05 (0.02, 0.20)	0.00	0.02 (0.02, 0.03)	0.00
Temporal_Pole_Mid_L							0.00	0.03 (0.02, 0.04)	0.00	0.08 (0.02, 0.21)	0.33 (0.02, 2.23)	0.02 (0.02, 0.03)	0.02 (0.02, 0.03)	0.02 (0.02, 0.03)	0.03 (0.02, 0.05)
Temporal_Pole_Mid_R							0.06 (0.03, 0.18)		0.00	0.05 (0.02, 0.10)	0.06 (0.03, 0.12)	0.04 (0.03, 0.06)	0.13 (0.02, 0.86)	0.03 (0.03, 0.05)	0.02 (0.02, 0.03)
Temporal_Inf_L									0.03 (0.02, 0.04)	0.03 (0.02, 0.05)	0.02 (0.02, 0.03)	0.02 (0.02, 0.02)	0.02 (0.02, 0.03)	0.05 (0.03, 0.10)	0.08 (0.03, 0.31)
Temporal_Inf_R										0.02 (0.02, 0.03)	0.02 (0.02, 0.03)	0.02 (0.02, 0.03)	0.02 (0.02, 0.03)	0.02 (0.01, 0.02)	0.03 (0.02, 0.04)
Fusiform_L											0.00	0.06 (0.03, 0.10)	0.04 (0.02, 0.07)	0.09 (0.03, 0.45)	0.06 (0.03, 0.14)
Fusiform_R												0.06 (0.04, 0.08)	0.24 (0.03, 1.80)	0.03 (0.02, 0.05)	0.03 (0.03, 0.04)
Hippocampus_L													0.00	0.21 (0.02, 1.34)	0.00
Hippocampus_R														0.00	0.04 (0.03, 0.14)
ParaHippocampal_L															0.00

Table 2.13: Negative emotion data of Temporal Region Matrix from the Proposed Sparse Method

application of these approaches to neuroimaging meta-analysis datasets in the Section 2.4. We demonstrate the ability of our proposed sparse method estimates by comparing measures such as the average MSE, sensitivity, specificity, and false discovery rate.

From the simulation study, we observed that our proposed method increases in accuracy as the sample size increases and that the resulting network is impacted by the sparsity of the data as well as the co-activation threshold used for the posterior probability. The simulation studies used to produce those results showcase the utility of the method to identify co-activation patterns. Our approaches addresses sparsity and contributes inference about co-activation in the brain compared to previous models.

Within the data analysis we found the positive emotion generally created stronger signals and differences in the estimated co-activation. Previous work has explored various hypotheses and stimuli as it relates to emotion. Lindquist et al. (2015) concluded that positive and negative emotions are supported by a flexible and interchanging set of brain regions. Overwhelmingly the results found the temporal and frontal lobes most active (Liu et al., 2011; Lindquist et al., 2015). Although, they (Lindquist et al., 2015) did not find unique activation to represent positive and negative emotion, they

agreed it is possible to find differences in the co-activation of positive and negative emotions Bartra et al. (2013); Liu et al. (2011). The interpretation of such results only lend itself to relative preference for one emotion over the other, not independent brain function.

It is important to note, that meta-analysis data includes multiple studies which may have differing procedures. Some effects of these differing procedure may influence the estimated results. The results are also limited by the data resolution of the original study.

An extension to our model could include exploring p-way interactions between regions. In addition, random effects could be used to better model study-level clustering and study modality. Also, to improve the model a set of weights could be applied to each study based on it's sample size, significance threshold used, and whether adjustments were made for multiple comparisons. Kang et al. (2011) mentions including the probability of a negative study not being published to the model. Future work could account for publication bias of the data used on our model. The proposed Sparse PG approach to meta-analysis data helps to extend the reach of current methods by including measures of inference within the framework.

Chapter 3

Estimation of United States (US) Influenza-Associated Mortality Model

This chapter is joint work with Dr. Howard Chang, Dr. Michael Haber and Dr. Danielle Iuliano.

3.1 Introduction

Influenza is a highly contagious viral infection affecting populations worldwide. It is one of the most common transmissible infectious diseases of the respiratory tract. Influenza illness is primarily caused by either influenza A or influenza B viruses (Blahd, 2015). Influenza A viruses can be more specifically labeled by the two proteins on the surface of the virus: hemagglutinin (H) and neuraminidase (N) (Centers for Disease Control and Prevention, National Center for Immunization and Respiratory Diseases (NCIRD), 2016). The A virus infects humans and animals, while the B virus solely infects humans. The reaction to an Influenza B infection is generally less severe, and as a result most of the annual disease burden of influenza is attributed to Influenza A virus infections.

Influenza is spread person to person by respiratory droplets and formites (Cox et al., 2004). Genetic changes during the influenza virus replication causes what is known as an antigenic shift (Cox et al., 2004). This shift is the reason why new vaccines must be created each season to prevent the virus from causing a global pandemic (Morens and Fauci, 2007). Influenza A viruses are known to have a more drastic antigenic shift than the Influenza B virus.

Prior studies have demonstrated a significant benefit to vaccination, and the CDC recommends that everyone older than 6 months should receive the vaccine before each influenza season. The particular strains of influenza in circulation vary each year, necessitate the need to customize immunization to address the primary strains in circulation. The changing strains also open the door for pandemic spread of unanticipated strains, often with very high infection rates. Although the majority of infections

are mild, many subpopulations (e.g., older adults) can be at risk due to preexisting conditions or complications (Wu et al., 2012). Chronic illnesses can exacerbate an infection or result in increased susceptibility to fatal bacterial infections (Weinberger et al., 2012). Some influenza strains can lead to fatal complications, and are the cause of substantial morbidity and mortality worldwide (Wu et al., 2012).

3.1.1 Global Impact

Influenza is a major concern globally. The global impact of influenza is disconcerting. There are 3 to 5 million estimated severe cases (World Health Organization, 2004) and 291,243 to 645,832 estimated seasonal influenza-associated respiratory deaths annually (Iuliano et al., 2017). A study conducted by Lozano et al. (2013) similarly reports influenza is estimated to be responsible for 444,000 to 553,000 worldwide deaths annually. (There are many existing mortality estimation methods in the literature, thus producing many estimates of influenza-associated mortality.) The World Health Organization declared the first pandemic of the twenty-first century during the 2009 H1N1 influenza season (Gran et al., 2013).

The elderly are the most likely to be hospitalized or die from influenza illness. They account for up to 90% of influenza-related deaths per season (Nair et al., 2011). Deaths among the elderly and those chronically ill are a significant portion of the annual deaths associated with influenza, specifically those with chronic cardiopulmonary disease. Chronically-ill individuals include those with chronic heart or lung disease, asthma and HIV/AIDS (Nair et al., 2011). Among children less than five years of age, influenza is responsible for 28,000 to 111,500 deaths (Nair et al., 2011). Based on existing literature, seasonal epidemics affect 20 to 30% of children and 5 to 10% of adults (Kuster et al., 2011). World Health Organization (2012) recommends influenza vaccination for high risk groups such as pregnant women, children ages 6 to 59 months, elderly individuals, select chronically-ill individuals and health care

professionals. To alleviate some of the disease burden globally, influenza vaccination has been promoted and expanded in many countries. Countries are working toward a significant reduction in morbidity and mortality caused by the influenza illness.

While warmer regions of the world are affected by influenza throughout the year suggesting climatic influences in disease dynamics, temperate countries, like the United States, typically anticipate flu season once a year during the winter months (Moura, 2010).

3.1.2 USA Impact

Each year, influenza is estimated to be responsible for 36,000 deaths, 225,000 hospitalization and $87 billion in health care costs in the United States, according to the Centers for Disease Control and Prevention (CDC) (Thompson et al., 2003, 2004). In 2009, President Barack Obama declared a national emergency in the USA as a result of the 2009 H1N1 pandemic. The outbreak was declared a pandemic due to its rapid increase in incidence and the limited availability of healthcare resources (Larson and Heymann, 2010). The availability of appropriate vaccinations could have limited the number of people infected. Kostova et al. (2013) in their study of influenza and hospitalizations averted in the United States found that vaccination averted 5 million influenza infections and 40,400 hospitalizations during the 2010-2011 influenza season.

The measure of disease burden is based on a proxy for influenza incidence because it is impossible to test an entire population for infection. The incidence proxy is often defined as the proportion of positive specimens for the influenza isolate of interest of patients seeking treatment for influenza-like-illness (ILI). While the number of individuals experiencing ILI represents the sick population who get specimens tested, the positive result of a specimen test indicates ILI that are indeed influenza-related.

3.1.3 Motivation

Estimates of influenza-associated death are important for policy makers to make informed decisions about resource allocation when challenged with public health demands and to expand our understanding of the impact of influenza on populations. Two simple approaches to estimate influenza-associated excess mortality include counting influenza-confirmed deaths and modeling the national mortality rate using the primary cause of death in conjunction with nationally representative influenza surveillance (Gran et al., 2013; Nicoll et al., 2012). Counting laboratory-confirmed influenza deaths or ICD-coded influenza deaths may underestimate the true burden because testing for influenza is not always performed and most deaths are not coded as influenza due to lack of testing or diagnosis of another cause of death (Gran et al., 2013; Nicoll et al., 2012; Gran et al., 2010). Death may occur several weeks after infection, and by the time the patient develops severe complications, influenza virus may not be detectable, and not listed as a cause of death on records. For example, if a patient is tested for influenza and experiences a heart attack, their cause of death will most likely be attributed to cardiovascular causes. Using influenza surveillance data to calculate influenza deaths directly may also result in a biased sample because children, older adults, individuals with chronic conditions, or patients with severe symptoms are more likely to consult a health professional and to be tested for influenza than other population groups.

More recently, complex statistical models are increasingly being used to estimate influenza-associated excess mortality, where excess deaths are calculated as a proportion of the total number of deaths. Specifically, these models first estimate the temporal association between mortality and proxies for influenza activity (if available), adjusting for temporal trends or environmental variables (e.g. temperature, dew point, air pollution, or humidity), or through the use of splines (Goldstein et al., 2012; Cohen et al., 2017). Proxies of influenza activity include information from inpa-

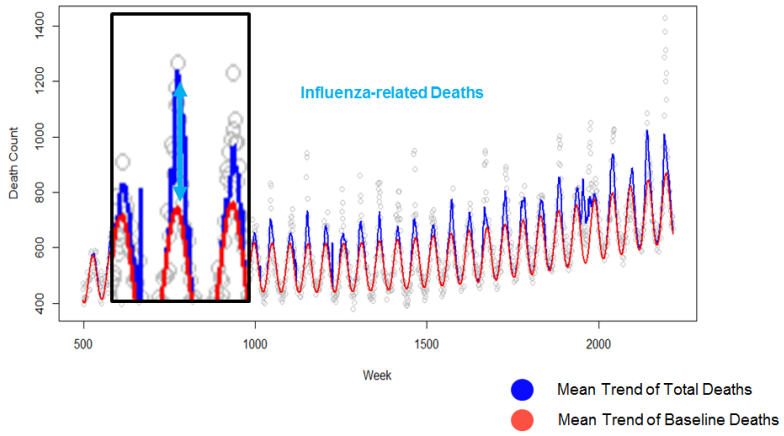

Figure 3.1: Influenza-related Mortality Calculation based on the mean trend of total deaths and mean trend of baseline deaths.

tient or outpatient influenza surveillance systems, which typically provide the number of specimens tested for influenza and the number that test positive for influenza virus types or subtypes (Goldstein et al., 2012). Influenza-associated excess mortality is calculated by taking the difference between the estimated total death count and a counterfactual baseline death count where influenza activity is assumed to be absent. A graphic representation can be found in Figure 3.1.

However, analyzing time-series count data presents two analytic challenges. First, mortality time-series exhibit temporal autocorrelation and models that do not account for autocorrelation may result in incorrect standard error estimation (biased downward) (Kim and Yeasmin, 2005; Schwartz, 1994). For example, the mortality at the current time point is influenced by mortality at previous time points. Second, overdispersion is common when death count data are modeled using Poisson log-linear models, assuming equal mean and variance. While different statistical models have been used to estimate the disease burden of influenza from time-series data, only a few modeling techniques account for both autocorrelation and overdispersion. Methods used to account for overdispersion include quasi-Poisson (Gran et al., 2013) and negative binomial models (Feng et al., 2012). To account for autocorrelation in the data, autoregressive integrated moving average models (Thompson et al., 2009;

Stroup et al., 1988) and bootstrapping methods have been used (Goldstein et al., 2012).

Using United States (U.S.) weekly respiratory vital records mortality data from 1981 to 2014 as a case study, our objective was to evaluate two approaches for jointly addressing autocorrelation and overdispersion. First, we extended a parametric bootstrap approach developed for a linear regression model (Goldstein et al., 2012) to a negative binomial model to account for overdispersion and autocorrelation in the residuals. Second, we considered a Poisson random intercept model with autoregressive random effects in the mean structure to account for overdispersion. Finally, we compared the first two approaches with simple methods for calculating influenza-associated excess deaths and conducted a simulation study.

3.2 Methodology

3.2.1 History of Influenza Mortality Models and Current Methods

There are many models that have been used to estimate influenza-associated mortality. Statistical modeling has been used to assess the disease burden of influenza for the last few decades (Gran et al., 2013). Some use viral surveillance data , while others use no surveillance data at all. Generally, each model uses some variation of information to determine a baseline number of deaths that would occur in the absence of influenza.

The Serfling model is a linear regression model technique used when viral surveillance data is not available (Serfling, 1963; Simonsen, Clarke, Williamson, Stroup, Arden and Schonberger, 1997; Simonsen et al., 2005). The model uses the mortality rate as the outcome and cyclic and harmonic terms as the covariates (Muscatello et al., 2008). Simonsen, Clarke, Williamson, Stroup, Arden and Schonberger (1997)

suggestd that five years of baseline data are required for accuracy of the model. This method is said to be appropriate for temperate countries and in modeling influenza epidemics and pandemics (Serfling, 1963; Simonsen, Clarke, Williamson, Stroup, Arden and Schonberger, 1997; Simonsen et al., 2005; Thompson et al., 2006). A limitation of this model is its assumption of the seasonal pattern of non-influenza mortality being the same each year (Muscatello et al., 2008).

Goldstein et al. (2012) introduced a variation of the Serfling model. The method involved bootstrapping a linear regression model of death counts data with viral surveillance included as predictors. The bootstrap method, introduced by Goldstein et al. (2012), can be divided into two parts. The first bootstrap is used to estimate the bias-corrected auto regressive parameter (Kim and Yeasmin, 2005). Without adjusting for the autoregressive (AR) structure of the model residuals, the estimate is found to be biased downward (Kim and Yeasmin, 2005; Schwartz, 1994). Once the model is setup and fit, the best autoregressive structure can be determined and we let ρ represent the correlation between the residuals at the selected AR structure. For example, if an AR(1) structure is assumed $\hat{\rho}$ is the correlation between th residual at the time point t and time point $t-1$. The bias of the autoregressive parameter is estimated via bootstrap by defining the difference between the residual at time t and the product of ρ and the residual at time point $t-1$. The second bootstrap is used to correctly estimate the regression parameters(Kim and Yeasmin, 2005). In this step, similar procedures are followed as the aforementioned bootstrap, but replacing the estimate of ρ with the bias-corrected ρ value. (To date the bootstrapping approach has been restricted to linear regression models.)

In order to determine the autoregressive structure of the bootstrap models's residuals, the partial autocorrelation coefficient function (PACF) is used. The PACF is a measure of conditional correlation between the residuals at each time point. An AR(1) structure of the model residuals means the current residual is function of the

previous time point. Similarly, an AR(2) structure for the model residuals translates to the correlation between the current residual and the residuals at two time points back given the knowledge of the time point one time point back.

Similar to the Serfling model, generalized additive models (GAM) is also a linear model with mortality rate as the outcome. The linear model can be represented as a sum of smoothed functions of covariates. An advantage of smoothing functions is the ability to examine non-linear effects of a covariate and to control for confounders flexibly. Muscatello et al. (2013) employed a semi-parameteric GAM to replace seasonal harmonic terms with a smoothing spline of time. This model was able to improve model fit up to 20% compared to the Serfling model (Muscatello et al., 2013). Estimates of influenza-related mortality have also been obtained using a Bayesian approach (Foppa et al., 2015).

Most recent literature includes Poisson and negative binomial regression models for influenza-associated death counts. These count regression model utilizes viral surveillance data by influenza type and subtype, adjusting for temporal trends and environmental variables (Goldstein et al., 2012) to estimate influenza mortality contribution. This model is said to not be particularly useful for pandemics, but does have the benefit of adjusting the model for RSV (respiratory syncytical virus) circulation for temperate countries during epidemics (Thompson et al., 2003, 2006).

Current modeling techniques can estimate the mortality due to influenza, but are limited by questionable methodological assumptions and data uncertainty (Goldstein et al., 2012). Thus, in response to these knowledge gaps, we propose research to evaluate the uncertainty around estimates of influenza-associated excess mortality specific to a country. We propose to employ both a hierarchical Bayesian framework and bootstrap methods to estimate influenza-related excess mortality and its precision for each influenza season.

3.2.2 US National Mortality, Population, and Influenza Surveillance Data

We obtained the weekly count of respiratory coded deaths for the U.S. population during the period 19812014 for three age groups (<65, 65-74, ≥75 years) from the National Center for Health Statistics. Each death in the U.S. is registered in the National Vital Statistics System and is systematically coded using the International Classification of Diseases, Ninth Revision (ICD-9) or International Classification of Diseases, Tenth Revision (ICD-10) codes. For this analysis, we used respiratory deaths that were coded from 460 to 519.9 in ICD-9 and from J00 to J99 in ICD-10. Weekly U.S. population count for each age group was defined as the mid-year estimate from the Census Bureau International Database. National influenza virus surveillance data were obtained from the U.S. Centers for Disease Control and Prevention (CDC). The weekly influenza percent positive was calculated as the number of specimens testing positive in a given week divided by the total number tested in the same week and was used as proxies for influenza activity. Each influenza proxy is lagged by one week to account for the time lapsed between infection and detection. These proxies included the weekly percent positive for influenza virus A(H1N1), influenza A(H1N1)pdm09, influenza A(H3N2), and influenza B. The dominant circulating strain each season is defined as the subtype with the largest proportion of positive specimens (Figure B.3).

3.2.3 Time-Series Model for Estimating Influenza-Associated Deaths

We first describe the time-series model for estimating influenza-associated mortality (Gran et al., 2013; Goldstein et al., 2012; Thompson et al., 2009; Muscatello et al., 2013) which was compared to models that account for overdispersion and autocorrelation. In this model, let Y_t denote the total respiratory mortality for a specific age

group for week $t = 1, \ldots, T$. The negative binomial log-linear model for the expected number of total respiratory deaths $E(Y_t)$ is given by:

$$\begin{aligned} logE(Y_t) =& log\alpha_t + \beta_0 + g(t) + \beta_1 sin(\frac{2\pi t}{52.179}) + \beta_2 cos(\frac{2\pi t}{52.179}) + \\ & \beta_3 H1N1_t + \beta_4 H3N2_t + \beta_5 H1N1pdm09_t + \beta_6 B_t \end{aligned} \tag{3.1}$$

where the model includes

- the at-risk population size α_t as an offset,
- a weekly long-term temporal trend $g(t)$ (e.g. polynomial functions),
- a seasonal trend (here specified as cyclical harmonics with a period of 52.179 weeks), and
- influenza subtype percent positive ($H1N1_t$, $H3N2_t$, $H1N1pdm09_t$, B_t).

Specific model specifications for US data are given in the Application to the Subsection 3.2.6 of US Mortality Data.

Week-specific influenza-associated excess deaths were estimated by taking the difference between (1) expected respiratory deaths ($\hat{Y}_t$) based on the observed covariate values and estimated regression coefficients and (2) expected baseline deaths ($\hat{Y}_{base,t}$). Baseline mortality was determined by removing the impact of the influenza subtype variables in the model by setting the values of influenza proxies to zero. Week-specific deaths were summed to calculate estimates for each influenza season. Standard errors were derived from the variance-covariance matrix of the regression coefficients using the Delta method.

3.2.4 Accounting for Temporal Correlation Using Residuals

The first method we examined to account for temporal autocorrelation incorporates the autocorrelation of the residuals using a parametric bootstrap (Efron and

Tibshirani, 1994). Temporal autocorrelation in the residuals refers to the correlation between the residuals at adjacent points in time (e.g., correlation dependence between estimates from the previous week(s) to the current). We extended the method described previously by Goldstein et al. (2012) for a Normal distributed outcome to generalized linear models for better handling count outcomes (e.g. using Poisson or negative binomial distributions).

Specifically, we let e_t denote the Pearsons standardized residual at time t defined as $\frac{(Y_t - \hat{Y}_t)}{\sqrt{Var(\hat{Y})}}$. We assumed that e_t follows an autoregressive (AR) structure where the residual at each week is dependent on previous weeks residuals. Standardized residuals were used to better reflect the normality assumptions imposed on $e_t$in the AR model. The AR model of the Kth-order, denoted as AR-K, is given by $e_t = \sum_{k=1}^{K} \rho_k e_{t-k} + u_t$, where ρ_k is the autoregressive parameter associated with the residual at week lag k, and u_t is a time-series of independent Normal variable $u_t \sim N(0, \sigma^2)$. To determine the order of the AR model, k, the partial autocorrelation function (PACF) can be used to determine the conditional correlation between the current and a specified time point conditional on the time points between.

After the initial model estimation using Equation 3.1, the parametric bootstrap procedure was conducted in two stages. The first stage of the bootstrap procedure was used to estimate the autoregressive parameter because bias in regression coefficient estimates may be present when fitting the initial model while incorrectly assuming temporal independence, ignoring the present dependence (Kim and Yeasmin, 2005; Schwartz, 1994).

We describe the parametric bootstrap procedure for the AR-1 residual structure, and the procedure extends similarly to different AR orders. In the first stage, an AR parameter estimate $\hat{\rho}$ is obtained based on standardized residuals, e_t, from the initial model fit. Then for each week t, define $u_t = e_t - \hat{\rho} e_{t-1}$ (the error terms of the autoregressive model). For each bootstrap iteration i, we obtained a sample of

$u_t^{(i)}$ equal to the total number of weeks in the time-series dataset by resampling with replacement of the collection of u_t, and calculated the correlated residuals $e_t^{(i)} = \hat{\rho} e_{t-1}^{(i)} + u_t^{(i)}$. Bootstrap total death count outcomes were calculated as $Y_t^{(i)} = \hat{Y}_t + \tilde{e}_t^{(i)}$ where $\tilde{e}_t^{(i)}$ is the back-transformed raw residual $(Y_t - \hat{Y}_t)$ from the resampled standardized residual. A new set of standardized residuals and AR parameter $\hat{\rho}^{(i)}$ was obtained by regressing $Y_t^{(i)}$ on the full set of covariates using Equation 3.1. The above step was repeated 10,000 times to obtain a bootstrap estimate ρ_{boot} defined as $\hat{\rho}_{boot} = 2\hat{\rho} - \bar{\rho}$, where $\bar{\rho}$ is the mean of $\hat{\rho}^{(i)}$ across bootstrap iterations.

The second stage of the bootstrap procedure was used to estimate the regression coefficient parameters and their variance-covariance accounting for residual temporal correlation using the estimated AR coefficient from Stage 1. In the second stage of the bootstrap process, we used the same approach as in Stage 1 to calculate u_t, $u_t^{(i)}$, $e_t^{(i)}$, and $Y_t^{(i)}$, however, one difference was that the bootstrap AR parameter ρ_{boot} was used instead of $\hat{\rho}$. For each bootstrap iteration, we regressed $Y_t^{(i)}$ on the full set of covariates and used the resulting regression coefficients to calculate season-specific influenza-associated excess deaths, with the 95% confidence interval defined as the 2.5 and 97.5 percentiles of the bootstrap samples. Detailed step-by-step algorithms for the AR-1 residual structure is provided in Appendix B.

3.2.5 Accounting for the Temporal Correlation Using the Mean

We also considered a second model-based approach that allows for temporal correlations directly in the mean structure using a random intercept model. In this approach, we extended the mean structure defined in Equation 3.1 through the addition of a random intercept at each time point, θ_t, and assumed a Poisson distribution of the outcome. Preliminary analyses using a negative binomial model with random intercepts indicated that the additional overdispersion is negligible. Therefore, to ac-

count for temporal correlation in the mean using a random intercept model, a Poisson model was chosen over a negative binomial model. We assumed that θ_t follows an AR structure similarly to the method described when accounting for the temporal autocorrelation using the residual. The random intercept can be interpreted as the baseline log relative risk associated with weekly mortality counts not explained by influenza activity and other covariates. Estimation was accomplished under a Bayesian framework to account for the estimation uncertainty of random effects. The regression model parameters (βs), and the initial random effect ($t = 1$) were assumed to have flat Normal priors with mean zero and variance $1x10^4$. The AR parameter(s) were assumed to have a uniform distribution between -1 and 1, while the variance parameter σ^2 was assumed to have a non-informative inverse Gamma distribution (shape=0.1, scale=10).

3.2.6 Application to US Mortality Data

We applied the two approaches to account for temporal autocorrelation in the analysis of weekly U.S. mortality data. Influenza season was defined as beginning at the 27th week of each year for the US (approximately July 1 to June 30), using the Sunday-Saturday designation of a week. A negative binomial distribution was assumed for Y_t to address overdispersion (Foppa et al., 2015). Influenza viral terms were lagged by one week to account for delay between influenza infection and death. Models were fit separately for each age group and up to a 4th power polynomial was used to account for weekly long-term temporal trends, $g(t)$, over the 33-year study period. For all methods accounting for autocorrelation, both AR-1 and AR-2 correlation structures were examined. The estimated seasonal values of influenza-associated mortality and the 95% confidence/credible intervals were truncated at zero if the estimated value was less than zero (Thompson et al., 2009; Hardelid et al., 2013).

In addition to the proposed methods, we also investigated two simple methods to obtain influenza-associated mortality estimates and standard error for comparison: the Delta method (Severini, 2005) and the Newey-West Delta method (Newey and West, 2017). The Delta method is a technique for approximating moments of functions of random variables assuming the function of interest is continuously differentiable and asymptotically Normal. The Delta method does not account for temporal autocorrelation, but does account for overdispersion when negative binomial regression is used. By asymptotic theory and the conditions of the Delta method, we know that the negative binomial regression used to approximate influenza-associated mortality can be approximated by the Delta method. The Newey-West Delta approach is an alternative procedure to compute sandwich robust standard errors for time-series data in the presence of heteroscedasticity and residual autocorrelation of a known lag. Once autocorrelation is determined to be in the residual structure of the regression model, ignoring this would be incorrect and often biased downward.

We also conducted simulation studies in which the true influenza-associated mortality was assumed known to compare the accuracy and precision of various methods. Weekly mortality data for ages $\geq$75 years were simulated using regression coefficients (i.e. time trends and viral activities) from the Poisson model with temporal autocorrelated random intercepts. We examined two simulation scenarios that differed by how the random intercepts were generated. The first scenario generated random intercepts using estimated parameters from the AR structure. Specifically, a time-series of θ_t was generated based on the posterior mean of the autoregressive parameter ρ_k and the variance σ^2. The second simulation scenario generated data using the posterior means of the estimated random intercepts. Hence, the first scenario assumed the auto-correlated random intercepts are independent of the other temporal covariates in the model. In the second scenario, random intercepts may reflect residual temporal trends not accounted by other covariates.

Ten simulated datasets were generated for each scenario. The simulated data were modeled using the four analytical strategies under consideration (Delta, Newey-West Delta, autocorrelation within the residuals, autocorrelation within the mean). Estimates across simulated datasets were summarized by the mean of influenza-associated mortality and 95% confidence/credible interval.

All analysis was performed with R software, version 3.2.1 (R Core Team, 2017). Bayesian estimation was accomplished using the Markov Chain Monte Carlo (MCMC) technique performed with JAGS (Plummer, 2012). Five thousand posterior samples were used for inference from a total sample of 20,000 MCMC iterations, after a burn-in of 5,000 iterations. JAGS code is available in Appendix B.

3.3 Results

Overall, the annual percent positive for all influenza subtypes when specimens are tested ranged from 426%. Of the 33 observed influenza seasons, Influenza A(H3N2) was the dominant circulating strain for 17 seasons, Influenza B for 9 seasons, Influenza A(H1N1) for 4 seasons and A(H1N1)pdm09 for 3 seasons. A summary of the specimens testing positive for influenza viruses and the predominant circulating subtype is included in Appendix B Figures B.3, B.2, and B.3. From 1981 to 2014, the annual rate of respiratory deaths for all ages for the total population ranged from 60.6 to 98.7 per 100,000.

Estimates of parameters governing the temporal autocorrelation in weekly deaths are summarized in Figure B.1. For example, ρ_1 or ρ_2 value can be interpreted as the correlation of the respiratory deaths lagged by 1 or 2 weeks, respectively. All three age groups demonstrated temporal autocorrelation in the mean or in the residual, with stronger correlation observed when autocorrelation was modeled via the mean. In AR-2 models, the lag-2 autocorrelation is considerably weaker than the lag-1. The

two youngest age groups were determined to have an AR-1 structure given that the 95% credible intervals of ρ_2 included zeros when autocorrelation was modeled in the means. A graphical display of the autocorrelation relationship can be found in Figure B.4.

Overall, we found that accounting for temporal correlation in the residuals gave regression coefficient estimates similar to those obtained from the Newey-West and the Delta methods (see Figure B.2). We expect the Delta and Newey-West Delta methods to have the same point influenza-associated mortality estimates because these two methods do not influence the estimation of regression coefficients. However, the Newey-West method resulted in large increases in standard errors, as shown in Figure B.2 (sometimes more than 50% as in the 0-65 age group). Accounting for temporal correlation in the means gave smaller regression coefficient estimates compared to the other methods, except for the A(H1N1)pdm09 estimate among those aged 75 or greater. Standard errors were also larger when the autocorrelation was modeled in the means versus the residuals. The choice of AR-1 versus AR-2 autocorrelation structure did not have a large impact on coefficient estimates or their standard errors. Regression coefficients for the influenza subtypes estimated from different methods are summarized in Figure B.2.

For brevity, Figure B.1 shows estimated influenza-associated respiratory mortality for seasons 2003 to 2014 for each age group estimated using different methods. As determined by the estimated autocorrelation parameters in Figure B.1, we present estimates from an AR-1 model whenever the confidence or posterior interval of theρ_2 parameter includes zero. The AR-1 structure is presented for the Newey-West Delta method because lag-1 is significant for all age groups. Accounting for temporal autocorrelation in the mean gave influenza-associated mortality estimates that are consistently smaller, compared to methods that account for temporal autocorrelation in the residual methods, including the Delta and Newey-West Delta methods. The

Figure 3.2: Influenza-associated Excess Mortality for each age group by season, 2003-2014

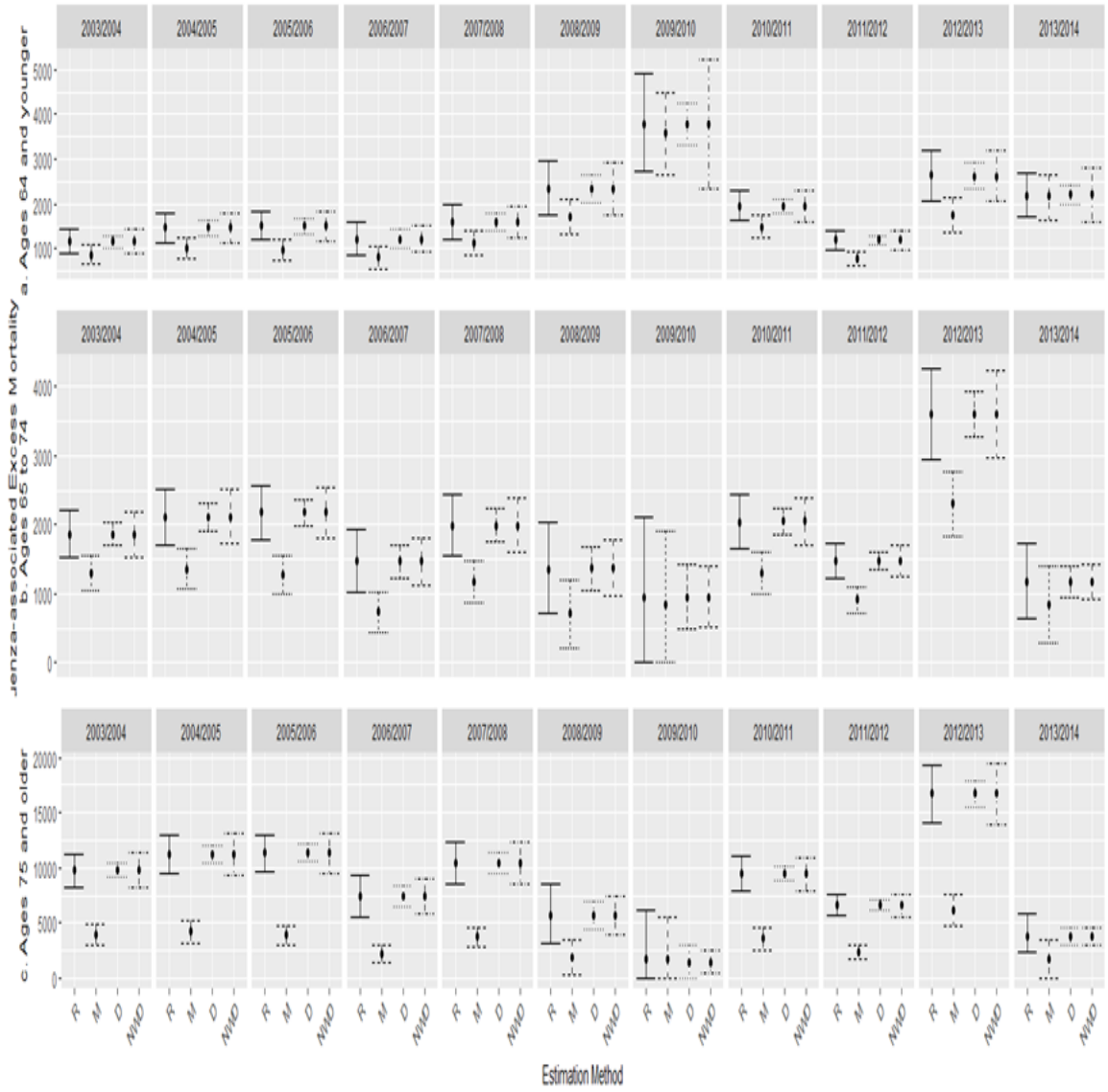

most significant difference between methods occurred within the oldest age group ($\geq$ 75 years). Differences in interval length closely follow the standard error associated with the estimated regression coefficients in Figure B.2. For example, for <65 year age group, the smallest confidence interval was associated with the Delta method, while the largest interval was produced by the Newey-West Delta method (with the exception of season 2006/2007). For 6574 year age group, the smallest confidence interval was typically produced by the Delta method, while none of the other methods consistently produced the largest interval. Our analyses also highlighted the increase in deaths during the 2009/2010 season among the youngest age group because of the emergence of the A(H1N1)pdm09 virus. The 2012/2013 season increase for the two oldest age groups is likely due to a mismatch in the vaccine, causing low vaccine effectiveness for those $\geq$ 65 years of age McLean et al. (2014). Estimates and 95% confidence or credible intervals are provided in Appendix B FigureB.4.

Results from the simulation study for both scenarios are provided in Tables B.5 and B.6. When autocorrelated random intercepts were generated independently of other covariates, all four methods estimated season-specific influenza-associated mortality with minimal bias from the truth. However, the Newey-West method gave a large standard error, followed by accounting for autocorrelation in the means, accounting for autocorrelation in the residuals, and the Delta method. However, when random intercepts were simulated based on the US data, methods that only account for autocorrelation in the residuals overestimated season-specific influenza-associated mortality. This implies that the use of random intercepts may capture additional temporal variability in mean mortality counts not accounted for by the long-term and seasonal trends. Hence, the exclusion of random intercepts may result in residual confounding for the influenza proxy coefficients.

3.4 Discussion

We proposed two approaches to estimate influenza-associated excess mortality using time-series analysis when temporal autocorrelation is present. The first approach specifies temporal correlation directly in the residuals; while the second approach induces temporal correlation by using time-dependent random intercepts in the mean structure. Both approaches account for overdispersion in the time-series count data. In our US respiratory mortality case study, we found that accounting for autocorrelation using either method resulted in larger uncertainty intervals compared to estimates that ignored autocorrelation.

The two simpler methods, Delta and Newey-West Delta, were less than optimal compared to our two proposed methods. The Delta method is not appropriate for weekly time-series of deaths because it assumes autocorrelation does not exist in the residuals, which will results in smaller standard errors and incorrect quantification of uncertainty for the estimate of interest (Kim and Yeasmin, 2005; Schwartz, 1994). The Newey-West Delta method also accounts for autocorrelation in residuals and is computationally faster. However, it requires the specification of a maximum lag for the autocorrelation structure that determines the weighting scheme (Newey and West, 2017). Other weighting schemes exist (Andrews, 1991; Lumley and Heagerty, 1999) and their finite sample behaviors may warrant further investigations.

Overall, smaller mortality estimates were associated with models that account for autocorrelation in the mean using random effects. We note that the means from these two approaches should be interpreted differently: a marginal interpretation (over all weeks) for the residual approach versus a conditional interpretation for the random effect model. However, in the simulation study, we found that when autocorrelated random intercepts were generated independently of other covariates, the influenza-associated excess mortality estimates were comparable (Appendix B Table B.5). Hence, the smaller excess death estimates associated with the random effect

model may be due to better control for temporal residual confounding of the viral proxy associations. The resulting influenza-associated mortality estimates increase and decrease similarly to seasonal estimates reported in Morbidity and Mortality Weekly Report (MMWR) (n.d.), while the mean method often provides a lower estimate.

Another difference between the two approaches is that the residual method enables researchers to specify the mean model and the variance model separately. This has the advantage of defining more complex variance structures as quasi-likelihood methods can be employed. However, this approach also assumes that the mean model is correctly defined. Alternatively, the use of random effects allows for a more flexible mean structure because the baseline mortality rate is allowed to vary across time points. However, this likelihood-based approach requires the specification of the random effect distribution. Another limitation is that the use of the flexible random effects may induce a bias towards the null for the influenza proxies, especially when these covariates are subject to measurement error (Reich et al., 2006).

While differences in the two approaches exist, both do not rely on large sample asymptotic and the computation time for each is similar. However, the random effect method may be more accessible due existing software for hierarchical models with dependence random effects (e.g. JAGS). The residual approach may be helpful when long-term temporal trends and unmeasured confounders are believed to be adequately accounted for in the model. While the random effect approach is more conservative and is recommended when the model lacks predictors dependent on long-term temporal trends. In practice, determining which method is most appropriate can be based on the confidence in the mean structure being correctly specified. Analyses may benefit from exploring both methods.

Our methods to account for autocorrelation do not account for other potential limitations associated with estimating influenza-associated excess mortality. To start,

our influenza-associated excess death results may be influenced by potential measurement errors in influenza activity data. Additionally, the likelihood that an influenza-infected person seeks medical care or is tested for influenza is small (Cauchemez et al., 2012). As a result, the sample of influenza proxy measures does not represent what is occurring in the population. Furthermore, prior to the 2008/2009 influenza season, the commonly used influenza detection tests were not as sensitive to the influenza virus as current laboratory testing methods. As a result, the percent positive over time may have increased to due to this change.

As more countries continue to leverage improvements in influenza virus surveillance with increasing availability of vital records data, time-series modeling may be used to estimate influenza-associated excess deaths or deaths due to any cause. A time-series modeling approach is likely to become more prevalent with increasing availability and quality of administrative databases and influenza surveillance systems. We describe several solutions to some of the challenges associated with these type of analyses. While US respiratory mortality served as the motivating case study, the modeling approaches could be widely applied in other settings. The overall recommendation is that methods that account for overdispersion and autocorrelation should be employed in estimating the influenza-associated health burden with time-series data.

Chapter 4

Addressing Long-term and Seasonal Trends in Influenza-Associated Mortality Model

This chapter is joint work with Dr. Howard Chang and Dr. Danielle Iuliano.

4.1 Introduction

Data sequentially recorded at regular time intervals is defined as time-series data. Time-series data are often collected in econometrics and biomedical research in order to answer critical questions. While the focus of the econometrics discipline is to forecast future changes in the time-series data (i.e. stock market prices), the focus of the biomedical analysis is largely to determine associations among time-series variables (Bhaskaran et al., 2013). Specifically, this chapter explores associations among week-to-week variation in influenza activity levels by subtype and respiratory mortality.

Influenza data is unique in that the incidence flucuates over time. Over the course of a year incidence will peak during influenza season and drop once the infectious period has ended (Lopman et al., 2004; Domínguez et al., 2007). The influenza proxies represent the exposure of the population. Because influenza activity varies by season, it can also be confounded by season. In other words, the relationship between respiratory mortality and influenza proxies may be confounded by factors on a similar timescale. See Figure 4.1 for graphical representation. In additon, influenza time-series data is not independent at each time point. Autocorrelation exists in the data. Long-term patterns and seasonality heavily influences our data. In our proposed analysis, we aim to control for the long-term and seasonal trend to explain the short-term associations.

There are many approaches to analyze influenza time-series data with a focus on removing the confounding. Common approaches can be categorized as regression models, time-series methods, non-influenza years approach, and non-influenza seasons of the same year approach (Jackson, 2009). Less common approaches, like ARIMAX (a combination of ARIMA and time-series for noninfluenza mortality pre-

Figure 4.1: Graphical representation of confounding

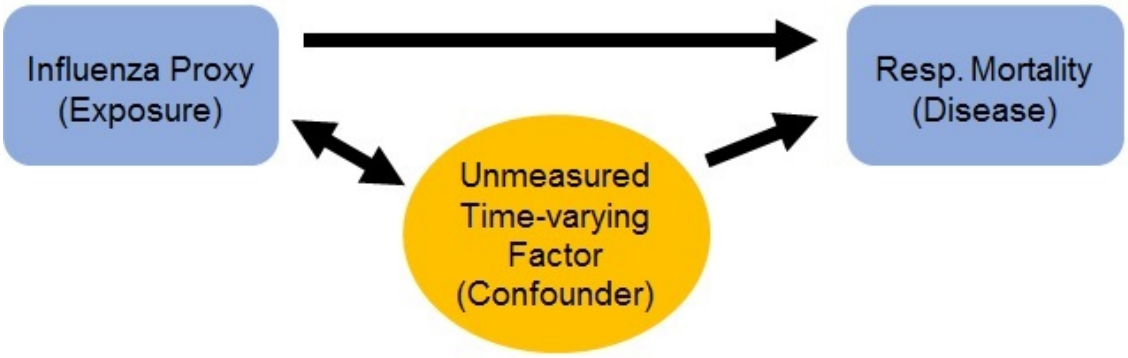

dictors), LOESS seasonal decomposition (separates time-series into trend, seasonal and remainder effect; the seasonal effect can be regression) (Partonen et al., 2004) and artificial neural networks (Guan et al., 2004), exist but will not be highlighted here.

Time-series regression analysis is not entirely different from general regression analysis although some key features of the data (autocorrelation and confounding) must be addressed in the analysis. To quantify short-term effects of environmental exposures (i.e. air pollution, pollen dust, or other weather variables) on health outcomes (i.e. mortality, myocardial infarction, or disease-specific hospitalization), many studies have employed time-series regression (Bhaskaran et al., 2013; Jiménez et al., 2010; Bhaskaran et al., 2010; Basu, 2009). It is an alternative to explain the short-term variation of an outcome, in our case respiratory deaths, as the exposure changes (i.e. influenza activity). The regression approach allows control over multiple potential confounding factors.

An often used regression method is the Serfling method, introduced by Robert Serfling as a way to model cyclic regression (Serfling, 1963; Izurieta et al., 2000; Simonsen, Clarke, Stroup, Williamson, Arden and Cox, 1997). The Serfling model uses only functions of time as explanatory variables for the time-series outcome. In

order to use the Serfling model, one must assume the amplitude of the mortality cycle is consistent across peaks and troughs. This means we assume winter maximums in mortality relative to the average mortality is equivalent to the summer minimums. In addition, we assume the seasonal confounder of the relationship between time and mortality has a consistent timescale and magnitude across seasons (Jackson, 2009). An advantage of this method is its use of changes in mortality during the fall and spring to inform estimates of non-influenza mortality. While this method requires little data compared to other methods, it does require several years worth of data for stable inference. A significant limitation of this approach is that all regression assumptions may not hold.

To address the confounding that may be present in the Serfling model, researchers choose to include explanatory variables to adjust for the potential confounding to more accurately measure mortality rate (Jackson, 2009; Sprenger et al., 1989). Variables such as rates of respiratory disease, circulation of non-influenza viruses, temperature, and other weather measure are seasonal confounders which vary seasonally in incidence and timing. In this regression model investigators assume they have included relevant and properly measured confounder in the model. While this model controls seasonal factors that are potential confounders, it is not often that data on potential confounders is collected or even collected on a timescale useful to be included in the model. Similar to the Serfling model, a model including explanatory variables cannot always assume the regression assumptions will hold and several years of data are required in order to fit this model.

As an extension of the previous models and a way to better measure influenza-associated mortality, a regression model including influenza circulation as a predictor is employed (Jackson, 2009; Thompson et al., 2003). This model is beneficial because it allows the explicit modeling of the contribution of influenza on the observed mortality. By including influenza circulation in the regression model, we assume the

influenza surveillance is sufficient to represent the disease burden of influenza on the population. In addition, we assume the influenza surveillance is consistent across seasons and the subpopulation being modeled. This model requires comprehensive surveillance data and makes assumptions about the temporal lag between influenza infection and influenza-related death. Influenza-associated mortality is determined by taking the difference between the expected total deaths and expected baseline mortality (expected deaths when impact of influenza proxy terms are removed from the model).

In Jackson (2009)'s comparison of the regression methods, he concluded that the choice of regression model strongly impacts the estimated influena-associated excess mortaltiy. The regression models that include predictors in addition to time almost always estimated lower influenza-associated deaths compared to the Serfling regression model. This suggests that the Serfling regression method may falsely attribute noninfluenza related deaths to influenza. Regression models adjusting for potential confounders are also more flexible in that they don't assume consistent strength and timing of confounder across time.

According to Bhaskaran et al. (2013), once selecting a regression model to employ the challenges within the model are controlling for seasonality and long-term trends, considering immediate and delayed effects between the exposure and the outcome, confounding, and adjusting for delayed exposure effects. This research addresses confounding by accounting for long-term and seasonal trends. Generally, there are three ways of accounting for long-term and seasonal trends. The simplest approach is to stratify the model by time indicator variables. Another option is to use periodic functions of time, such as sine and cosine terms, to smoothly model regular cycles. While this option can smoothly long-term trend with relatively few parameters, it forces the seasonal pattern to be the same each year. In response to this limitation, many researcher add polynomial functions of time to the model. The final option is

spline functions of time. Spline can smoothly capture the trends and allow changes in the seasonal trend each year. A graphical display of each approach is shown in Figure 4.2.

Influenza-associated mortality models have included splines in various ways. Some models include splines as a function of time from begin to end of data period (Muscatello et al., 2013; Rizzo et al., 2007; Yang et al., 2012; Nielsen et al., 2011), others as a function of an environmental factor (i.e. temperture, humidity) (Aungkulanon et al., 2015), a function of certified influenza deaths (Wong et al., 2015) and function of seasonal week (week 1 to 52) (Goldstein et al., 2012). Because no gold standard exist in assessing when long-term trend and seasonality are fully accounted for, multiple measures have been used in studies. But once the trends are accounted for the residual variation can be used investigate the relationship between the outcome and exposure.

In this paper, we provide a specific model characterization of model choice and model uncertainty in time series studies of influenza activity and respiratory mortality with a focus on adjusting seasonal and long-term trends confounding. First, we define our model using parametric (natural cubic) splines to model the smooth function of time. Then, within a simulation study we explore goodness-of-fit measures to select the degrees of freedom of the splines and evaluate each measure under different statistical frameworks. Finally, we apply our confounding adjustment to the US influenza mortality dataset. To summarize the impact of our approach, we quantify model uncertainty in short-term effect estimates of influenza activity effects and influenza-associated mortality estimates.

In our model we account for both the seasonal and long-term trends in the data as we did in Chapter 3. The long-term trend accounts for increases or decreases in the data over time, while seasonal trend accounts for changes over time within a fixed period. Without including both trends, we may miss patterns in the data.

Figure 4.2: Visualization of the three approaches to account for long-term and seasonal trends in the data from Bhaskaran et al. (2013)

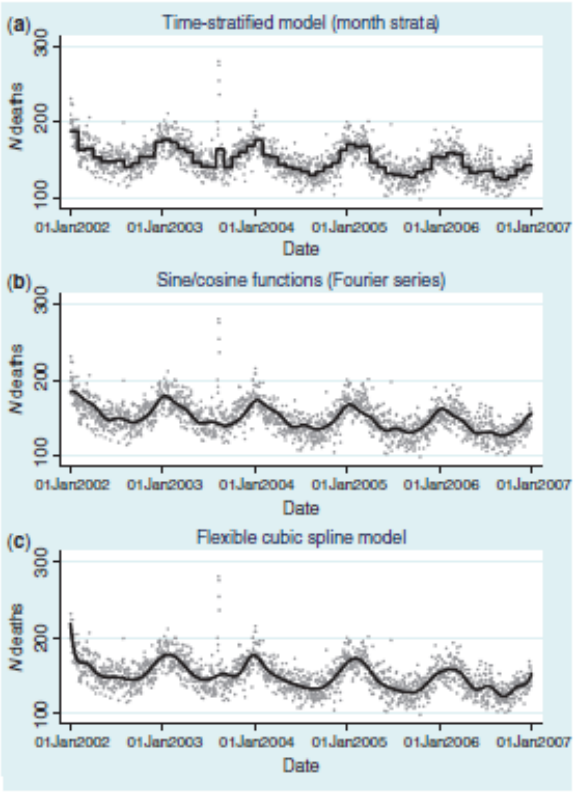

Our existing mortality model from Chapter 3 is updated with natural cubic spline functions to account for the long-term temporal trends and seasonal trends. For ages <65, our weekly time-series negative binomial regression models is used to assess the relationship between respiratory death counts and flu activity.

The negative binomial distribution is assumed for respiratory deaths to address overdispersion. The natural cubic spline basis function is used for the time trends. Recent models include harmonic functions for the cyclic seasonal component, and polynomial terms to describe the long-term trend are each replaced with a single function of time. Thus, our model will use two functions of time, one to address the long-term trend and the other to address seasonality. The spline terms model trend, which is believed to control for confounding effects.

The level of smoothness the function provides is integral to how the time trend

will capture the relationship between influenza activity and mortality. The effects of the levels of smoothness for long-term and seasonal trends on the beta regression coefficient of influenza activity, a measure of impact on the respiratory deaths, will be explored. Secondly, effects of the level of smoothness on the influenza-associated mortality will be investigated and compared to those obtained in Chapter 3.

4.2 Application to US Mortality Data

To illustrate how our approach can be applied to a realistic influenza dataset, we use United States data provided by the U.S. Centers for Disease Control and Prevention (CDC) comprising of weekly time-series of respiratory mortality, population count and influenza surveillance. The weekly count of respiratory coded deaths for the U.S. population during the period 1981–2014 for three age groups ($<$65, 65-74, $\geq$75 years) from the National Center for Health Statistics. Each death in the U.S. is registered in the National Vital Statistics System and is systematically coded using the International Classification of Diseases, Ninth Revision (ICD-9) or International Classification of Diseases, Tenth Revision (ICD-10) codes. For this analysis, we used respiratory deaths that were coded from 460 to 519.9 in ICD-9 and from J00 to J99 in ICD-10. Weekly U.S. population count for each age group was defined as the mid-year estimate from the Census Bureau International Database. National influenza virus surveillance data were obtained from the CDC. The weekly influenza percent positive was calculated as the number of specimens testing positive in each week divided by the total number tested in the same week and was used as proxies for influenza activity. These proxies included the weekly percent positive for influenza virus A(H1N1), influenza A(H1N1)pdm09, influenza A(H3N2), and influenza B. Each influenza proxy is lagged by one week to account for the time lapsed between infection and detection. Figures 4.3 and 4.4 shows scatterplots of each influenza A(H3N2) proxy and

respiratory mortality.

Figure 4.3: Plot showing exposure, Influenza A(H3N2), over time for ages less than 65.

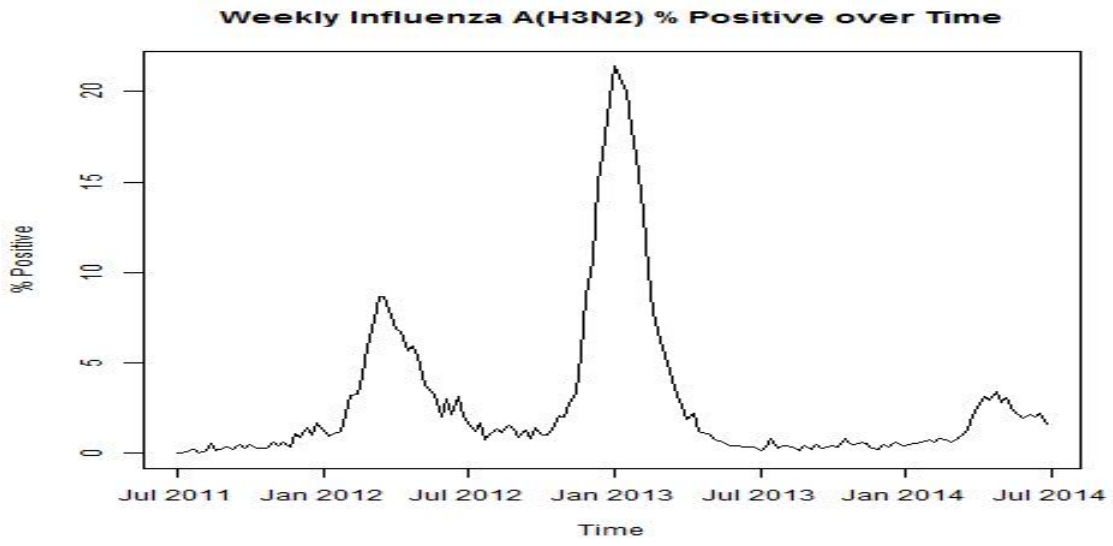

The model used to analyze the data is similar to the model described in the Simulation Study (see Section 4.3), but differing by the distribution assumed for the mortality outcome. Here the mortality outcome is assumed to have a negative binomial distribution for each age group.

$$log(E(Y_t)) = log(\alpha_t) + intercept + \beta_1 H1N1_t + \beta_2 H3N2_t + \beta_3 PDM_t + \beta_4 B_t + f(time, df) + h(weekofyear, df)$$

The f function is a natural cubic spline of time in order to model long-term trend while the h function is a natural cubic spline of week of the year to model the seasonal variation in the data. In addition to the temporal terms, the model includes the at-risk population size α_t as an offset and influenza subtype percent positive $(H1N1_t, H3N2_t, H1N1pdm09_t, B_t)$.

Figure 4.4: Plot showing outcome, Influenza respiratory deaths, over time for ages less than 65.

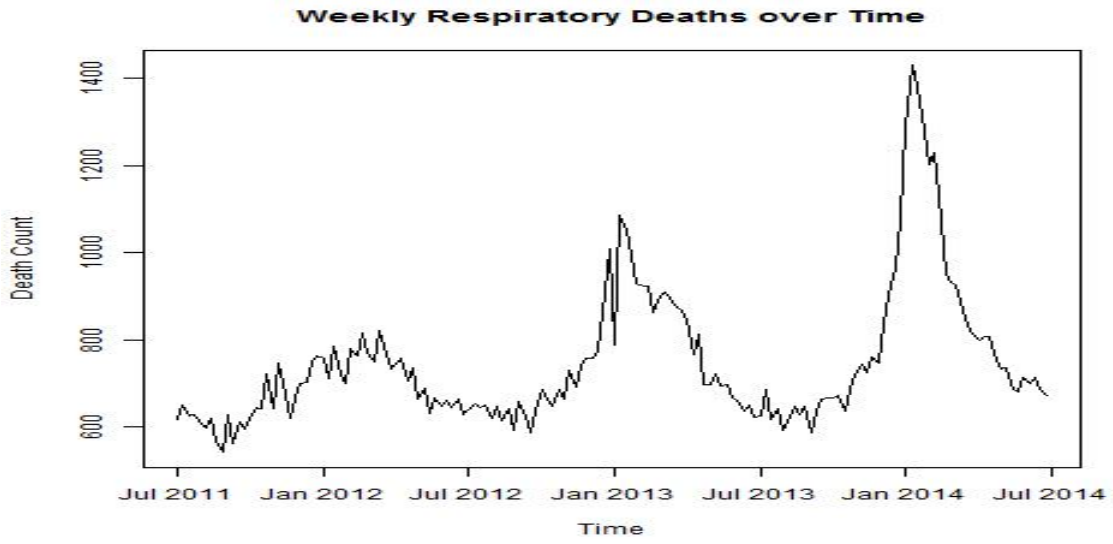

We calculate each of the beta regression coefficient and influenza-associated mortality of the aforementioned model to determine the best degrees of freedom (df) with which we can obtain each estimate. The tables in Appendix C summarizes the results.

When comparing the impact of long-term trend and seasonal trend smoothness, we find that generally the smoothness of the seasonal trend has the greatest impact on estimates. By not sufficiently controlling for both long-term and seasonal trend overestimation can occur (see Figures 4.7, 4.8, 4.5, and 4.6). Our results show that as we initially begin to account for the temporal trend, the greatest changes occur. Generally, ignoring temporal trend results in one of the largest estimates. As seasonal trend is accounted for most estimates decrease, while account for long-term trend causes minor fluctuations in the estimate. Influenza-associated mortality and most beta coefficients from influenza proxies of experienced the greatest decrease in estimation and variance between one to three DF for seasonal trend. Increasing the complexity of our model with additional degrees of freedom for each time trend con-

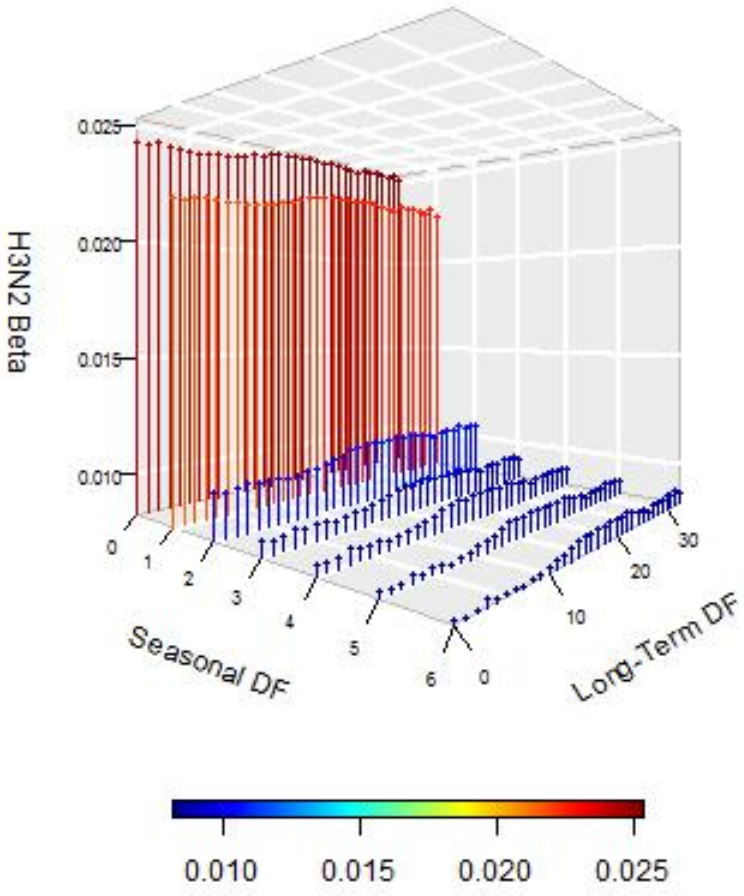

Figure 4.5: Estimate beta coefficients of Influenza A(H3N2) as the degrees of freedom for long-term and seasonal trends vary

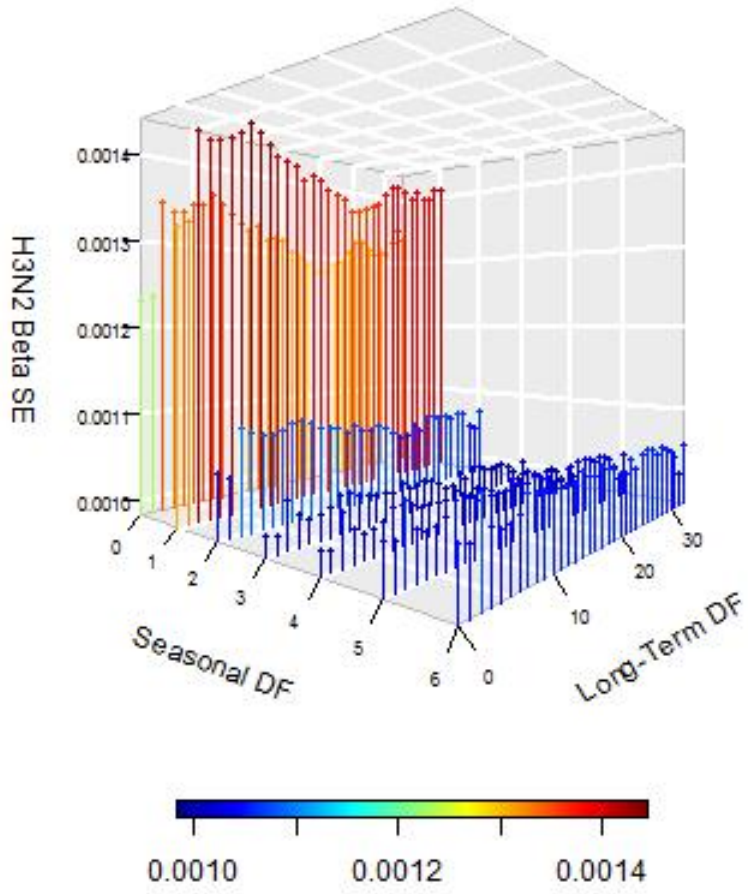

Figure 4.6: Beta coefficients standard error of Influenza A(H3N2) as the degrees of freedom for long-term and seasonal trends vary

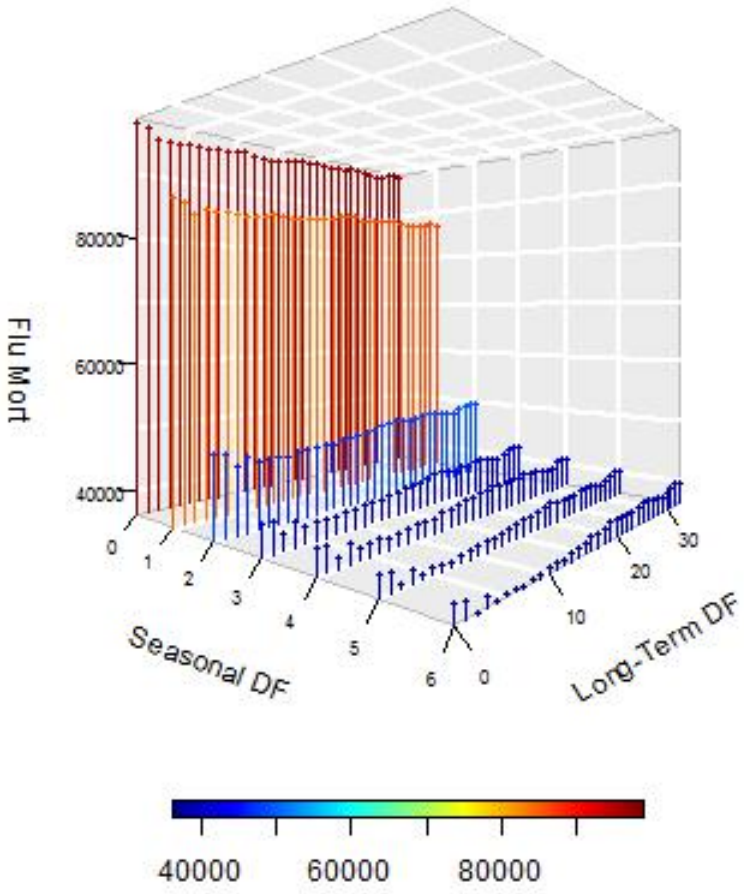

Figure 4.7: Estimate of total influenza-associated mortality as the degrees of freedom for long-term and seasonal trends vary

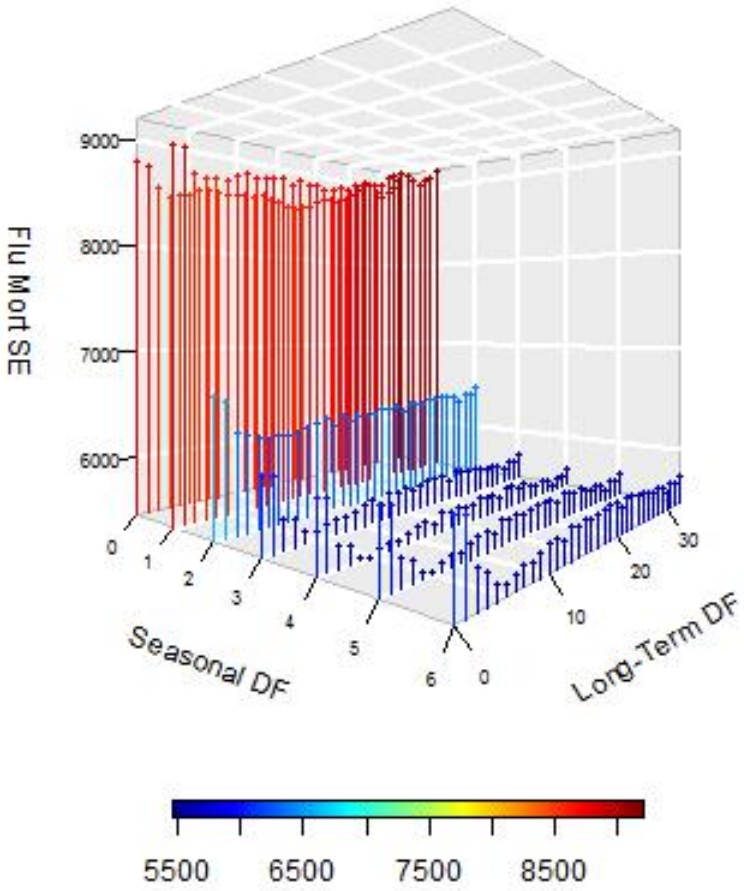

Figure 4.8: Standard error of total influenza-associated mortality as the degrees of freedom for long-term and seasonal trends vary

Ages	Variable	Mean	Standard Deviation
	Influenza A(H1N1)	0.8373	2.6332
	Influenza A(H3N2)	2.1575	4.0386
<65	Influenza A(H1N1)pdm09	0.7272	4.0453
	Influenza B	1.9533	4.3962
	Respiratory Mortality	589	132.1517
	Influenza A(H1N1)	0.8373	2.6332
	Influenza A(H3N2)	2.1575	4.0386
$65-74$	Influenza A(H1N1)pdm09	0.7272	4.0453
	Influenza B	1.9533	4.3962
	Respiratory Mortality	848.5	164.7635
	Influenza A(H1N1)	0.8373	2.6332
	Influenza A(H3N2)	2.1575	4.0386
≥ 75	Influenza A(H1N1)pdm09	0.7272	4.0453
	Influenza B	1.9533	4.3962
	Respiratory Mortality	2610	774.0633

Table 4.1: Descriptive Statistics of Influenza Proxies and Respiratory Mortality

tinued to decrease the total influenza-associated mortality. We constraint our model to what is reasonable based on the frequency of data collected and the total number of observations. As a reference point, Samet et al. (2000) used 7 degrees of freedom per year of data when information was collected daily and Peng et al. (2006) reports as little as 4 degrees of freedom per year in the notes from Joel Schwartz and Braga et al. (2000) study. Less dominant influenza proxies (e.g. Influenza A(H1N1)pdm09 and B) show behavior differing from influenza-associated mortality and the other influenza proxies. For example, the regression coefficient for A(H1N1)pdm09 seems to be impacted more by long-term DF. The estimate greatly decreases after two DF are added.

Similar to the point estimates, a large decrease in standard error occurred after reaching at least two seasonal DF. After reaching at least three seasonal DF, the standard error drop and then increases as long-term DF increases. Dominant influenza

proxies, A(H1N1) and A(H3N2), decrease as DF from temporal trends increase. While the less dominant influenza proxies' standard error vary at less control of the temporal trend, but stabilizes as DF increases. The error surrounding the model is heavily influenced by the length of the series (e.g. number of weeks), the number of events (e.g. respiratory deaths) per week, and the amount of overdispersion within the data (Bhaskaran et al., 2013). Air pollution time series analysis requires thousands of days of data with an average of tens of events to estimate a reliable precision measure (Bhaskaran et al., 2013). With close to 2,000 weeks worth of data and hundreds of respiratory deaths per week, our results are credible.

In Chapter 3, the Residual method (AR-2) estimated a total of 40,376 (SE = 5,265) deaths for age group 1, while the mean method (AR-1) estimated 29,404 (SE = 3,875) deaths. In comparison, the spline temporal trend model estimated 37, 962 (SE = 5,490) influenza-associated deaths (long-term DF = 6, seasonal DF = 4). The estimate was selected based on the stability of estimation and those in its surrounding degrees of freedom and minimum standard error. See Table 4.2 for summarized results. Our previous methods contained residual confounding. By controlling for the trends in the data, we are able to estimate the short-term impact of the influenza proxy exposures on death. The mean method may allow for the maximum amount of flexibility in accounting for trend.

4.3 Simulations

We designed a simulation study to assess the bias and variance of $\hat{\beta}$ when time is represented by a natural spline and the degrees of freedom of the natural spline is selected by beta regression coefficient estimates and estimate influenza-associated mortality. In effort to represent realistic data analysis, we generate data under four predetermined confounding scenarios and evaluate our proposed evaluation proce-

	GLM with natural spline	Mean	Residual
Total Influenza-associated Mortality	37,962	29,404	40,376
SE	5,490	3,875	5,266
Influenza A(H1N1)	1.68	1.9	2.6
SE	0.76	1	0.8
Influenza A(H3N2)	9.28	6.5	9.7
SE	0.98	0.9	0.5
Influenza B	3.46	1.8	0.3
SE	1.07	0.5	0.05
Influenza A(H1N1)pdm09	6.7	7.9	8.3
SE	1.39	1.1	0.5

SE - standard error
Beta estimates and SE are x1,000

Table 4.2: Parameter estimates for ages less then 65

dures under each. The scenarios vary by the timescale of confounding and the relationship between the influenza proxies and seasonal trend.

Our simulation model takes the following framework:

$$Y_t \sim Poisson(\mu_t)$$

$$log(\mu_t) = log(\alpha_t) + \beta_0 + f(t, w)$$

$$f(t, w) = \sum_{j=1}^{m_1} a_j B_j(t) + \sum_{j=1}^{m_2} c_j D_j(w)$$

$$FLU_{t,scaled} \sim Beta$$

$$probit(E(FLU_{t,scaled})) = g_{FLU}(t, w)$$

$$g(t, w) = \sum_{j=1}^{m_{flu}} b_j H_j(t) + \sum_{j=1}^{m_{flu2}} d_j K_j(w)$$

where α_t is the at-risk population size as the log offset, FLU_t represents each weekly time series percentage of specimens testing positive ($H1N1_t$, $H3N2_t$, PDM_t,

and B_t for Influenza A(H1N1), A(H3N2), A(H1N1pdm09), and B, respectively). Both functions f and g model temporal trend over time (t) and seasonal trend variations (w) using natural cubic splines. Within f and g, m_1, m_2, m_{flu} and m_{flu2} are the degrees of freedom of the functions while B_j, D_j, H_j and K_j are basis functions.

After selecting the degrees of freedom for each temporal trend spline (m_1, m_2, m_{flu} and m_{flu2}), a log-linear Poisson regression model is fit to the US influenza mortality dataset. Then, a probit-link Beta regression model is fit with g, the influenza temporal spline, for each influenza activity proxy (rescaled to be from 0 to 1) as the outcome. From each of the beta regressions, we scale each Pearson's residual variances to inform our concurvity of the simulated data. The raw residuals are solved from the Person's residuals. To simulate each influenza proxy, the autocorrelated raw residuals are added to the influenza proxy's mean trend.

In a similar manner, we generate the mean trend of mortality data without the effect of influenza. For the simulation study, we assume no influence of influenza on mortality in order to better observe any false effect of the influenza proxies within each scenario.

The following four scenarios are simulated for examination:

1. both spline trends of $g(t, w)$ are smoother than both spline trends of $f(t, w)$ and there is moderate concurvity between g and f,

2. both spline trends of $g(t, w)$ are smoother than both spline trends of $f(t, w)$ and there is high concurvity between g and f,

3. both spline trends of $g(t, w)$ are rougher than both spline trends of $f(t, w)$ and there is moderate concurvity between g and f, and

4. both spline trends of $g(t, w)$ are rougher than both spline trends of $f(t, w)$ and there is high concurvity between g and f.

Concurvity is defined as the correlation between f and g in a nonparameteric setting. High concurvity indicates that the influenza proxies are tightly correlated with the timescale for mortality, $f(t, w)$. While under moderate concurvity, factors with shorter cycles than the influenza proxies could effect mortality. In other words, concurvity is analogous to collinearity between predictors. A summary of the four scenarios is shown in Table 4.3.

Scenario	*Concurvity*	σ^2	m_1	m_2	m_{flu}	m_{flu2}
$g(t,w)$ smoother than $f(t,w)$	Moderate	σ^2_{FLU}	15	4	8	2
$g(t,w)$ smoother than $f(t,w)$	High	$\frac{\sigma^2_{FLU}}{5}$	15	4	8	2
$g(t,w)$ rougher than $f(t,w)$	Moderate	σ^2_{FLU}	8	2	15	4
$g(t,w)$ rougher than $f(t,w)$	High	$\frac{\sigma^2_{FLU}}{5}$	8	2	15	4

Table 4.3: Simulation Study Scenarios

In 50 simulated datasets, each influenza proxy is assumed to have no effect on the mortality in the Poisson regression model. The natural spline function degrees of freedom range from 0 to 33 for the overall trend spline and 0 to 6 for the seasonal variation spline. Zero indicates no temporal trend in the model. Beta regression coefficients and influenza-associated mortality are estimated for each of the 50 generated datasets. The performance of the simulation study points to the conditions under which our model may incorrectly find an effect for the influenza proxies or overestimate of influenza-associated mortality.

All simulations and analysis were conducted in R (R Core Team, n.d.) using the `glm` function for regression modeling and the `ns` function from the splines package for natural cubic spline smoothing of the time trend.

The purpose of the simulation study is to highlight the effects of smoothing and confounding via concurvity. When the mortality temporal trends and influenza proxy temporal trends are correlated on similar timescales there is said to be concurvity (multicollinearity). Similar to the analysis of the influenza dataset, the initial degrees of freedom added to the seasonal trend were not sufficient to reduce bias. This can

be seen in the large drop after 2 degrees of freedom. A smoother g (influenza proxy) function (fewer degrees of freedom) causes less bias beta regression and influenza-associated mortality estimates and decreased variance. This can particularly be seen when the seasonal degrees of freedom reaches 2. From the simulation study we find the higher concurvity between f and g, often causes an increase in the estimate bias as well as the variance. In addition, there is a slower decline in bias over the seasonal trend and a less consistent approach to the truth. Generally we can conclude more DF decreases the bias while only creating slight changes in the standard error. Dominici et al. (2004) suggests using at least as many DF needed to predict the exposure variable.

4.4 Discussion

Influenza time-series data modeling can greatly benefit from these findings. While employing splines is not the only smooth function for time, it is widely used and understood. Most importantly, it highlights an additional approach to controlling for trends compared to the popular polynomial and sine/cosine terms. Polynomial and sine/cosine terms modeling the temporal trend can account for trends smoothly using fewer parameters than spline terms. However, the temporal trend is forced to be the same each cycle. This may not match the data very well. While the spline terms provide a more flexible model, allowing differences in one cycle to the next, the terms are considered to be mathematically complex and research has not concluded on a gold standard approach to determining the optimum number of knots. The optimum number of knots will depend on the temporal trends within the data. The amount of smoothness greatly impacts the estimate. Deciding how to smooth has yet to reach a consensus among researchers.

Many critical choices are made throughout the modeling process of influenza time-

series data. Ultimately, the best model for one's data will depend on the characteristics of the data itself. Researchers must try to determine under which scenario their data is likely occurring. Concurvity can be determined by calculating the correlation between the exposure measurements and the fitted values from the exposure regressed on potential confounders (Ramsay et al., 2003). Similar to the research in the previous two chapters, investigators should carefully consider each implementation of the model. Sensitivity analysis should be conducted at each decision to determine how a different decision may change results. Sensitivity analysis will include the choice of the amount of control of temporal trends and others based on timescale of the data, autocorrelation, availability of data on possible confounder variables and other properties when selecting the appropriate analytical method.

Many researcher may consider employing a generalized additive model (GAM) as opposed to the generalized linear model used here. Current literature, has made no decision on the preference between the models, but recent computational software have shown some error. The direct computation for the standard error is difficult and it was found to be incorrectly calculated in many often used software programs. Investigators should use caution when implementing GAM.

Determining the optimal degrees of freedom for temporal splines requires more research. Thus, future work suggested by this chapter includes possible goodness-of-fit measures. In particular the often used Akaike information criterion (AIC), a relative measure of the quality of a statistical model based on likelihood and number of estimated parameters, cannot be applied to autocorrelated data. When AIC is used to for time series analysis or autocorrelated data, it is likely to select a more complex model as the number of observations increases (Ripley, 2007; Shibata, 1976). Although controlling for temporal trends usually reduces the autocorrelation, a special goodness-of-fit measure for autocorrelated time series data with selection based on confounding not prediction would be a significant contribution to the field. Another

area of future interest is to address complex overdispersion. Our current methods address the simplest form of overdispersion in which we assume overdispersion is constant over time. More complex structures of overdispersion can be addressed in future research.

Appendix A

Appendix for Chapter 2

Listing A.1: Sparse Poisson-Gamma Model

```
# JAGS sparse model description
JAGS_SparsePGG = function() {
# Likelihood
for (contrast in 1:num_contrasts) {
for (region in 1:num_regions) {
X[contrast, region] ~ dpois(mean[contrast, region])
X_pred[contrast, region] ~ dpois(mean[contrast, region])
mean[contrast, region] <- inprod(theta[contrast, region, ],delta[
   ↪ region,])
theta[contrast, region, region] ~ dgamma(lambda[region, region], 1)
for (region_1 in (region + 1):num_regions) {
theta[contrast, region, region_1] ~ dgamma(lambda[region, region_1],
   ↪ 1)
#symmetric
theta[contrast, region_1, region] <- theta[contrast, region, region_1]
}
```

```
}
}


# Prior for lambda and delta
for (region in 1:num_regions) {
delta[region,region] = 1
lambda[region, region] ~ dgamma(0.001, 0.001)
for (region_1 in (region + 1):num_regions) {
lambda[region, region_1] ~ dgamma(0.001, 0.001)
delta[region,region_1] ~ dbern(0.2)
#symmetric
lambda[region_1, region] <- lambda[region, region_1]
delta[region_1,region] <- delta[region,region_1]
}
}
}
```

Appendix B

Appendix for Chapter 3

AR-1 Residual (Bootstrap) Method

The residual approach is conducted in two stages. The first stage of the method is used to estimate the autoregressive (AR) parameter by resampling the AR structure error and adding it back into the model. The second stage is used to estimate the regression parameters and their variance-covariance accounting for residual temporal correlation using the estimated AR coefficient from stage 1. Let Y_t be the mortality data, $\hat{Y}_t$ be the estimates, $e_t = Y_t - \hat{Y}_t$ be the residuals.

- Stage 1: Bootstrap estimation of the autoregressive parameter

    1. Calculate the Pearsons standardized residuals from the original mortality data, $e_t = \frac{Y_t - \hat{Y}_t}{\sqrt{Var(\hat{Y}_t)}}$.
    2. Fit AR-1 model, $e_t = \rho e_{t-1} + u_t$, to obtain $\hat{}$ where the error of our autoregressive structure $u_t \sim N(0, \sigma^2)$.
    3. Obtain residual autoregressive structure error at each time point t, $u_t = e_t - \hat{\rho} e_{t-1}$.
    4. Sample with replacement from the set of u_t to get 10,000 sets of u_t^*.
    5. Calculate $e_t^* = \hat{\rho} e_{t-1}^* + u_t$ as uncorrelated over time residuals for each set,

			Methods				
			Residual		Mean		
Age Group	**ARStructure**	**ARParameter(s)**	**Mean**	**SE**	**Mean**	**SE**	**CI**
Ages 0-64	**AR-1**	ρ	0.65	0.04	0.79	0.02	(0.76, 0.83)
	AR-2	ρ_1	0.57	0.05	0.88	0.05	(0.77, 0.98)
		ρ_2	0.13	0.05	-0.08	0.05	(-0.18, 0.01)
Ages 65-74	**AR-1**	ρ	0.67	0.04	0.81	0.02	(0.78, 0.85)
	AR-2	ρ_1	0.56	0.05	0.87	0.05	(0.77, 0.96)
		ρ_2	0.16	0.05	-0.06	0.05	(-0.15, 0.04)
Ages $\geq$ 75	**AR-1**	ρ	0.80	0.03	0.87	0.01	(0.84, 0.9)
	AR-2	ρ_1	0.83	0.05	0.99	0.01	(0.97, 1)
		ρ_2	-0.04	0.05	-0.15	0.01	(-0.18, -0.12)

SE - standard error
CI - credible interval
AR - autogressive

Table B.1: Autoregressive (AR) Parameter estimates for AR-1 and AR-2 models when temporal correlation is accounted for via the residual vs. via the mean

where $e_1^* = e_1$.

6. Obtain $Y_t^* = \hat{Y}_t + \tilde{e_t^*}$for each set, where $\tilde{e_t^*}$is not a standardized residual (rescaled to appropriately be added to the data).

7. Regress Y_t^* to the influenza activity, temporal trends and seasonal covariates for each set.

8. Calculate $e_{2,t}^* = \frac{Y_t^* - \hat{Y_t^*}}{\sqrt{Var(\hat{Y_t^*})}}$ for each set.

9. Determine ρ^*, given an AR-1 model, $e_{2,t}^* = \rho^* e_{2,t-1}^* + u_{2,t}$, is applied on the standardized residuals $e_{S,2,t}^*$ for each set.

10. Calculate $Bias = \bar{\rho^*} - \hat{\rho}$ where $\bar{\rho^*}$is the mean of bootstrap samples ρ^*.

11. Calculate bootstrap autoregressive parameter $\rho_{boot} = \hat{\rho} - Bias$.

- Stage 2: Bootstrap estimation of the regression parameters

1. Calculate $u_{boot,t} = e_t - {}_{boot}e_{t-1}$.

			Viral Proxies							
			A(H3N2)		A(H1N1)		B		A(H1N1)pdm09	
	Methods		β	SE(β)	β	SE(β)	β	SE(β)	β	SE(β)
Ages 0-64	Delta		9.6	0.6	2.6	0.8	3.0	0.5	8.4	0.5
	Newey-West	AR(1)	9.6	1.1	2.6	0.9	3.0	0.9	8.4	1.5
		AR(2)	9.6	1.2	2.6	1.0	3.0	0.9	8.4	1.8
	Residual	AR(1)	9.6	0.6	2.6	0.8	3.0	0.5	8.3	0.5
		AR(2)	9.7	0.5	2.6	0.8	3.0	0.5	8.3	0.5
	Mean	AR(1)	6.5	0.9	1.9	1.0	1.8	0.5	7.9	1.1
		AR(2)	6.3	0.9	1.8	1.0	1.8	0.5	7.8	1.1
Ages 65-74	Delta		11.2	0.5	1.5	0.7	1.8	0.4	1.7	0.4
	Newey-West	AR(1)	11.2	1.0	1.5	0.9	1.8	0.8	1.7	0.4
		AR(2)	11.2	1.1	1.5	1.0	1.8	0.8	1.7	0.5
	Residual	AR(1)	11.2	0.5	1.5	0.7	1.8	0.4	1.7	0.4
		AR(2)	11.3	0.5	1.5	0.7	1.8	0.4	1.7	0.4
	Mean	AR(1)	7.4	0.8	0.1	0.8	0.6	0.4	1.5	1.1
		AR(2)	7.2	0.8	0.0	0.8	0.6	0.4	1.5	1.1
Ages $\geq$ 75	Delta		15.5	0.5	1.6	0.7	3.0	0.5	0.7	0.5
	Newey-West	AR(1)	15.5	1.2	1.6	1.0	3.0	1.0	0.7	0.3
		AR(2)	15.5	1.4	1.6	1.2	3.0	1.0	0.7	0.3
	Residual	AR(1)	15.5	0.5	1.6	0.7	3.0	0.5	0.7	0.5
		AR(2)	15.5	0.5	1.6	0.7	3.0	0.5	0.7	0.5
	Mean	AR(1)	6.2	0.7	0.2	0.7	0.8	0.3	1.2	1.2
		AR(2)	5.7	0.7	0.1	0.7	0.7	0.3	0.9	1.2

AR - autoregressive structure
SE - standard error

Table B.2: Regression Coefficient Estimates and Standard Error (x1,000) for viral proxies using various methods of analysis

2. Sample with replacement for the set of $u_{boot,t}$, to get 10,000 sets of $u^*_{boot,t}$.
3. Determine $e^*_{3,t} = \rho_{boot} e_{3,t-1} + u^*_{2,t}$ for each set.
4. Obtain $Y^*_{boot} = \hat{Y}_t + e^*_{3,t}$ for each set, where $\tilde{e^*_{3,t}}$is not a standardized residual (rescaled to appropriately be added to the data).
5. Fit Y^*_{boot} to the influenza activity, temporal trends and seasonal covariates for each set.

Negative Binomial Delta Method

From asymptotic normality, we know $\hat{\beta} \sim N(\beta, \Sigma_{\hat{\beta}})$.

Using the Delta method, we know $g(\hat{\beta}) \sim N(g(\beta), \nabla g(\beta)^T \Sigma_{\hat{\beta}} \nabla g(\beta))$, where $\nabla g(\beta)$ is a vector of partial derivatives with respect to each β.

In the case of the influenza mortality model, $g(\beta) = \sum_{t=1}^{T} population_t * exp(X_{1t}\beta_1 + X_{2t}\beta_2) - \sum_{t=1}^{T} population_t * exp(X_{1t}\beta_1)$, where the time trend variables are represented by X_{1t} and the influenza proxies of interest are represented by X_{2t}.

Listing B.1: Mean (Bayesian) Method JAGS Code

```
LogPool <- function() {
for (i in 1:N){
resp[i] ~ dpois(mu[i])
log(mu[i]) <- logpop[i] + beta[1] + beta[2]*((deathwk[i]-m1)/sd1) +
beta[3]*((pow(deathwk[i],2)-m2)/sd2) + beta[4]*((pow(deathwk[i],3)-m3)
    ↪ /sd3) +
beta[5]*((pow(deathwk[i],4)-m4)/sd4) + beta[6]*cos(2*3.141593*deathwk[
    ↪ i]/52.179) +
beta[7]*sin(2*3.141593*deathwk[i]/52.179) + beta[8]*lpH3N2[i] + beta
    ↪ [9]*lpH1N1[i] +
```

```
beta[10]*lpB[i] + beta[11]*lpH1N1pdm09[i] + eps[i]
}
for ( j in 1:11 ) {
beta[j] ~ dnorm( 0, 0.0001 )
}
eps[1] ~ dnorm(0,0.0001)
p ~ dunif(-1,1)
k ~ dgamma(0.1,0.1)
for (i in 1:(N-1)){
eps[i+1] <- (p * eps[i]) + gam[i+1]
gam[i+1] ~ dnorm(0,k)
}
}

lpH1N1 <- data$lperc_sH1N1
lpH1N1pdm09 <- data$lperc_H1N1pdm09
lpH3N2 <- data$lperc_sH3N2
lpB <- data$lperc_sB
deathwk <- data$deathwk
resp <- data$resp
pop <- data1$population
logpop <- data$logpop

death.nb <- function(a){
model <- glm(resp ~ offset(logpop) + I((deathwk-mean(data$deathwk))/sd
   ↪ (data$deathwk)) +
 ((deathwk^2-mean(data$deathwk^2))/sd(data$deathwk^2)) + I((deathwk^3-
```

```
    ↪ mean(data$deathwk^3))/sd(data$deathwk^3)) +
  I((deathwk^4-mean(data$deathwk^4))/sd(data$deathwk^4)) + cos(2*
     ↪ 3.141593*deathwk/52.179) +
   sin(2*3.141593*deathwk/52.179) + lperc_sH3N2 + lperc_sH1N1 + lperc_
      ↪ sB + lperc_H1N1pdm09,
    family = "poisson", data = a)
}

jags.dat = list ("resp"=resp, "deathwk"=deathwk,
 "lpH1N1pdm09"=lpH1N1pdm09, "lpH3N2"=lpH3N2, "lpB"=lpB, "logpop" =
    ↪ logpop, "lpH1N1" = lpH1N1,
  "N" = nrow(data), "m1" = mean(data$deathwk), "m2" = mean(data$
     ↪ deathwk^2),
   "m3" = mean(data$deathwk^3), "m4" = mean(data$deathwk^4), "sd1" =
      ↪ sd(data$deathwk),
    "sd2" = sd(data$deathwk^2), "sd3" = sd(data$deathwk^3), "sd4" = sd
       ↪ (data$deathwk^4))
jags.param = c("beta","mu","eps","p","gam","k")
jags.inits <- function() {
list(
"beta" = summary(death.nb(data))$coefficient[1:11],
"p" = 0,
"k" = 1
)}

jagsfit <- jags(data=jags.dat, inits=jags.inits, jags.param, n.iter
   ↪ =25000, model.file=LogPool, n.chains=1, n.burn=5000, n.thin=4 )
```

Simulation Study - Bayesian Model Data Generation In order to generate what is used as our observed data for the simulation study, we use values from our Bayesian model posterior distribution.

$\hat{Y}_t = population * exp(X\hat{\beta} + \hat{\epsilon}_t)$

$\epsilon_{t+1} = p * \epsilon_t + \gamma_{t+1}$

$\gamma_{t+1} \sim Normal(0, k)$

1. Find posterior mean of inverse variance of the autoregressive standard error term (k) denoted as $\bar{k_p}$.

2. Simulate $\gamma_t \sim N(0, \bar{k_p})$. (NOTE: 10 sets of number of observations - 1 values, and add the first row of zero values)

3. Solve $\epsilon_{t+1} = \bar{p_p} * \epsilon_t + \gamma_t$. (NOTE: For AR(1) autoregressive structure, the first ϵ_1 is simply the posterior mean at that time point)

4. Solve $\mu_t = log(population) * exp(X\bar{\beta}_p + \epsilon_t)$. (NOTE: $\mu_t \sim$ Negative Binomial$(p, \bar{r_p})$).

5. Solve for p.

6. Randomly generate data using negative binomial distribution. During the simulation study the generated sets are used as the observed data.

Regression Coefficients Interpretations

The means from the residual and mean approaches are interpreted differently. The residual approach has a marginal interpretation. The target inference is on the population-level (over all weeks). The mean method has a conditional interpretation. The target inference is on a subject-level (for a specific week). The mean given the random intercept (mean residual) of that specific week.

		Proportion of Positive Specimens Testing Positive for a Given Subtype (%)				
Season	% Positive specimens of total tested	A(H1N1)	A(H3N2)	A(H1N1)pdm	B	Predominant Subtype
1981/1982	3.96	23.70	0.32	0.00	75.97	B
1982/1983	9.41	10.65	77.60	0.00	11.75	A(H3N2)
1983/1984	12.85	50.81	3.84	0.00	45.36	A(H1N1)
1984/1985	13.35	0.10	97.27	0.00	2.63	A(H3N2)
1985/1986	11.65	0.08	23.54	0.00	76.38	B
1986/1987	10.07	99.28	0.23	0.00	0.50	A(H1N1)
1987/1988	8.76	7.33	76.37	0.00	16.30	A(H3N2)
1988/1989	17.32	32.25	5.37	0.00	49.38	B
1989/1990	11.32	1.10	78.69	0.00	19.82	A(H3N2)
1990/1991	9.81	3.80	6.04	0.00	85.48	B
1991/1992	12.54	15.64	59.17	0.00	0.93	A(H3N2)
1992/1993	11.99	1.62	14.48	0.00	70.98	B
1993/1994	11.59	0.35	67.99	0.00	0.82	A(H3N2)
1994/1995	9.83	1.35	48.12	0.00	26.23	A(H3N2)
1995/1996	12.39	31.72	22.42	0.00	15.33	A(H1N1)
1996/1997	16.11	0.03	34.90	0.00	22.36	A(H3N2)
1997/1998	17.13	0.08	39.93	0.00	0.67	A(H3N2)
1998/1999	14.40	0.21	17.92	0.00	22.96	B
1999/2000	17.07	1.73	41.44	0.00	0.75	A(H3N2)
2000/2001	14.49	28.47	0.81	0.00	46.17	B
2001/2002	18.70	0.58	43.07	0.00	15.18	A(H3N2)
2002/2003	14.83	28.83	11.65	0.00	42.47	B
2003/2004	21.50	0.01	40.67	0.00	0.97	A(H3N2)
2004/2005	19.45	0.10	34.68	0.00	24.45	A(H3N2)
2005/2006	15.62	3.87	41.69	0.00	17.34	A(H3N2)
2006/2007	16.92	28.57	17.32	0.00	22.66	A(H1N1)
2007/2008	23.04	9.96	28.46	0.00	30.34	B
2008/2009	26.16	14.94	8.50	49.99	12.93	A(H1N1)pdm09
2009/2010	17.26	0.18	0.42	92.23	0.20	A(H1N1)pdm09
2010/2011	10.35	0.00	47.51	29.09	21.97	A(H3N2)
2011/2012	4.98	0.00	63.40	17.72	16.92	A(H3N2)
2012/2013	12.93	0.00	70.20	3.81	24.95	A(H3N2)
2013/2014	9.39	0.00	10.80	75.43	12.71	A(H1N1)pdm09

Table B.3: Proportion of positive specimens tested by season and influenza subtype

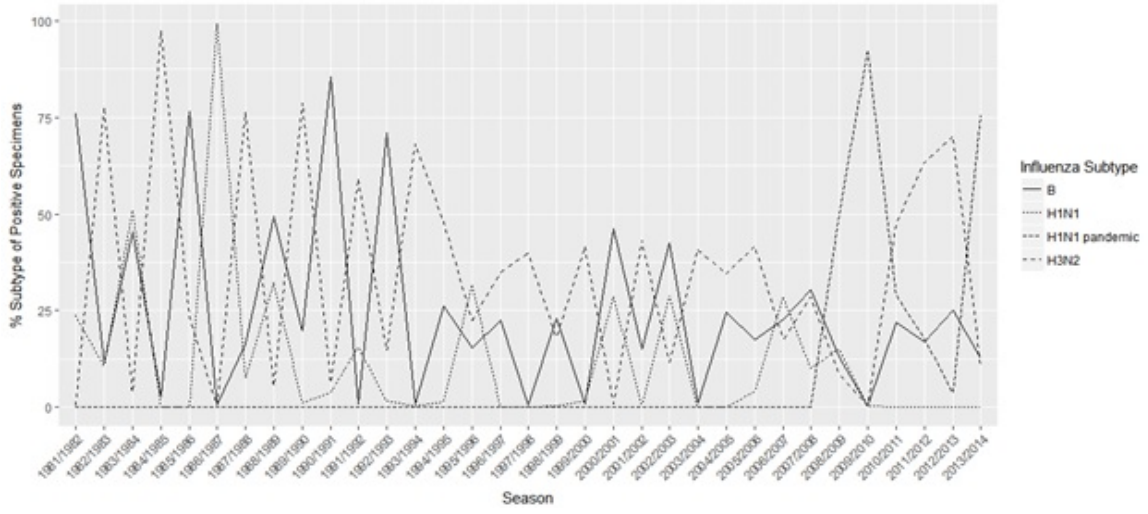

Figure B.1: Percentage of influenza subtype for all age groups during each season, given the specimen tested positive

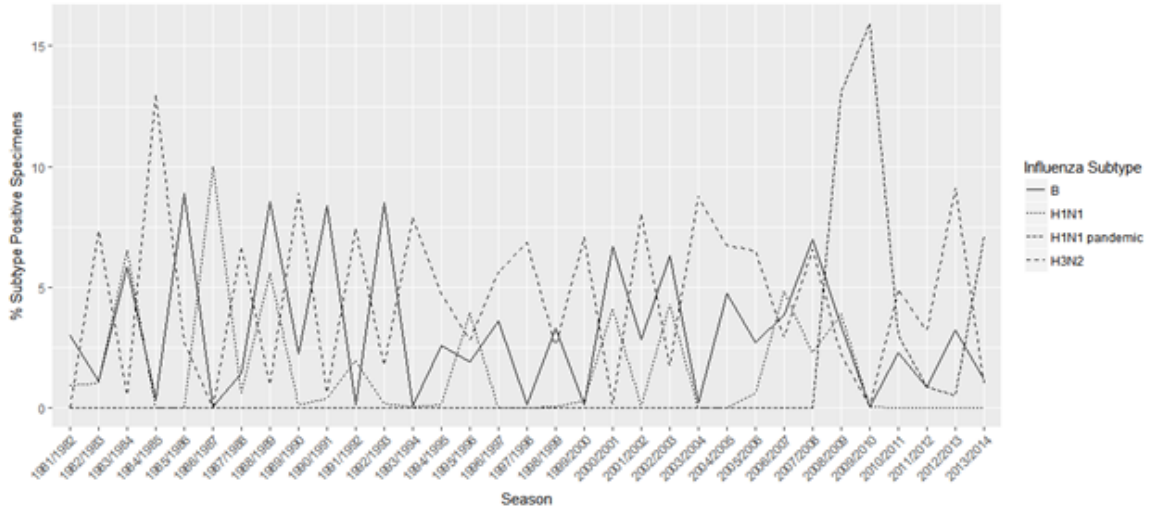

Figure B.2: Percentage of specimens testing positive for all age groups by influenza subtype during each season

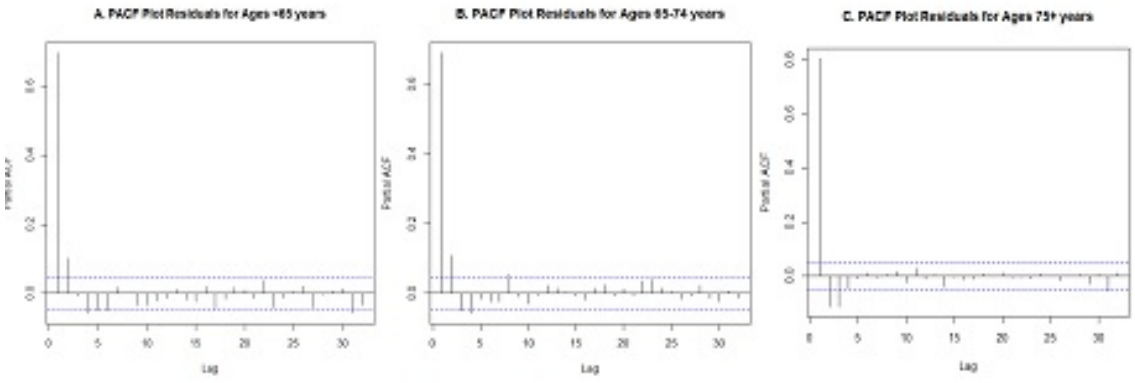

Figure B.3: PACF Plots by Age Group

	Delta		Newey-West Delta		Residual		Mean	
Season	**Deaths**	**SE**	**Deaths**	**SE**	**Deaths**	**SE**	**Deaths**	**SE**
1981/1982	507	68.84	507	135.95	510	137.48	122	54.39
1982/1983	5,482	196.23	5,482	446.51	5,502	430.55	2,176	236.51
1983/1984	2,930	257.68	2,930	459.70	2,942	520.82	834	217.42
1984/1985	9,333	335.60	9,333	817.00	9,346	773.10	4,003	429.23
1985/1986	3,205	187.09	3,205	415.96	3,201	365.16	1,261	176.11
1986/1987	733	317.55	733	449.43	790	601.84	112	300.12
1987/1988	6,265	221.26	6,265	513.63	6,259	480.88	2,642	287.19
1988/1989	2,692	279.29	2,692	494.94	2,690	571.17	816	252.40
1989/1990	8,663	297.63	8,663	724.69	8,655	674.52	3,657	393.50
1990/1991	2,748	258.87	2,748	527.24	2,763	501.38	797	197.35
1991/1992	7,216	272.72	7,216	617.46	7,214	594.27	3,013	334.81
1992/1993	5,536	307.49	5,536	682.47	5,530	602.47	1,972	268.34
1993/1994	8,419	291.58	8,419	721.99	8,419	670.14	3,837	416.93
1994/1995	7,270	319.15	7,270	724.85	7,275	651.41	2,661	305.18
1995/1996	4,797	263.57	4,797	464.53	4,801	541.65	1,756	262.03
1996/1997	7,591	294.12	7,591	685.80	7,590	621.21	3,316	367.50
1997/1998	7,163	241.01	7,163	597.07	7,168	554.85	3,589	392.56
1998/1999	3,557	144.28	3,557	330.16	3,556	296.94	1,532	177.78
1999/2000	8,514	292.99	8,514	706.86	8,523	660.94	3,725	407.27
2000/2001	2,339	327.59	2,339	583.21	2,343	672.37	576	283.09
2001/2002	11,574	426.06	11,574	1000.41	11,579	919.28	4,510	492.59
2002/2003	4,835	375.86	4,835	669.34	4,838	763.67	1,491	307.48
2003/2004	9,782	338.34	9,782	826.72	9,791	778.50	3,935	461.05
2004/2005	11,276	412.86	11,276	966.41	11,274	891.33	4,224	499.95
2005/2006	11,354	395.43	11,354	919.94	11,352	865.00	3,891	456.71
2006/2007	7,435	473.93	7,435	777.57	7,443	969.02	2,237	422.10
2007/2008	10,441	473.72	10,441	971.28	10,437	966.24	3,730	487.92
2008/2009	5,708	619.83	5,708	874.15	5,736	1,361.68	1,914	804.64
2009/2010	1,437	827.45	1,437	530.47	1,797	1,814.09	1,674	2042.68
2010/2011	9,459	345.34	9,459	752.82	9,444	793.32	3,578	508.41
2011/2012	6,611	220.79	6,611	511.31	6,606	502.10	2,412	295.06
2012/2013	16,716	599.32	16,716	1,413.75	16,717	1,339.59	6,235	714.20
2013/2014	3,750	388.61	3,750	396.12	3,798	942.04	1,800	888.79

SE - standard error

Table B.4: Regression Mortality Estimates by Season for ages older than 75

	Delta		Newey-West Delta		Residual		Mean		PosteriorTruth
Season	**Deaths**	**SE**	**Deaths**	**SE**	**Deaths**	**SE**	**Deaths**	**SE**	**Deaths**
1981/1982	119	18.68	125	143.15	123	19.52	125	28.45	121
1982/1983	2,076	48.81	2,065	428.59	2,065	51.48	2,060	76.22	2,156
1983/1984	830	67.55	849	461.03	836	70.66	846	102.69	828
1984/1985	3,559	76.71	3,528	730.71	3,531	81.11	3,521	118.18	3,967
1985/1986	1,127	50.54	1,127	423.69	1,132	52.78	1,131	76.11	1,250
1986/1987	113	69.85	140	443.60	115	74.97	124	132.09	114
1987/1988	2,381	56.30	2,369	499.20	2,367	59.29	2,368	88.30	2,618
1988/1989	761	74.93	784	513.26	769	78.48	784	113.95	811
1989/1990	3,332	72.06	3,306	677.30	3,307	76.07	3,308	112.44	3,623
1990/1991	804	69.71	821	551.06	819	72.30	822	106.41	792
1991/1992	2,777	67.40	2,761	588.69	2,751	71.06	2,761	104.58	2,985
1992/1993	1,918	83.12	1,919	695.08	1,925	86.78	1,926	125.81	1,955
1993/1994	3,287	69.84	3,258	673.01	3,258	73.79	3,263	109.05	3,801
1994/1995	2,657	78.84	2,647	680.34	2,652	82.66	2,651	120.49	2,637
1995/1996	1,707	69.87	1,715	475.27	1,698	73.31	1,712	107.26	1,740
1996/1997	2,823	76.54	2,809	673.57	2,814	80.25	2,816	118.31	3,285
1997/1998	2,839	59.63	2,814	574.68	2,814	63.02	2,811	93.88	3,555
1998/1999	1,340	39.30	1,335	339.68	1,338	41.16	1,337	60.92	1,518
1999/2000	3,337	72.76	3,311	681.10	3,307	76.80	3,305	114.34	3,690
2000/2001	551	88.54	583	614.52	564	92.67	582	135.38	574
2001/2002	4,328	108.22	4,304	965.45	4,310	113.70	4,308	167.29	4,469
2002/2003	1,532	100.81	1,557	693.73	1,538	105.59	1,555	153.35	1,479
2003/2004	3,789	80.57	3,756	771.12	3,758	85.13	3,754	125.64	4,192
2004/2005	4,255	105.68	4,231	943.46	4,238	111.03	4,235	163.55	4,502
2005/2006	4,330	101.22	4,306	903.14	4,306	106.58	4,314	158.75	4,156
2006/2007	2,568	125.14	2,590	802.25	2,557	131.21	2,578	193.31	2,449
2007/2008	3,720	122.64	3,723	956.14	3,710	128.61	3,722	187.74	4,011
2008/2009	2,321	166.40	2,354	922.24	2,333	174.57	2,376	252.61	2,262
2009/2010	2,264	218.62	2,236	585.65	2,298	231.31	2,333	334.54	2,220
2010/2011	3,968	89.82	3,939	750.71	3,954	94.71	3,964	140.33	3,882
2011/2012	2,717	57.29	2,696	516.63	2,703	60.50	2,704	91.05	2,595
2012/2013	6,336	143.34	6,291	1,314.06	6,302	151.04	6,304	220.02	6,655
2013/2014	2,182	105.20	2,164	418.78	2,196	111.03	2,209	162.08	2,100

SE - standard error

Table B.5: Poisson model using data generated from random intercept produced using parameters from the auroregressive structure simulation results of influenza-associated deaths from ages older than 75 for various methods of analysis

	Delta		Newey-West Delta		Residual		Mean		PostriorTruth
Season	**Deaths**	**SE**	**Deaths**	**SE**	**Deaths**	**SE**	**Deaths**	**SE**	**Deaths**
1981/1982	461	17.83	464	139.44	461	151.11	158	56.1	121
1982/1983	5,543	48.37	5,553	439.9	5,552	447.32	2,646	235.46	2,156
1983/1984	2,778	66.39	2,791	464.24	2,781	568.59	1,078	221.96	828
1984/1985	9,522	80.66	9,534	807.35	9,525	776.57	4,829	421.17	3,967
1985/1986	3,168	47.8	3,179	418.66	3,156	391.68	1,521	179.69	1,250
1986/1987	559	83.72	562	473.76	670	616.3	248	306.61	114
1987/1988	6,313	54.02	6,325	503.15	6,298	490.99	3,220	287.45	2,618
1988/1989	2,507	72.06	2,520	502.33	2,489	636.43	1,057	257.1	811
1989/1990	8,815	71.71	8,827	715.54	8,798	678.75	4,430	389.9	3,623
1990/1991	2,602	66.55	2,616	536.15	2,623	542.03	998	203.42	792
1991/1992	7,321	67.18	7,330	620.66	7,310	612.49	3,683	333.29	2,985
1992/1993	5,503	78.66	5,522	687.39	5,482	647.65	2,399	275.17	1,955
1993/1994	8,629	70.15	8,639	724.24	8,621	672.95	4,648	412.59	3,801
1994/1995	7,310	79.93	7,328	719.58	7,301	681.39	3,238	308.45	2,637
1995/1996	4,735	68.05	4,746	470.03	4,724	602.06	2,202	265.84	1,740
1996/1997	7,681	73.2	7,698	683.72	7,666	645.17	4,013	367.79	3,285
1997/1998	7,344	57.98	7,352	599.62	7,341	557.39	4,357	391.2	3,555
1998/1999	3,583	36.26	3,591	329.26	3,574	311.92	1,861	180.16	1,518
1999/2000	8,691	70.94	8,701	710.86	8,690	667.19	4,534	406.8	3,690
2000/2001	2,106	84.9	2,121	596.04	2,096	743.13	772	289.1	574
2001/2002	11,701	104.71	11,723	989.63	11,685	942.43	5,466	492.06	4,469
2002/2003	4,623	96.93	4,641	675.14	4,603	850.26	1,886	312.76	1,479
2003/2004	9,966	81.04	9,978	824.58	9,963	778.78	5,136	458.28	4,192
2004/2005	11,351	101.08	11,373	951.25	11,330	909.66	5,502	499.71	4,502
2005/2006	11,414	95.86	11,433	902.05	11,394	875.44	5,119	457.49	4,156
2006/2007	7,205	121.87	7,223	780.6	7,198	1,061.07	3,121	428.19	2,449
2007/2008	10,283	118.42	10,308	954.21	10,254	1,021.65	4,961	489.44	4,011
2008/2009	5,468	161.17	5,491	889.63	5,468	1,520.94	2,713	828.52	2,262
2009/2010	1,810	215.17	1,822	573.17	2,136	2,039.96	2,110	2,142.64	2,220
2010/2011	9,563	84.53	9,580	735.9	9,534	811.25	4,664	516.03	3,882
2011/2012	6,678	53.16	6,687	499.51	6,663	503.81	3,154	297.32	2,595
2012/2013	16,838	144.32	16,866	1,393.42	16,814	1,344.76	8,088	705.62	6,655
2013/2014	3,908	100.87	3,920	403.87	3,940	1,035.60	2,325	935.83	2,100

SE - standard error

Table B.6: Poisson model using data generated from random intercept produced from the posterior means simulation results of influenza-associated deaths from ages older than 75 for various methods of analysis

Appendix C

Appendix for Chapter 4

	0	1	2	3	4	5	6
0	9.37	5.60	-1.69	-1.49	-1.49	-1.49	-1.49
1	9.55	5.83	-1.60	-1.37	-1.37	-1.36	-1.37
2	9.58	5.76	-1.95	-1.71	-1.70	-1.69	-1.70
3	11.40	7.53	-0.08	0.08	0.10	0.10	0.10
4	10.76	6.86	-0.59	-0.46	-0.44	-0.44	-0.45
5	10.99	7.09	-0.31	-0.22	-0.21	-0.21	-0.21
6	11.07	7.19	-0.19	-0.12	-0.11	-0.10	-0.11
7	11.10	7.22	-0.19	-0.13	-0.11	-0.11	-0.11
8	11.02	7.08	-0.48	-0.40	-0.39	-0.38	-0.39
9	11.07	7.15	-0.44	-0.35	-0.33	-0.33	-0.33
10	11.13	7.20	-0.39	-0.30	-0.28	-0.28	-0.28
11	11.28	7.35	-0.31	-0.21	-0.20	-0.19	-0.20
12	11.37	7.42	-0.27	-0.17	-0.16	-0.15	-0.16
13	11.48	7.54	-0.15	-0.06	-0.05	-0.05	-0.05
14	11.57	7.62	-0.11	-0.03	-0.01	-0.01	-0.01
15	11.57	7.63	-0.16	-0.07	-0.05	-0.05	-0.05
16	11.62	7.66	-0.22	-0.12	-0.10	-0.10	-0.10
17	11.78	7.81	-0.16	-0.05	-0.03	-0.03	-0.03
18	11.82	7.83	-0.12	-0.01	0.01	0.01	0.01
19	11.85	7.87	-0.07	0.03	0.04	0.05	0.05
20	11.84	7.86	-0.08	0.02	0.04	0.04	0.04
21	11.83	7.84	-0.15	-0.04	-0.02	-0.02	-0.02
22	11.86	7.85	-0.27	-0.16	-0.14	-0.13	-0.13
23	12.09	8.07	-0.14	-0.03	-0.01	-0.00	-0.01
24	12.07	8.06	-0.12	-0.01	0.01	0.02	0.01
25	12.02	8.00	-0.24	-0.11	-0.10	-0.09	-0.09
26	12.03	8.01	-0.26	-0.13	-0.12	-0.11	-0.11
27	12.12	8.07	-0.31	-0.17	-0.15	-0.15	-0.15
28	12.17	8.11	-0.33	-0.19	-0.17	-0.16	-0.17
29	12.27	8.20	-0.30	-0.16	-0.14	-0.13	-0.13
30	12.40	8.28	-0.40	-0.25	-0.23	-0.22	-0.23
31	12.50	8.37	-0.29	-0.14	-0.12	-0.12	-0.12
32	12.34	8.26	-0.28	-0.13	-0.11	-0.10	-0.11
33	12.34	8.24	-0.34	-0.19	-0.17	-0.17	-0.17

Table C.1: Simulation Study Results of $g(t, w)$ smoother than $f(t, w)$ and moderate concurvity:
Beta regression coefficient estimates (x1,000) for Influenza H1N1 at varying DFs for long-term (vertical) and seasonal (horizontal) trends for ages less than 65 years

	0	1	2	3	4	5	6
0	18.56	13.81	1.22	2.21	2.31	2.31	2.31
1	19.61	14.73	1.25	2.38	2.50	2.50	2.50
2	19.07	13.99	-0.14	0.99	1.10	1.10	1.10
3	18.59	13.54	-0.87	0.26	0.37	0.37	0.37
4	18.80	13.73	-0.77	0.37	0.48	0.49	0.48
5	18.84	13.76	-0.88	0.28	0.39	0.39	0.39
6	18.96	13.85	-0.97	0.22	0.33	0.34	0.33
7	19.18	13.97	-1.26	-0.01	0.11	0.11	0.10
8	19.29	14.03	-1.41	-0.12	-0.01	-0.01	-0.01
9	19.45	14.16	-1.47	-0.16	-0.04	-0.04	-0.05
10	19.47	14.15	-1.60	-0.27	-0.16	-0.16	-0.16
11	19.59	14.26	-1.59	-0.26	-0.15	-0.14	-0.15
12	19.72	14.37	-1.60	-0.26	-0.14	-0.14	-0.14
13	19.81	14.44	-1.65	-0.31	-0.19	-0.18	-0.19
14	19.94	14.57	-1.61	-0.26	-0.14	-0.14	-0.14
15	20.05	14.68	-1.61	-0.25	-0.13	-0.12	-0.13
16	20.21	14.81	-1.59	-0.22	-0.10	-0.09	-0.10
17	20.34	14.93	-1.58	-0.20	-0.07	-0.07	-0.07
18	20.43	14.99	-1.63	-0.24	-0.12	-0.11	-0.12
19	20.51	15.05	-1.65	-0.26	-0.14	-0.13	-0.14
20	20.66	15.19	-1.67	-0.27	-0.14	-0.14	-0.15
21	20.77	15.28	-1.66	-0.25	-0.12	-0.12	-0.13
22	20.91	15.39	-1.68	-0.26	-0.13	-0.12	-0.13
23	20.90	15.40	-1.68	-0.25	-0.12	-0.12	-0.12
24	21.07	15.54	-1.70	-0.26	-0.13	-0.12	-0.13
25	21.19	15.64	-1.70	-0.25	-0.11	-0.11	-0.12
26	21.31	15.75	-1.72	-0.25	-0.12	-0.11	-0.12
27	21.41	15.83	-1.76	-0.29	-0.15	-0.15	-0.15
28	21.45	15.87	-1.77	-0.29	-0.15	-0.15	-0.16
29	21.48	15.90	-1.76	-0.28	-0.14	-0.13	-0.14
30	21.65	16.06	-1.73	-0.24	-0.10	-0.10	-0.11
31	21.76	16.15	-1.80	-0.30	-0.16	-0.16	-0.16
32	21.80	16.20	-1.78	-0.28	-0.14	-0.13	-0.14
33	21.66	16.08	-1.78	-0.29	-0.15	-0.15	-0.16

Table C.2: Simulation Study Results of $g(t, w)$ smoother than $f(t, w)$ and moderate concurvity:
Beta regression coefficient estimates (x1,000) for Influenza H3N2 at varying DFs for long-term (vertical) and seasonal (horizontal) trends for ages less than 65 years

	0	1	2	3	4	5	6
0	6.20	6.69	7.20	7.14	7.15	7.16	7.16
1	8.15	8.16	7.27	7.40	7.41	7.43	7.43
2	4.05	3.87	2.19	2.37	2.37	2.38	2.38
3	2.21	2.07	0.13	0.38	0.38	0.39	0.39
4	2.45	2.31	0.28	0.56	0.56	0.56	0.56
5	2.54	2.38	0.34	0.61	0.61	0.62	0.62
6	2.41	2.29	0.37	0.62	0.62	0.63	0.63
7	2.29	2.26	0.60	0.81	0.80	0.81	0.81
8	2.26	2.29	0.79	0.98	0.97	0.98	0.98
9	2.24	2.27	0.79	0.96	0.96	0.97	0.97
10	2.36	2.36	0.83	1.01	1.01	1.02	1.02
11	2.33	2.34	0.79	0.98	0.98	0.99	0.99
12	2.00	2.03	0.48	0.70	0.70	0.71	0.71
13	1.57	1.63	0.02	0.29	0.28	0.28	0.29
14	1.38	1.45	-0.28	0.01	-0.00	0.00	0.01
15	1.38	1.47	-0.39	-0.08	-0.09	-0.09	-0.09
16	1.41	1.53	-0.41	-0.08	-0.10	-0.09	-0.09
17	1.39	1.53	-0.43	-0.09	-0.10	-0.10	-0.10
18	1.32	1.48	-0.47	-0.11	-0.12	-0.12	-0.12
19	1.25	1.41	-0.51	-0.14	-0.16	-0.15	-0.15
20	1.26	1.43	-0.53	-0.16	-0.18	-0.17	-0.17
21	1.35	1.49	-0.52	-0.15	-0.17	-0.16	-0.16
22	1.38	1.52	-0.49	-0.13	-0.15	-0.14	-0.14
23	1.39	1.54	-0.49	-0.14	-0.15	-0.15	-0.15
24	1.38	1.53	-0.50	-0.15	-0.17	-0.16	-0.16
25	1.36	1.51	-0.52	-0.17	-0.19	-0.18	-0.18
26	1.33	1.47	-0.54	-0.19	-0.21	-0.20	-0.20
27	1.33	1.47	-0.56	-0.20	-0.21	-0.21	-0.21
28	1.36	1.50	-0.56	-0.19	-0.21	-0.20	-0.20
29	1.42	1.56	-0.54	-0.17	-0.20	-0.19	-0.19
30	1.46	1.59	-0.53	-0.16	-0.18	-0.17	-0.17
31	1.45	1.58	-0.53	-0.16	-0.19	-0.18	-0.18
32	1.40	1.55	-0.55	-0.18	-0.20	-0.19	-0.19
33	1.38	1.52	-0.58	-0.20	-0.22	-0.22	-0.22

Table C.3: Simulation Study Results of $g(t, w)$ smoother than $f(t, w)$ and moderate concurvity:
Beta regression coefficient estimates (x1,000) for Influenza H1N1pdm09 at varying DFs for long-term (vertical) and seasonal (horizontal) trends for ages less than 65 years

	0	1	2	3	4	5	6
0	4.25	2.28	0.35	0.43	0.44	0.44	0.44
1	4.64	2.63	0.37	0.50	0.50	0.51	0.51
2	4.35	2.26	-0.12	0.01	0.01	0.02	0.02
3	4.58	2.50	0.13	0.24	0.25	0.25	0.25
4	4.52	2.44	0.08	0.19	0.20	0.20	0.20
5	4.49	2.43	0.07	0.19	0.19	0.20	0.20
6	4.56	2.48	0.07	0.19	0.19	0.20	0.20
7	4.60	2.50	0.00	0.14	0.14	0.15	0.15
8	4.62	2.50	-0.06	0.08	0.09	0.09	0.09
9	4.61	2.49	-0.07	0.07	0.07	0.08	0.08
10	4.59	2.46	-0.11	0.04	0.04	0.05	0.05
11	4.61	2.48	-0.11	0.04	0.04	0.05	0.05
12	4.63	2.50	-0.09	0.06	0.06	0.06	0.07
13	4.57	2.46	-0.14	0.01	0.02	0.02	0.02
14	4.59	2.47	-0.15	0.00	0.01	0.01	0.01
15	4.62	2.50	-0.15	0.00	0.01	0.01	0.01
16	4.60	2.48	-0.16	-0.01	-0.00	0.00	0.00
17	4.59	2.48	-0.16	-0.01	-0.00	0.00	0.00
18	4.59	2.49	-0.14	0.01	0.02	0.02	0.02
19	4.60	2.50	-0.15	0.01	0.01	0.02	0.02
20	4.60	2.50	-0.14	0.02	0.02	0.03	0.03
21	4.62	2.51	-0.16	0.00	0.01	0.01	0.01
22	4.61	2.52	-0.15	0.01	0.01	0.02	0.02
23	4.64	2.54	-0.15	0.02	0.02	0.03	0.03
24	4.62	2.53	-0.15	0.01	0.02	0.02	0.02
25	4.63	2.54	-0.15	0.01	0.02	0.02	0.02
26	4.65	2.55	-0.14	0.02	0.03	0.04	0.04
27	4.63	2.54	-0.16	0.01	0.01	0.02	0.02
28	4.63	2.53	-0.16	0.01	0.01	0.02	0.02
29	4.65	2.55	-0.15	0.02	0.02	0.03	0.03
30	4.64	2.55	-0.16	0.01	0.01	0.02	0.02
31	4.62	2.54	-0.17	0.00	0.00	0.01	0.01
32	4.65	2.55	-0.17	0.00	0.00	0.01	0.01
33	4.66	2.56	-0.17	-0.00	0.00	0.01	0.01

Table C.4: Simulation Study Results of $g(t, w)$ smoother than $f(t, w)$ and moderate concurvity:
Beta regression coefficient estimates (x1,000) for Influenza B at varying DFs for long-term (vertical) and seasonal (horizontal) trends for ages less than 65 years

	0	1	2	3	4	5	6
0	33.23	27.98	-15.03	-11.20	-10.98	-10.97	-11.00
1	31.86	30.19	-12.06	-6.21	-5.73	-5.69	-5.71
2	32.44	30.09	-16.61	-10.77	-10.34	-10.31	-10.34
3	47.44	45.42	-0.02	4.63	5.01	5.04	5.03
4	43.27	40.43	-6.52	-2.49	-2.20	-2.17	-2.18
5	45.51	42.76	-1.94	0.98	1.20	1.23	1.22
6	43.00	40.80	0.00	2.25	2.42	2.44	2.43
7	40.74	39.82	-0.43	2.08	2.29	2.31	2.30
8	42.57	42.44	-6.35	-2.09	-1.74	-1.71	-1.73
9	42.63	42.45	-6.37	-2.04	-1.70	-1.67	-1.69
10	43.08	42.75	-6.44	-2.11	-1.78	-1.75	-1.77
11	43.93	43.79	-6.03	-1.60	-1.25	-1.21	-1.23
12	44.42	44.53	-5.65	-1.14	-0.77	-0.74	-0.76
13	45.03	45.30	-5.01	-0.55	-0.17	-0.13	-0.16
14	45.18	45.65	-4.87	-0.41	-0.02	0.02	0.00
15	45.17	45.71	-5.03	-0.50	-0.11	-0.07	-0.09
16	45.09	45.64	-5.17	-0.61	-0.21	-0.17	-0.19
17	45.65	46.26	-5.02	-0.35	0.06	0.11	0.09
18	46.02	46.67	-4.91	-0.21	0.20	0.25	0.23
19	46.32	47.01	-4.71	-0.03	0.39	0.43	0.42
20	46.31	47.07	-4.67	-0.00	0.41	0.46	0.44
21	46.04	46.84	-5.06	-0.34	0.08	0.12	0.11
22	45.91	46.75	-5.57	-0.77	-0.35	-0.31	-0.33
23	46.52	47.41	-5.16	-0.34	0.08	0.13	0.11
24	46.57	47.49	-5.00	-0.22	0.20	0.25	0.23
25	46.45	47.40	-5.50	-0.63	-0.20	-0.16	-0.17
26	46.58	47.56	-5.59	-0.68	-0.25	-0.20	-0.22
27	46.56	47.60	-5.81	-0.87	-0.45	-0.40	-0.42
28	46.52	47.59	-5.96	-1.00	-0.56	-0.51	-0.53
29	46.71	47.82	-5.96	-0.93	-0.50	-0.45	-0.48
30	46.90	48.07	-6.38	-1.24	-0.80	-0.75	-0.77
31	47.41	48.62	-6.02	-0.89	-0.44	-0.38	-0.40
32	47.16	48.38	-5.93	-0.84	-0.39	-0.33	-0.36
33	47.21	48.43	-6.10	-1.04	-0.59	-0.54	-0.56

Table C.5: Simulation Study Results of $g(t, w)$ smoother than $f(t, w)$ and high concurvity:
Beta regression coefficient estimates (x1,000) for Influenza H1N1 at varying DFs for long-term (vertical) and seasonal (horizontal) trends for ages less than 65 years

	0	1	2	3	4	5	6
0	45.81	42.84	-3.32	3.12	3.94	3.95	3.92
1	48.35	47.29	0.52	9.87	11.12	11.17	11.15
2	49.19	47.75	-3.68	5.35	6.44	6.47	6.44
3	46.53	45.48	-7.06	1.91	2.94	2.98	2.95
4	47.30	46.26	-6.29	2.80	3.87	3.91	3.87
5	47.03	46.02	-7.08	2.18	3.26	3.30	3.27
6	47.44	46.53	-8.06	1.66	2.77	2.82	2.78
7	49.66	49.18	-12.17	-0.48	0.78	0.83	0.77
8	50.39	50.28	-14.92	-2.18	-0.87	-0.83	-0.89
9	50.53	50.39	-15.28	-2.38	-1.08	-1.03	-1.10
10	50.32	50.12	-15.96	-3.11	-1.83	-1.79	-1.86
11	50.34	50.22	-15.96	-3.01	-1.71	-1.67	-1.74
12	50.67	50.66	-15.61	-2.60	-1.26	-1.21	-1.28
13	51.13	51.20	-15.38	-2.41	-1.05	-0.99	-1.06
14	51.44	51.57	-15.13	-2.14	-0.76	-0.70	-0.76
15	51.57	51.73	-15.06	-2.08	-0.68	-0.62	-0.68
16	51.73	51.90	-15.06	-2.04	-0.62	-0.56	-0.62
17	51.77	51.96	-15.12	-2.03	-0.61	-0.54	-0.60
18	51.75	51.95	-15.31	-2.18	-0.76	-0.69	-0.76
19	51.77	52.00	-15.34	-2.20	-0.77	-0.71	-0.77
20	51.90	52.14	-15.42	-2.20	-0.76	-0.69	-0.76
21	52.00	52.28	-15.46	-2.17	-0.72	-0.65	-0.72
22	52.13	52.41	-15.55	-2.17	-0.71	-0.65	-0.71
23	52.03	52.34	-15.57	-2.18	-0.72	-0.66	-0.72
24	52.12	52.43	-15.71	-2.23	-0.76	-0.69	-0.76
25	52.19	52.51	-15.75	-2.22	-0.74	-0.67	-0.74
26	52.28	52.62	-15.80	-2.23	-0.74	-0.68	-0.74
27	52.40	52.76	-15.92	-2.29	-0.79	-0.73	-0.79
28	52.47	52.84	-15.91	-2.29	-0.78	-0.72	-0.78
29	52.45	52.84	-15.91	-2.28	-0.76	-0.70	-0.76
30	52.52	52.94	-15.90	-2.21	-0.69	-0.62	-0.69
31	52.53	52.96	-16.10	-2.36	-0.82	-0.76	-0.83
32	52.59	53.01	-16.09	-2.33	-0.80	-0.73	-0.80
33	52.51	52.93	-16.09	-2.37	-0.85	-0.79	-0.85

Table C.6: Simulation Study Results of $g(t, w)$ smoother than $f(t, w)$ and high concurvity:
Beta regression coefficient estimates (x1,000) for Influenza H3N2 at varying DFs for long-term (vertical) and seasonal (horizontal) trends for ages less than 65 years

	0	1	2	3	4	5	6
0	8.51	9.75	16.80	15.62	15.50	15.49	15.50
1	19.14	19.27	18.96	18.95	18.93	18.93	18.94
2	12.25	12.21	7.32	8.07	8.11	8.12	8.13
3	7.48	7.55	2.02	3.09	3.14	3.15	3.15
4	7.83	7.95	2.46	3.58	3.64	3.65	3.65
5	8.20	8.29	2.62	3.73	3.79	3.79	3.80
6	7.39	7.51	2.87	3.77	3.81	3.82	3.82
7	5.03	5.16	4.24	4.42	4.40	4.40	4.41
8	3.55	3.63	5.48	5.14	5.07	5.08	5.09
9	3.71	3.80	5.36	5.06	5.00	5.00	5.01
10	4.39	4.48	5.24	5.09	5.05	5.05	5.06
11	4.06	4.13	4.86	4.79	4.74	4.75	4.76
12	2.35	2.39	3.58	3.59	3.52	3.53	3.54
13	0.01	0.03	1.64	1.79	1.69	1.69	1.71
14	-1.60	-1.61	0.10	0.40	0.28	0.28	0.29
15	-2.01	-2.05	-0.51	-0.03	-0.18	-0.18	-0.17
16	-1.79	-1.84	-0.42	0.14	-0.02	-0.02	-0.01
17	-1.57	-1.62	-0.18	0.37	0.21	0.21	0.23
18	-1.52	-1.58	-0.09	0.44	0.29	0.30	0.31
19	-1.65	-1.71	-0.19	0.34	0.19	0.19	0.21
20	-1.86	-1.94	-0.36	0.17	0.02	0.02	0.03
21	-2.08	-2.18	-0.44	0.02	-0.14	-0.14	-0.12
22	-2.30	-2.42	-0.46	-0.05	-0.22	-0.22	-0.21
23	-2.20	-2.34	-0.39	-0.04	-0.21	-0.21	-0.20
24	-2.01	-2.15	-0.24	0.03	-0.14	-0.14	-0.12
25	-1.96	-2.09	-0.22	0.04	-0.12	-0.12	-0.11
26	-2.11	-2.25	-0.32	-0.02	-0.18	-0.18	-0.17
27	-2.38	-2.54	-0.42	-0.08	-0.25	-0.25	-0.24
28	-2.57	-2.75	-0.49	-0.10	-0.29	-0.29	-0.27
29	-2.52	-2.72	-0.47	-0.04	-0.24	-0.24	-0.23
30	-2.41	-2.63	-0.42	0.01	-0.20	-0.20	-0.19
31	-2.38	-2.60	-0.39	0.01	-0.19	-0.19	-0.18
32	-2.42	-2.63	-0.39	-0.01	-0.21	-0.21	-0.20
33	-2.41	-2.62	-0.41	-0.05	-0.23	-0.23	-0.22

Table C.7: Simulation Study Results of $g(t, w)$ smoother than $f(t, w)$ and high concurvity:
Beta regression coefficient estimates (x1,000) for Influenza H1N1pdm09 at varying DFs for long-term (vertical) and seasonal (horizontal) trends for ages less than 65 years

	0	1	2	3	4	5	6
0	0.93	-2.44	1.55	0.99	0.80	0.81	0.82
1	6.17	4.87	3.25	3.67	3.54	3.55	3.56
2	4.36	2.51	-0.72	-0.09	-0.18	-0.16	-0.16
3	5.55	4.11	1.12	1.60	1.52	1.53	1.55
4	5.21	3.61	0.53	0.97	0.88	0.89	0.90
5	5.02	3.47	0.62	1.03	0.94	0.95	0.96
6	5.72	4.34	0.58	1.17	1.09	1.11	1.12
7	6.08	5.40	-0.23	0.75	0.71	0.73	0.74
8	6.45	6.26	-1.38	-0.01	-0.01	0.01	0.02
9	6.27	6.05	-1.42	-0.06	-0.06	-0.04	-0.03
10	6.18	5.87	-1.58	-0.22	-0.23	-0.21	-0.20
11	6.27	6.07	-1.56	-0.17	-0.17	-0.15	-0.15
12	6.28	6.22	-1.35	0.02	0.02	0.04	0.04
13	6.03	6.07	-1.43	-0.08	-0.09	-0.07	-0.07
14	5.98	6.12	-1.45	-0.09	-0.10	-0.08	-0.07
15	5.92	6.10	-1.46	-0.10	-0.10	-0.08	-0.08
16	5.77	5.96	-1.52	-0.16	-0.17	-0.15	-0.14
17	5.67	5.89	-1.55	-0.18	-0.19	-0.17	-0.16
18	5.66	5.91	-1.44	-0.09	-0.10	-0.08	-0.07
19	5.63	5.90	-1.46	-0.10	-0.11	-0.09	-0.08
20	5.59	5.89	-1.42	-0.06	-0.07	-0.05	-0.05
21	5.60	5.94	-1.46	-0.09	-0.10	-0.08	-0.07
22	5.55	5.91	-1.42	-0.05	-0.06	-0.04	-0.03
23	5.57	5.96	-1.41	-0.02	-0.03	-0.01	-0.00
24	5.48	5.87	-1.41	-0.02	-0.04	-0.02	-0.01
25	5.44	5.85	-1.40	-0.02	-0.04	-0.02	-0.01
26	5.40	5.84	-1.39	-0.00	-0.02	0.00	0.01
27	5.35	5.80	-1.41	-0.03	-0.05	-0.03	-0.02
28	5.31	5.79	-1.41	-0.03	-0.05	-0.03	-0.02
29	5.32	5.83	-1.37	0.01	-0.01	0.01	0.01
30	5.25	5.78	-1.37	0.01	-0.02	0.01	0.01
31	5.15	5.70	-1.38	-0.02	-0.04	-0.02	-0.01
32	5.16	5.72	-1.40	-0.02	-0.05	-0.03	-0.02
33	5.20	5.75	-1.40	-0.02	-0.04	-0.02	-0.01

Table C.8: Simulation Study Results of $g(t, w)$ smoother than $f(t, w)$ and high concurvity:
Beta regression coefficient estimates (x1,000) for Influenza B at varying DFs for long-term (vertical) and seasonal (horizontal) trends for ages less than 65 years

	0	1	2	3	4	5	6
0	9.72	5.84	-1.56	-1.53	-1.60	-1.60	-1.60
1	10.08	6.18	-1.48	-1.45	-1.52	-1.51	-1.51
2	9.64	5.67	-2.24	-2.20	-2.29	-2.30	-2.30
3	11.97	7.97	0.07	0.17	0.08	0.08	0.08
4	11.82	7.60	-0.53	-0.42	-0.52	-0.52	-0.52
5	12.42	8.14	-0.13	-0.00	-0.09	-0.10	-0.10
6	12.44	8.17	-0.11	0.01	-0.08	-0.09	-0.08
7	12.39	8.16	-0.08	0.05	-0.05	-0.05	-0.05
8	12.21	7.89	-0.46	-0.34	-0.44	-0.45	-0.44
9	12.00	7.67	-0.74	-0.61	-0.72	-0.72	-0.72
10	12.01	7.73	-0.54	-0.41	-0.51	-0.52	-0.52
11	11.92	7.72	-0.48	-0.36	-0.46	-0.47	-0.47
12	11.76	7.62	-0.58	-0.46	-0.56	-0.57	-0.57
13	12.02	7.75	-0.63	-0.50	-0.61	-0.62	-0.62
14	12.42	7.99	-0.64	-0.50	-0.61	-0.62	-0.62
15	12.57	8.10	-0.61	-0.47	-0.59	-0.60	-0.60
16	12.46	8.02	-0.62	-0.48	-0.59	-0.60	-0.60
17	12.52	8.09	-0.57	-0.43	-0.54	-0.55	-0.55
18	12.57	8.15	-0.59	-0.45	-0.56	-0.57	-0.57
19	12.64	8.18	-0.64	-0.51	-0.62	-0.63	-0.63
20	12.75	8.26	-0.60	-0.46	-0.58	-0.59	-0.59
21	12.74	8.27	-0.60	-0.47	-0.59	-0.59	-0.60
22	12.79	8.31	-0.61	-0.47	-0.58	-0.59	-0.59
23	12.75	8.30	-0.59	-0.45	-0.56	-0.57	-0.57
24	12.83	8.34	-0.63	-0.49	-0.61	-0.62	-0.62
25	13.05	8.55	-0.50	-0.35	-0.47	-0.48	-0.48
26	13.05	8.56	-0.48	-0.33	-0.45	-0.46	-0.46
27	12.93	8.46	-0.57	-0.43	-0.55	-0.56	-0.56
28	13.17	8.71	-0.40	-0.26	-0.38	-0.39	-0.39
29	13.19	8.70	-0.46	-0.32	-0.44	-0.45	-0.45
30	13.18	8.69	-0.49	-0.34	-0.46	-0.47	-0.47
31	13.34	8.84	-0.41	-0.27	-0.39	-0.40	-0.40
32	13.36	8.86	-0.40	-0.26	-0.38	-0.39	-0.39
33	13.21	8.70	-0.52	-0.37	-0.49	-0.51	-0.51

Table C.9: Simulation Study Results of $g(t, w)$ rougher than $f(t, w)$ and moderate concurvity

Beta regression coefficient estimates (x1,000) for Influenza H1N1 at varying DFs for long-term (vertical) and seasonal (horizontal) trends for ages less than 65 years

	0	1	2	3	4	5	6
0	19.37	14.30	2.17	2.17	2.14	2.15	2.16
1	20.14	14.92	2.17	2.19	2.15	2.16	2.17
2	19.54	14.19	1.01	1.03	0.99	0.99	0.99
3	19.18	13.94	0.61	0.67	0.63	0.63	0.63
4	19.33	14.06	0.58	0.64	0.60	0.59	0.60
5	19.42	14.17	0.62	0.69	0.64	0.64	0.64
6	19.47	14.20	0.55	0.62	0.57	0.57	0.57
7	19.61	14.28	0.46	0.53	0.48	0.48	0.48
8	19.71	14.36	0.41	0.48	0.44	0.43	0.43
9	19.94	14.57	0.51	0.59	0.54	0.53	0.53
10	20.07	14.67	0.50	0.57	0.52	0.52	0.52
11	20.24	14.79	0.47	0.54	0.49	0.49	0.49
12	20.49	14.97	0.43	0.51	0.46	0.45	0.45
13	20.74	15.17	0.45	0.53	0.47	0.47	0.47
14	21.08	15.42	0.43	0.51	0.45	0.45	0.45
15	21.23	15.52	0.41	0.49	0.43	0.43	0.43
16	21.40	15.65	0.41	0.49	0.43	0.43	0.43
17	21.49	15.73	0.38	0.45	0.40	0.39	0.40
18	21.61	15.84	0.39	0.46	0.41	0.41	0.41
19	21.68	15.87	0.34	0.41	0.36	0.35	0.35
20	21.85	16.02	0.36	0.43	0.38	0.37	0.37
21	21.96	16.11	0.36	0.43	0.38	0.37	0.37
22	22.07	16.20	0.33	0.40	0.35	0.34	0.34
23	22.24	16.35	0.34	0.42	0.36	0.35	0.35
24	22.36	16.44	0.28	0.36	0.30	0.30	0.30
25	22.50	16.56	0.32	0.40	0.34	0.34	0.34
26	22.69	16.73	0.32	0.40	0.34	0.34	0.34
27	22.71	16.73	0.21	0.29	0.23	0.23	0.23
28	22.96	16.94	0.28	0.37	0.31	0.30	0.30
29	23.07	17.05	0.31	0.39	0.33	0.33	0.33
30	23.22	17.19	0.34	0.43	0.37	0.36	0.36
31	23.34	17.27	0.27	0.36	0.30	0.29	0.29
32	23.45	17.38	0.29	0.38	0.32	0.31	0.31
33	23.24	17.21	0.30	0.38	0.32	0.31	0.32

Table C.10: Simulation Study Results of $g(t, w)$ rougher than $f(t, w)$ and moderate concurvity

Beta regression coefficient estimates (x1,000) for Influenza H3N2 at varying DFs for long-term (vertical) and seasonal (horizontal) trends for ages less than 65 years

	0	1	2	3	4	5	6
0	7.33	7.51	6.89	6.91	6.92	6.92	6.92
1	8.95	8.73	6.98	7.02	7.02	7.03	7.03
2	4.17	3.81	1.44	1.48	1.46	1.47	1.46
3	2.36	2.11	-0.44	-0.42	-0.43	-0.43	-0.44
4	2.47	2.23	-0.35	-0.33	-0.34	-0.35	-0.35
5	2.83	2.53	-0.16	-0.15	-0.16	-0.17	-0.17
6	2.87	2.56	-0.14	-0.13	-0.14	-0.15	-0.15
7	2.87	2.62	0.02	0.03	0.02	0.02	0.02
8	2.98	2.77	0.20	0.22	0.21	0.21	0.20
9	2.95	2.74	0.12	0.14	0.13	0.13	0.12
10	2.89	2.67	0.05	0.07	0.06	0.05	0.05
11	2.87	2.67	0.06	0.08	0.07	0.06	0.06
12	2.72	2.61	0.10	0.11	0.11	0.10	0.10
13	2.37	2.44	0.11	0.12	0.12	0.11	0.11
14	2.00	2.22	0.08	0.09	0.09	0.08	0.08
15	1.91	2.20	0.09	0.10	0.10	0.09	0.09
16	2.05	2.30	0.11	0.12	0.12	0.11	0.11
17	2.15	2.36	0.11	0.12	0.11	0.11	0.11
18	2.11	2.33	0.10	0.11	0.11	0.10	0.10
19	2.02	2.27	0.09	0.10	0.10	0.09	0.09
20	1.97	2.24	0.07	0.08	0.08	0.07	0.07
21	1.99	2.25	0.07	0.09	0.08	0.08	0.08
22	2.06	2.32	0.12	0.14	0.14	0.13	0.13
23	2.14	2.39	0.15	0.17	0.17	0.16	0.16
24	2.15	2.39	0.14	0.16	0.15	0.15	0.15
25	2.11	2.35	0.12	0.13	0.13	0.12	0.12
26	2.05	2.30	0.09	0.10	0.10	0.09	0.09
27	2.07	2.34	0.09	0.10	0.10	0.09	0.09
28	2.21	2.49	0.11	0.12	0.12	0.11	0.11
29	2.40	2.67	0.14	0.16	0.15	0.15	0.15
30	2.53	2.78	0.17	0.18	0.18	0.17	0.17
31	2.48	2.73	0.17	0.19	0.18	0.17	0.17
32	2.34	2.61	0.14	0.16	0.16	0.15	0.15
33	2.29	2.56	0.14	0.16	0.16	0.15	0.15

Table C.11: Simulation Study Results of $g(t, w)$ rougher than $f(t, w)$ and moderate concurvity
Beta regression coefficient estimates (x1,000) for Influenza H1N1pdm09 at varying DFs for long-term (vertical) and seasonal (horizontal) trends for ages less than 65 years

	0	1	2	3	4	5	6
0	2.64	0.36	0.16	0.19	0.15	0.15	0.15
1	2.90	0.58	0.18	0.21	0.16	0.17	0.16
2	2.59	0.22	-0.26	-0.24	-0.30	-0.30	-0.30
3	2.82	0.47	-0.01	0.08	0.02	0.03	0.02
4	2.81	0.46	-0.03	0.06	0.00	0.00	0.00
5	2.84	0.50	0.01	0.11	0.05	0.05	0.05
6	2.83	0.50	0.02	0.12	0.06	0.06	0.06
7	2.82	0.48	-0.01	0.09	0.03	0.03	0.03
8	2.77	0.43	-0.08	0.02	-0.04	-0.04	-0.04
9	2.76	0.41	-0.09	0.01	-0.06	-0.06	-0.06
10	2.76	0.42	-0.07	0.03	-0.03	-0.03	-0.03
11	2.77	0.43	-0.09	0.01	-0.05	-0.05	-0.05
12	2.76	0.43	-0.09	0.01	-0.06	-0.06	-0.06
13	2.85	0.49	-0.06	0.04	-0.03	-0.03	-0.03
14	2.88	0.52	-0.06	0.04	-0.02	-0.02	-0.03
15	2.86	0.50	-0.08	0.02	-0.04	-0.04	-0.05
16	2.85	0.50	-0.06	0.04	-0.02	-0.02	-0.03
17	2.82	0.47	-0.07	0.03	-0.04	-0.04	-0.04
18	2.82	0.48	-0.06	0.04	-0.02	-0.02	-0.02
19	2.85	0.49	-0.06	0.04	-0.02	-0.02	-0.03
20	2.82	0.47	-0.07	0.03	-0.03	-0.03	-0.04
21	2.82	0.47	-0.06	0.04	-0.03	-0.03	-0.03
22	2.80	0.47	-0.05	0.05	-0.02	-0.02	-0.02
23	2.80	0.45	-0.08	0.02	-0.05	-0.05	-0.05
24	2.79	0.45	-0.07	0.03	-0.03	-0.03	-0.04
25	2.76	0.43	-0.08	0.02	-0.05	-0.05	-0.05
26	2.78	0.45	-0.08	0.03	-0.04	-0.04	-0.05
27	2.80	0.47	-0.07	0.03	-0.04	-0.04	-0.04
28	2.74	0.43	-0.10	0.01	-0.06	-0.06	-0.06
29	2.77	0.45	-0.09	0.01	-0.06	-0.06	-0.06
30	2.76	0.45	-0.10	0.00	-0.07	-0.07	-0.07
31	2.74	0.44	-0.11	-0.00	-0.07	-0.07	-0.08
32	2.74	0.43	-0.10	0.00	-0.07	-0.07	-0.07
33	2.76	0.44	-0.10	0.01	-0.06	-0.06	-0.06

Table C.12: Simulation Study Results of $g(t, w)$ rougher than $f(t, w)$ and moderate concurvity

Beta regression coefficient estimates (x1,000) for Influenza B at varying DFs for long-term (vertical) and seasonal (horizontal) trends for ages less than 65 years

	0	1	2	3	4	5	6
0	27.17	26.29	-4.16	-4.19	-4.19	-4.18	-4.17
1	32.67	32.18	0.68	0.63	0.77	0.92	0.92
2	30.43	29.52	-9.17	-8.97	-9.28	-9.25	-9.25
3	38.23	37.36	0.22	0.41	0.14	0.11	0.12
4	37.95	36.86	-2.58	-2.30	-2.70	-2.73	-2.72
5	46.82	45.65	1.08	1.48	1.07	1.05	1.06
6	47.61	46.49	0.99	1.35	0.98	0.95	0.96
7	45.49	44.64	1.61	1.92	1.57	1.54	1.55
8	45.58	44.43	-1.19	-0.83	-1.36	-1.41	-1.40
9	41.69	40.50	-4.25	-3.79	-4.55	-4.59	-4.58
10	34.15	33.05	-1.63	-0.96	-1.98	-2.01	-2.00
11	28.54	27.80	-0.94	-0.28	-1.26	-1.28	-1.27
12	27.73	27.30	-1.01	-0.44	-1.31	-1.33	-1.32
13	30.30	29.68	-0.68	0.04	-1.10	-1.13	-1.12
14	38.42	37.90	-1.08	-0.14	-1.64	-1.66	-1.66
15	37.97	37.69	-0.93	0.08	-1.55	-1.59	-1.58
16	36.53	36.24	-0.92	0.02	-1.46	-1.50	-1.49
17	33.65	33.40	-0.79	0.12	-1.29	-1.34	-1.33
18	35.15	34.95	-1.11	-0.14	-1.68	-1.72	-1.72
19	36.59	36.45	-1.25	-0.20	-1.86	-1.90	-1.89
20	36.64	36.48	-0.98	0.08	-1.60	-1.64	-1.64
21	36.40	36.23	-0.78	0.25	-1.39	-1.43	-1.43
22	36.69	36.56	-0.81	0.22	-1.45	-1.49	-1.48
23	37.22	37.15	-0.88	0.20	-1.50	-1.54	-1.54
24	37.08	37.04	-0.84	0.27	-1.46	-1.49	-1.49
25	37.33	37.30	-0.41	0.69	-1.02	-1.05	-1.05
26	36.42	36.38	-0.54	0.55	-1.16	-1.20	-1.19
27	35.98	35.99	-0.70	0.42	-1.29	-1.33	-1.33
28	36.59	36.65	-0.49	0.66	-1.04	-1.07	-1.07
29	36.75	36.81	-0.43	0.70	-1.04	-1.07	-1.06
30	36.65	36.74	-0.40	0.76	-0.97	-1.01	-1.00
31	35.90	35.99	-0.65	0.51	-1.21	-1.25	-1.25
32	36.08	36.19	-0.60	0.56	-1.19	-1.22	-1.22
33	36.52	36.63	-0.63	0.55	-1.17	-1.20	-1.20

Table C.13: Simulation Study Results of $g(t, w)$ rougher than $f(t, w)$ and high concurvity

Beta regression coefficient estimates (x1,000) for Influenza H1N1 at varying DFs for long-term (vertical) and seasonal (horizontal) trends for ages less than 65 years

	0	1	2	3	4	5	6
0	58.85	53.98	7.18	7.20	7.20	7.31	7.31
1	65.63	63.71	14.77	15.25	15.54	15.91	15.91
2	64.72	61.77	3.97	4.14	3.65	3.73	3.74
3	62.60	59.58	-1.78	-1.39	-1.80	-1.84	-1.83
4	62.71	59.74	-1.44	-1.06	-1.48	-1.52	-1.51
5	62.62	60.13	-0.47	-0.00	-0.37	-0.39	-0.38
6	62.37	59.79	-0.81	-0.35	-0.70	-0.73	-0.72
7	63.33	60.90	-1.00	-0.52	-0.93	-0.98	-0.96
8	63.42	60.93	-1.12	-0.71	-1.22	-1.29	-1.27
9	64.21	61.77	-0.16	0.23	-0.29	-0.36	-0.34
10	66.08	63.64	-0.75	-0.41	-0.78	-0.85	-0.83
11	67.94	65.59	-1.00	-0.68	-1.04	-1.11	-1.09
12	69.21	67.13	-1.00	-0.64	-1.07	-1.14	-1.12
13	70.14	68.41	-1.22	-0.84	-1.28	-1.35	-1.33
14	70.14	69.11	-1.14	-0.68	-1.29	-1.36	-1.35
15	72.33	71.78	-1.54	-1.04	-1.71	-1.78	-1.77
16	72.39	71.79	-1.18	-0.69	-1.32	-1.40	-1.38
17	73.04	72.47	-1.23	-0.74	-1.36	-1.44	-1.42
18	73.02	72.56	-1.29	-0.80	-1.48	-1.56	-1.54
19	73.02	72.66	-1.36	-0.86	-1.55	-1.63	-1.61
20	73.15	72.79	-1.31	-0.80	-1.48	-1.55	-1.53
21	73.30	72.95	-1.34	-0.83	-1.50	-1.58	-1.56
22	73.57	73.28	-1.29	-0.78	-1.49	-1.57	-1.55
23	73.54	73.31	-1.31	-0.79	-1.50	-1.57	-1.56
24	73.77	73.57	-1.21	-0.70	-1.40	-1.47	-1.46
25	73.94	73.79	-1.27	-0.74	-1.44	-1.51	-1.50
26	74.21	74.07	-1.34	-0.81	-1.52	-1.61	-1.59
27	74.41	74.31	-1.22	-0.67	-1.39	-1.47	-1.45
28	74.31	74.26	-1.28	-0.71	-1.44	-1.51	-1.49
29	74.52	74.48	-1.18	-0.64	-1.37	-1.45	-1.43
30	74.71	74.71	-1.35	-0.80	-1.54	-1.62	-1.59
31	74.95	74.99	-1.34	-0.77	-1.52	-1.60	-1.58
32	75.05	75.10	-1.29	-0.73	-1.48	-1.56	-1.53
33	74.89	74.93	-1.19	-0.62	-1.34	-1.41	-1.39

Table C.14: Simulation Study Results of $g(t, w)$ rougher than $f(t, w)$ and high concurvity

Beta regression coefficient estimates (x1,000) for Influenza H3N2 at varying DFs for long-term (vertical) and seasonal (horizontal) trends for ages less than 65 years

	0	1	2	3	4	5	6
0	14.52	14.63	13.92	13.94	13.93	13.92	13.93
1	28.30	27.84	19.05	19.29	19.46	19.55	19.55
2	21.64	20.47	3.88	4.04	3.66	3.69	3.69
3	18.03	16.81	-2.32	-2.02	-2.36	-2.38	-2.38
4	17.98	16.78	-2.11	-1.81	-2.16	-2.19	-2.18
5	19.88	18.81	-1.11	-0.75	-1.06	-1.08	-1.07
6	20.60	19.50	-1.21	-0.85	-1.15	-1.18	-1.17
7	20.08	19.17	-0.67	-0.35	-0.64	-0.68	-0.66
8	20.52	19.60	-0.14	0.14	-0.21	-0.25	-0.24
9	20.81	19.88	-0.24	0.03	-0.34	-0.38	-0.37
10	20.43	19.49	-0.35	-0.06	-0.42	-0.46	-0.45
11	19.00	18.12	-0.22	0.11	-0.31	-0.34	-0.33
12	16.70	16.08	-0.20	0.12	-0.29	-0.33	-0.31
13	13.40	13.07	-0.20	0.07	-0.26	-0.30	-0.28
14	8.73	8.69	-0.17	0.03	-0.18	-0.22	-0.20
15	5.10	5.13	-0.09	0.08	-0.05	-0.09	-0.08
16	5.91	5.92	-0.14	0.05	-0.11	-0.15	-0.14
17	7.23	7.22	-0.12	0.10	-0.12	-0.15	-0.14
18	7.49	7.49	-0.03	0.20	-0.03	-0.07	-0.05
19	6.96	6.97	0.03	0.22	0.04	-0.00	0.01
20	6.47	6.49	0.03	0.19	0.05	0.01	0.03
21	6.25	6.28	-0.02	0.13	0.00	-0.04	-0.02
22	6.15	6.18	-0.07	0.10	-0.06	-0.10	-0.08
23	6.02	6.06	-0.04	0.15	-0.03	-0.07	-0.05
24	5.75	5.78	-0.01	0.16	-0.01	-0.04	-0.02
25	5.69	5.71	-0.03	0.14	-0.02	-0.05	-0.04
26	6.04	6.06	-0.09	0.06	-0.10	-0.13	-0.12
27	6.76	6.79	-0.27	-0.10	-0.28	-0.32	-0.30
28	7.67	7.70	-0.36	-0.18	-0.38	-0.41	-0.39
29	8.20	8.23	-0.33	-0.13	-0.36	-0.39	-0.37
30	8.11	8.14	-0.25	-0.05	-0.27	-0.30	-0.28
31	7.66	7.68	-0.18	0.01	-0.19	-0.22	-0.21
32	7.15	7.18	-0.19	-0.01	-0.20	-0.23	-0.22
33	6.91	6.94	-0.31	-0.14	-0.32	-0.36	-0.34

Table C.15: Simulation Study Results of $g(t, w)$ rougher than $f(t, w)$ and high concurvity

Beta regression coefficient estimates (x1,000) for Influenza H1N1pdm09 at varying DFs for long-term (vertical) and seasonal (horizontal) trends for ages less than 65 years

	0	1	2	3	4	5	6
0	-9.66	-13.22	1.03	1.50	1.20	1.28	1.25
1	-6.88	-8.23	1.73	3.21	3.86	4.04	4.00
2	-7.69	-9.76	0.38	0.50	-0.49	-0.42	-0.45
3	-7.66	-9.77	0.85	1.55	0.66	0.66	0.65
4	-7.69	-9.78	1.00	1.66	0.73	0.73	0.73
5	-8.58	-10.32	0.66	1.49	0.73	0.73	0.73
6	-8.79	-10.61	0.77	1.63	0.86	0.86	0.86
7	-8.65	-10.35	0.61	1.43	0.61	0.61	0.61
8	-8.92	-10.69	0.50	1.11	0.12	0.11	0.10
9	-8.81	-10.56	0.51	1.10	0.04	0.03	0.03
10	-9.01	-10.73	0.52	1.19	0.20	0.19	0.19
11	-9.24	-10.88	0.54	1.23	0.21	0.20	0.20
12	-9.39	-10.76	0.49	1.15	0.13	0.12	0.12
13	-10.05	-11.20	0.53	1.22	0.15	0.15	0.14
14	-10.26	-10.93	0.49	1.15	0.04	0.04	0.03
15	-11.42	-11.77	0.60	1.27	0.16	0.15	0.15
16	-11.39	-11.77	0.51	1.20	0.11	0.11	0.10
17	-11.39	-11.75	0.51	1.21	0.11	0.11	0.10
18	-11.49	-11.79	0.53	1.20	0.07	0.07	0.06
19	-11.60	-11.84	0.60	1.28	0.15	0.15	0.14
20	-11.73	-11.97	0.55	1.24	0.12	0.12	0.11
21	-11.81	-12.05	0.55	1.24	0.13	0.13	0.12
22	-12.01	-12.20	0.49	1.16	0.03	0.03	0.02
23	-11.95	-12.12	0.55	1.24	0.11	0.11	0.10
24	-12.09	-12.23	0.53	1.23	0.10	0.09	0.09
25	-12.21	-12.33	0.49	1.19	0.07	0.07	0.06
26	-12.22	-12.33	0.49	1.19	0.06	0.05	0.05
27	-12.21	-12.30	0.49	1.21	0.08	0.08	0.07
28	-12.16	-12.22	0.51	1.25	0.13	0.13	0.13
29	-12.33	-12.38	0.42	1.13	-0.01	-0.01	-0.02
30	-12.41	-12.44	0.50	1.22	0.09	0.09	0.08
31	-12.40	-12.40	0.55	1.27	0.15	0.14	0.14
32	-12.53	-12.53	0.51	1.23	0.09	0.09	0.08
33	-12.50	-12.51	0.53	1.27	0.15	0.15	0.14

Table C.16: Simulation Study Results of $g(t, w)$ rougher than $f(t, w)$ and high concurvity

Beta regression coefficient estimates (x1,000) for Influenza B at varying DFs for long-term (vertical) and seasonal (horizontal) trends for ages less than 65 years

	0	1	2	3	4	5	6
0	13.31	11.44	2.19	1.67	1.56	1.40	1.28
1	13.37	11.50	2.27	1.74	1.63	1.46	1.35
2	12.90	11.06	1.81	1.27	1.16	0.99	0.86
3	13.84	12.01	2.67	2.12	2.01	1.83	1.71
4	13.85	11.88	2.19	1.58	1.47	1.27	1.14
5	13.84	11.87	2.17	1.57	1.45	1.26	1.13
6	13.74	11.78	2.13	1.54	1.43	1.23	1.10
7	13.78	11.83	2.17	1.58	1.47	1.27	1.13
8	13.73	11.78	2.12	1.53	1.41	1.21	1.08
9	13.69	11.74	2.09	1.49	1.38	1.18	1.05
10	13.75	11.78	2.13	1.53	1.41	1.21	1.08
11	13.52	11.54	1.97	1.38	1.26	1.06	0.93
12	13.38	11.43	1.93	1.37	1.25	1.05	0.92
13	13.74	11.79	2.19	1.59	1.47	1.27	1.14
14	13.97	12.02	2.31	1.68	1.55	1.36	1.23
15	14.00	12.06	2.32	1.69	1.56	1.37	1.24
16	14.11	12.23	2.50	1.89	1.76	1.57	1.44
17	14.04	12.17	2.48	1.89	1.76	1.57	1.44
18	14.11	12.25	2.53	1.92	1.80	1.61	1.48
19	14.02	12.17	2.51	1.91	1.79	1.60	1.47
20	14.21	12.32	2.62	2.00	1.88	1.68	1.56
21	14.26	12.38	2.64	2.03	1.91	1.71	1.58
22	14.02	12.20	2.53	1.93	1.81	1.62	1.49
23	14.35	12.50	2.72	2.09	1.96	1.77	1.64
24	14.47	12.58	2.86	2.27	2.14	1.95	1.82
25	14.59	12.69	3.11	2.54	2.42	2.23	2.10
26	14.64	12.71	3.16	2.58	2.46	2.26	2.13
27	14.02	12.17	2.80	2.25	2.14	1.94	1.81
28	14.40	12.59	2.89	2.36	2.25	2.05	1.92
29	14.32	12.49	2.64	2.11	1.98	1.78	1.65
30	14.74	12.79	2.94	2.37	2.24	2.04	1.90
31	15.10	13.11	3.37	2.82	2.69	2.50	2.36
32	15.07	13.03	3.18	2.63	2.50	2.30	2.15
33	14.56	12.62	2.98	2.46	2.34	2.14	2.00

Table C.17: Data Analysis Results:
Beta regression coefficient estimates (x1,000) for Influenza H1N1 at varying DFs for long-term (vertical) and seasonal (horizontal) trends for ages less than 65 years

	0	1	2	3	4	5	6
0	24.31	21.59	10.09	8.79	8.62	8.44	8.34
1	24.23	21.52	9.99	8.71	8.55	8.37	8.26
2	24.44	21.72	10.02	8.74	8.58	8.39	8.28
3	24.36	21.76	10.17	8.90	8.75	8.56	8.45
4	24.36	21.74	10.06	8.78	8.62	8.42	8.30
5	24.36	21.75	10.07	8.80	8.64	8.43	8.32
6	24.34	21.74	10.05	8.78	8.62	8.41	8.30
7	24.37	21.75	9.96	8.69	8.53	8.31	8.20
8	24.43	21.82	10.04	8.77	8.61	8.39	8.28
9	24.50	21.89	10.11	8.83	8.67	8.46	8.35
10	24.51	21.92	10.15	8.88	8.72	8.51	8.40
11	24.62	22.05	10.25	8.97	8.80	8.60	8.48
12	24.80	22.21	10.36	9.06	8.89	8.68	8.57
13	24.85	22.31	10.47	9.16	8.99	8.79	8.68
14	25.02	22.49	10.62	9.28	9.11	8.91	8.80
15	25.11	22.60	10.69	9.33	9.16	8.96	8.85
16	25.12	22.62	10.70	9.32	9.15	8.95	8.84
17	25.18	22.68	10.75	9.36	9.19	8.99	8.88
18	25.18	22.70	10.76	9.37	9.20	9.00	8.89
19	25.19	22.71	10.77	9.37	9.20	9.00	8.89
20	25.19	22.72	10.77	9.37	9.20	9.00	8.90
21	25.15	22.68	10.72	9.32	9.15	8.95	8.84
22	25.22	22.74	10.80	9.39	9.22	9.02	8.91
23	25.15	22.69	10.76	9.35	9.19	8.99	8.88
24	25.07	22.62	10.68	9.26	9.09	8.89	8.79
25	25.09	22.65	10.63	9.20	9.03	8.84	8.73
26	24.97	22.54	10.47	9.04	8.87	8.67	8.57
27	25.27	22.80	10.63	9.18	9.00	8.80	8.70
28	25.18	22.73	10.62	9.20	9.02	8.83	8.72
29	25.24	22.78	10.67	9.22	9.05	8.85	8.74
30	25.20	22.77	10.75	9.30	9.13	8.93	8.83
31	25.05	22.68	10.60	9.20	9.04	8.85	8.75
32	25.36	22.97	10.70	9.28	9.11	8.91	8.81
33	25.10	22.68	10.61	9.16	8.98	8.79	8.69

Table C.18: Data Analysis Results:
Beta regression coefficient estimates (x1,000) for Influenza H3N2 at varying DFs for long-term (vertical) and seasonal (horizontal) trends for ages less than 65 years

	0	1	2	3	4	5	6
0	11.84	11.50	10.64	10.86	10.88	10.86	10.83
1	11.53	11.21	10.25	10.52	10.55	10.53	10.49
2	9.18	8.90	8.12	8.40	8.43	8.41	8.37
3	8.65	8.42	7.81	8.11	8.13	8.12	8.08
4	8.69	8.44	7.75	8.04	8.06	8.05	8.00
5	8.88	8.61	7.88	8.15	8.18	8.16	8.12
6	8.82	8.56	7.87	8.15	8.18	8.16	8.12
7	8.81	8.56	7.96	8.25	8.28	8.26	8.22
8	8.83	8.58	7.99	8.27	8.30	8.29	8.25
9	8.83	8.59	7.97	8.26	8.29	8.27	8.23
10	8.92	8.65	8.00	8.28	8.31	8.29	8.25
11	8.86	8.55	7.90	8.18	8.21	8.19	8.14
12	8.19	7.91	7.48	7.84	7.87	7.85	7.80
13	7.20	7.04	6.97	7.44	7.48	7.46	7.42
14	6.46	6.41	6.66	7.22	7.26	7.25	7.21
15	6.28	6.28	6.63	7.20	7.24	7.24	7.19
16	6.43	6.43	6.70	7.24	7.29	7.28	7.23
17	6.64	6.60	6.77	7.28	7.33	7.32	7.27
18	6.91	6.81	6.94	7.43	7.47	7.46	7.42
19	7.21	7.07	7.22	7.72	7.76	7.75	7.70
20	7.29	7.14	7.37	7.89	7.94	7.93	7.88
21	6.98	6.87	7.21	7.75	7.80	7.79	7.74
22	6.69	6.60	6.96	7.49	7.54	7.53	7.48
23	6.79	6.69	6.93	7.42	7.47	7.46	7.41
24	7.11	6.97	7.15	7.65	7.69	7.68	7.63
25	7.47	7.32	7.55	8.12	8.16	8.15	8.10
26	7.62	7.50	7.92	8.59	8.65	8.63	8.58
27	7.25	7.19	7.84	8.60	8.67	8.65	8.60
28	6.78	6.77	7.47	8.22	8.28	8.27	8.22
29	6.61	6.60	7.21	7.90	7.96	7.95	7.90
30	6.96	6.90	7.35	7.98	8.03	8.02	7.97
31	7.59	7.43	7.78	8.38	8.43	8.42	8.36
32	8.08	7.85	8.16	8.80	8.86	8.83	8.77
33	7.92	7.70	8.20	8.96	9.03	9.01	8.93

Table C.19: Data Analysis Results:
Beta regression coefficient estimates (x1,000) for Influenza H1N1pdm09 at varying DFs for long-term (vertical) and seasonal (horizontal) trends for ages less than 65 years

	0	1	2	3	4	5	6
0	10.07	7.15	5.74	3.60	3.36	3.25	3.22
1	10.06	7.15	5.73	3.60	3.36	3.25	3.23
2	10.11	7.21	5.72	3.64	3.43	3.32	3.29
3	10.15	7.35	5.90	3.86	3.64	3.53	3.50
4	10.14	7.33	5.81	3.76	3.54	3.43	3.40
5	10.14	7.34	5.84	3.80	3.58	3.46	3.43
6	10.19	7.39	5.86	3.81	3.60	3.48	3.45
7	10.16	7.36	5.82	3.78	3.56	3.44	3.41
8	10.20	7.41	5.86	3.82	3.60	3.48	3.45
9	10.24	7.44	5.86	3.81	3.59	3.47	3.44
10	10.36	7.56	5.94	3.89	3.67	3.55	3.52
11	10.44	7.61	5.95	3.89	3.67	3.54	3.51
12	10.34	7.54	5.91	3.87	3.65	3.52	3.49
13	10.52	7.75	6.04	3.99	3.78	3.65	3.62
14	10.48	7.76	6.05	4.01	3.79	3.67	3.64
15	10.54	7.85	6.10	4.05	3.84	3.72	3.69
16	10.61	7.91	6.14	4.07	3.86	3.74	3.71
17	10.64	7.94	6.13	4.05	3.83	3.71	3.68
18	10.69	7.99	6.20	4.11	3.90	3.77	3.74
19	10.73	8.04	6.25	4.16	3.95	3.83	3.79
20	10.68	8.00	6.22	4.14	3.92	3.80	3.77
21	10.62	7.95	6.18	4.10	3.88	3.76	3.73
22	10.78	8.08	6.23	4.12	3.90	3.77	3.74
23	10.80	8.10	6.29	4.18	3.97	3.84	3.81
24	10.76	8.09	6.27	4.17	3.95	3.83	3.80
25	10.76	8.07	6.25	4.12	3.90	3.79	3.76
26	10.76	8.05	6.26	4.11	3.88	3.76	3.74
27	10.68	7.94	6.17	3.98	3.75	3.63	3.61
28	10.63	7.87	6.22	3.99	3.76	3.64	3.62
29	10.69	7.97	6.28	4.08	3.86	3.74	3.71
30	10.65	7.97	6.15	3.97	3.75	3.63	3.60
31	10.66	7.88	6.30	4.08	3.85	3.73	3.71
32	10.40	7.69	6.25	4.06	3.84	3.72	3.70
33	10.80	8.03	6.26	4.04	3.80	3.68	3.65

Table C.20: Data Analysis Results:
Beta regression coefficient estimates (x1,000) for Influenza B at varying DFs for long-term (vertical) and seasonal (horizontal) trends for ages less than 65 years

	0	1	2	3	4	5	6
0	97918.90	85136.35	48437.63	40701.42	39724.33	38920.32	38479.02
1	97579.13	84820.96	47972.89	40339.68	39370.68	38550.09	38101.52
2	95954.02	83244.24	45900.15	38365.90	37464.56	36622.66	36146.92
3	96134.95	83926.73	47116.35	39725.68	38839.18	37984.71	37530.17
4	96146.69	83759.52	46207.08	38691.47	37784.52	36870.30	36387.81
5	96263.94	83928.25	46389.40	38894.16	37990.96	37070.19	36591.25
6	96202.83	83876.96	46344.89	38864.35	37962.35	37035.96	36556.88
7	96220.85	83881.57	46163.34	38679.65	37766.43	36818.35	36333.91
8	96403.83	84114.66	46404.09	38929.95	38016.06	37073.85	36592.30
9	96582.10	84283.36	46514.70	39025.82	38107.13	37171.75	36690.12
10	96925.41	84645.64	46853.94	39366.25	38445.47	37519.80	37039.54
11	97076.70	84735.89	46871.12	39348.63	38415.41	37475.64	36986.08
12	96603.19	84317.02	46648.65	39211.55	38285.25	37351.25	36859.78
13	96488.21	84472.55	46988.53	39575.03	38659.36	37743.88	37259.26
14	96283.10	84504.75	47187.47	39784.19	38874.04	37967.80	37488.06
15	96450.98	84813.87	47439.78	39987.84	39075.54	38168.50	37690.57
16	96777.02	85198.50	47742.64	40221.57	39305.56	38407.04	37934.11
17	97074.46	85482.97	47894.01	40294.26	39372.49	38467.24	37992.78
18	97408.08	85840.63	48224.43	40601.38	39682.45	38778.42	38305.36
19	97674.07	86098.98	48554.53	40936.44	40016.93	39113.41	38640.66
20	97788.02	86226.54	48741.59	41119.48	40200.35	39299.99	38829.78
21	97390.80	85852.43	48420.91	40814.70	39898.11	38990.17	38515.72
22	97400.32	85868.59	48400.22	40720.83	39802.65	38898.29	38423.28
23	97617.06	86123.34	48553.80	40851.08	39936.47	39034.84	38561.35
24	97756.18	86243.15	48639.64	40956.79	40042.53	39141.09	38669.71
25	98169.41	86636.48	49063.56	41358.07	40435.47	39545.81	39083.25
26	98097.08	86527.82	49054.82	41363.23	40433.60	39532.04	39067.11
27	97770.64	86195.62	48863.05	41165.25	40227.42	39325.82	38856.43
28	97418.13	85890.90	48711.76	41001.41	40071.48	39182.60	38716.68
29	97440.94	85982.92	48499.89	40757.34	39832.42	38925.49	38448.85
30	97893.64	86413.31	48823.36	41017.87	40084.00	39188.50	38716.57
31	98367.96	86765.15	49499.11	41726.36	40795.79	39925.10	39468.49
32	98896.54	87302.33	49750.93	42039.45	41108.41	40219.10	39749.51
33	98601.62	86877.40	49444.89	41693.29	40752.26	39847.74	39367.46

Table C.21: Data Analysis Results:
Influenza-associated Mortality estimates at varying DFs for long-term (vertical) and seasonal (horizontal) trends for ages less than 65 years

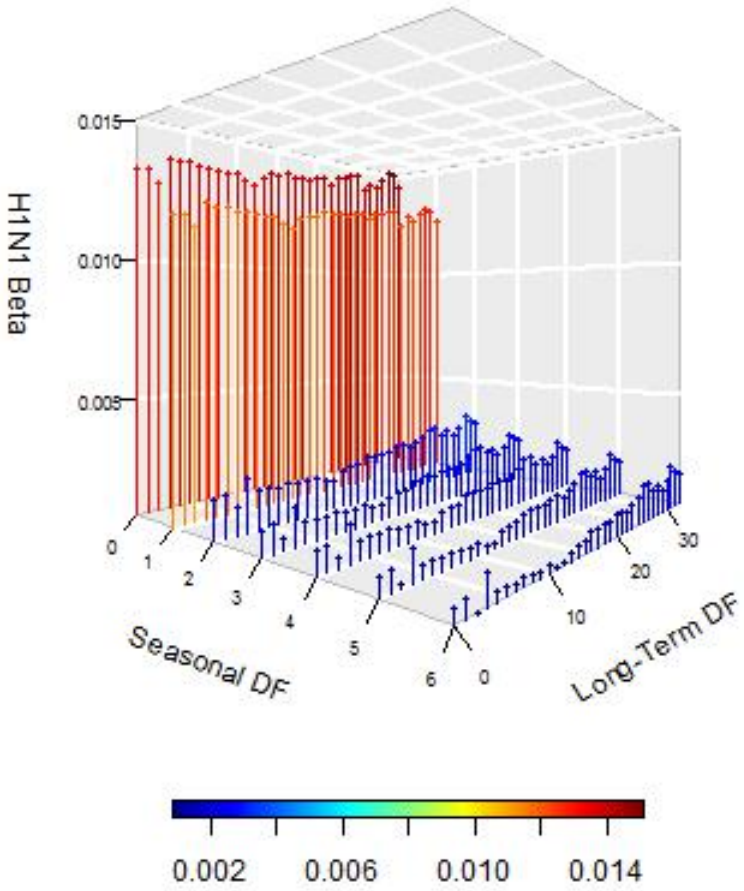

Figure C.1: Estimate beta coefficients of Influenza A(H1N1) as the degrees of freedom for long-term and seasonal trends vary

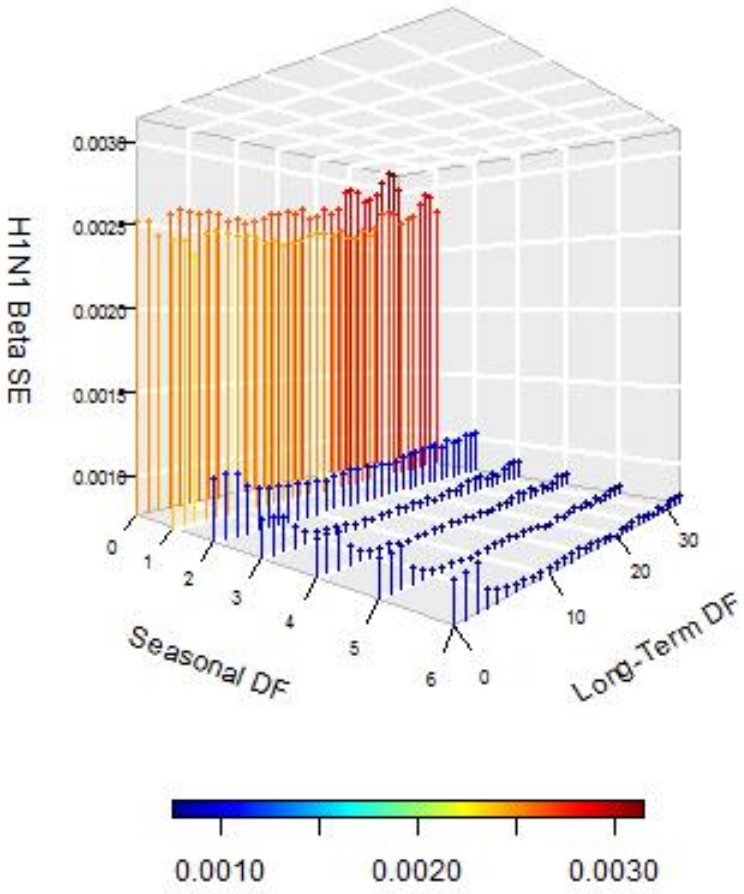

Figure C.2: Beta coefficients standard error of Influenza A(H1N1) as the degrees of freedom for long-term and seasonal trends vary

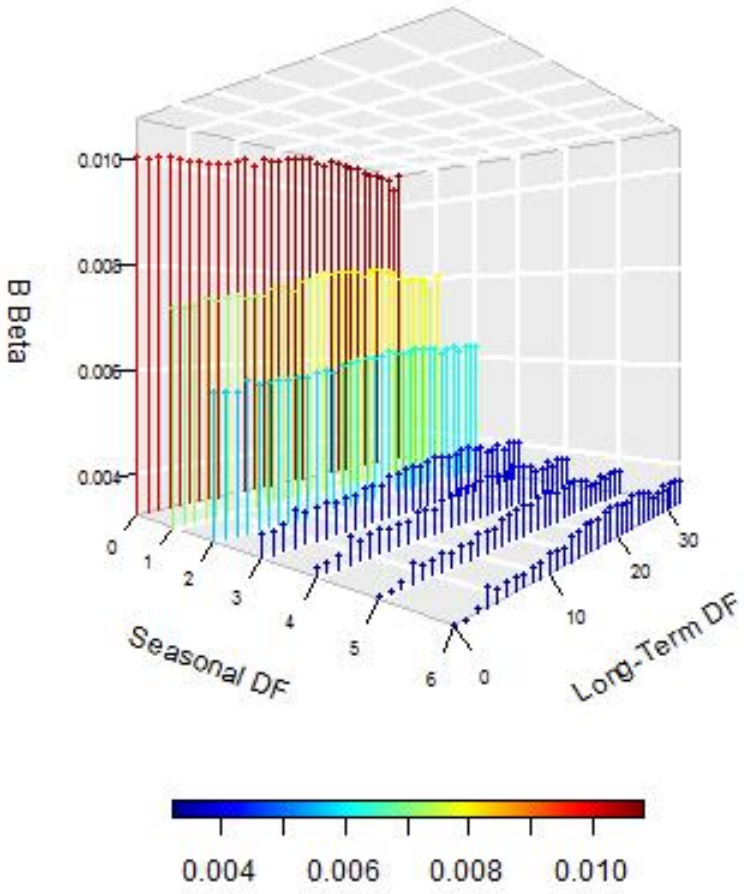

Figure C.3: Estimate beta coefficients of Influenza B as the degrees of freedom for long-term and seasonal trends vary

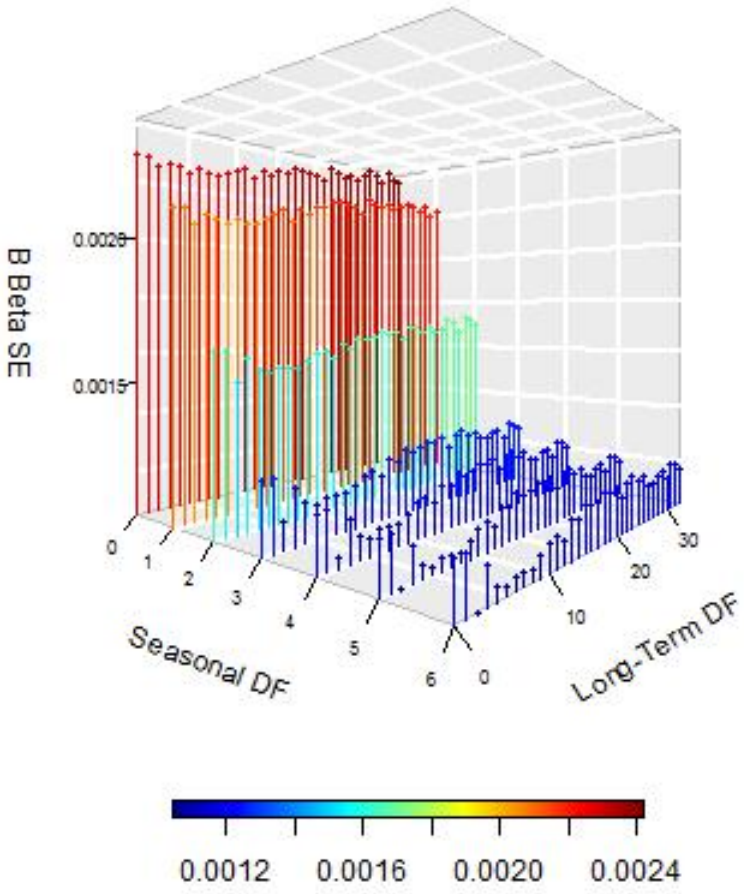

Figure C.4: Beta coefficients standard error of Influenza B as the degrees of freedom for long-term and seasonal trends vary

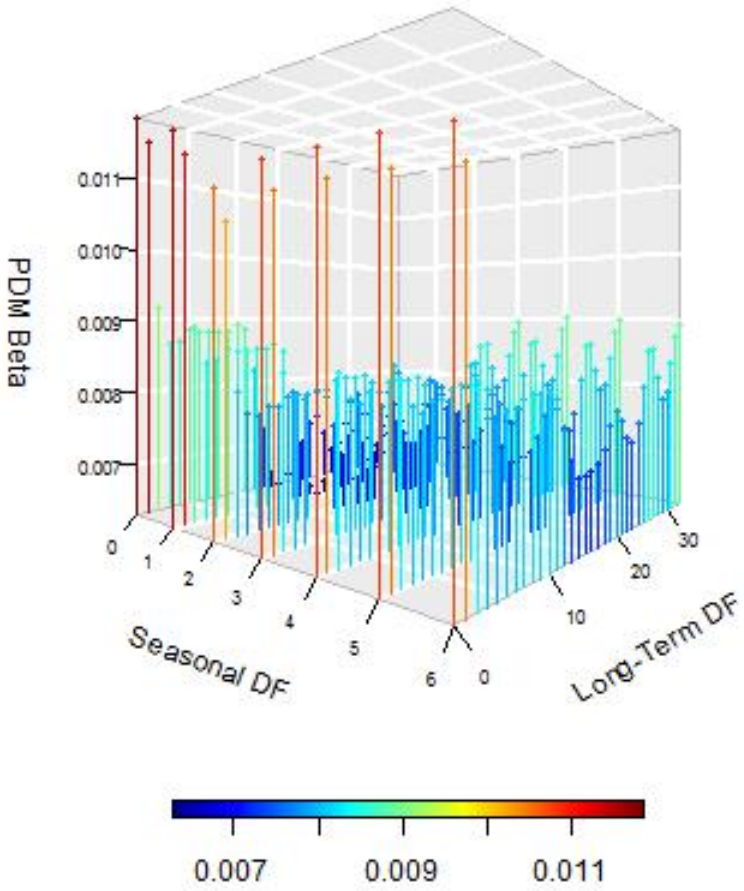

Figure C.5: Estimate beta coefficients of Influenza A(H1N1)pdm09 as the degrees of freedom for long-term and seasonal trends vary

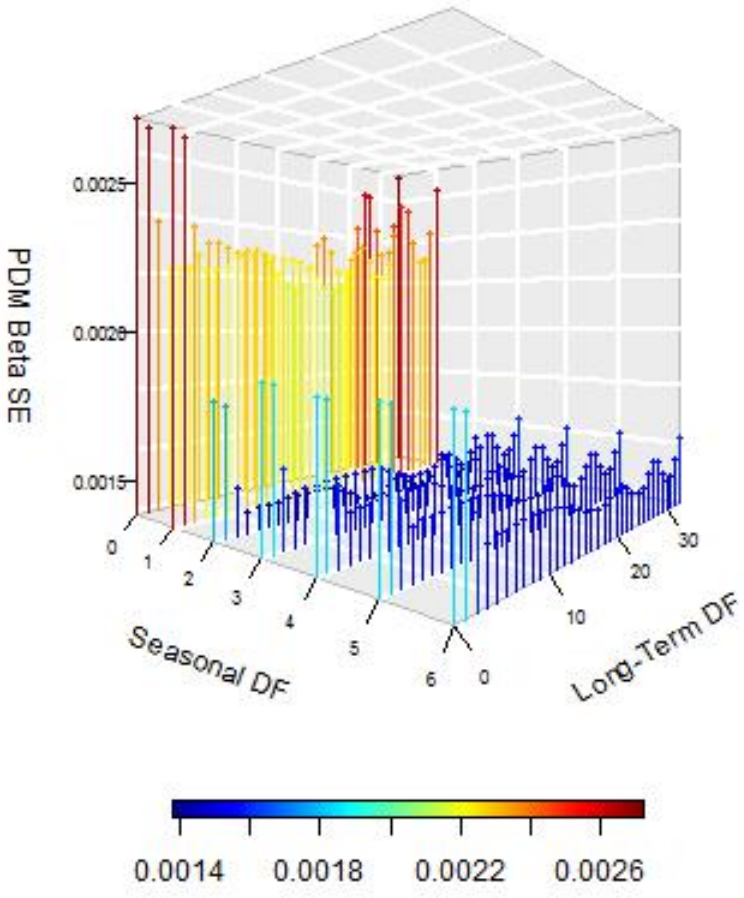

Figure C.6: Beta coefficients standard error of Influenza A(H1N1)pdm09 as the degrees of freedom for long-term and seasonal trends vary

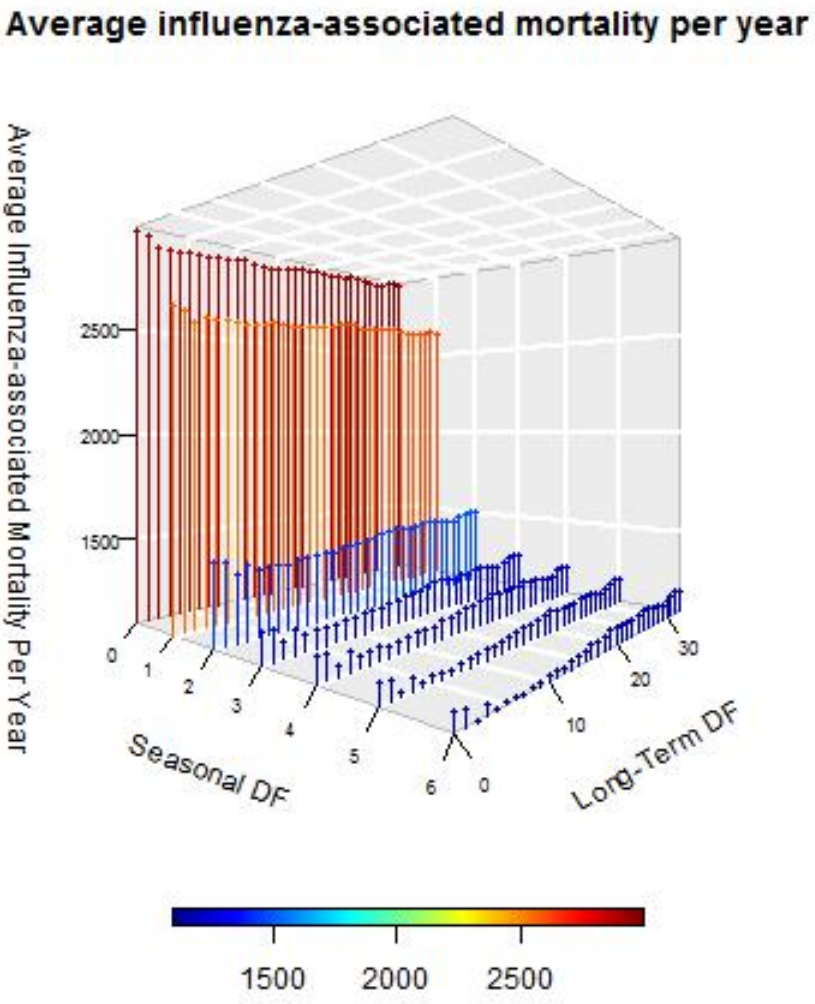

Figure C.7: Average annual total influenza-associated mortality as the degrees of freedom for long-term and seasonal trends vary

Bibliography

Akaike, H. (1998), Information theory and an extension of the maximum likelihood principle, in 'Selected Papers of Hirotugu Akaike', Springer, pp. 199–213.

Andrews, D. W. (1991), 'Heteroskedasticity and autocorrelation consistent covariance matrix estimation', Econometrica: Journal of the Econometric Society pp. 817–858.

Aungkulanon, S., Cheng, P.-Y., Kusreesakul, K., Bundhamcharoen, K., Chittaganpitch, M., Margaret, M. and Olsen, S. (2015), 'Influenza-associated mortality in thailand, 2006–2011', Influenza and other respiratory viruses **9**(6), 298–304.

Bartra, O., McGuire, J. T. and Kable, J. W. (2013), 'The valuation system: a coordinate-based meta-analysis of bold fmri experiments examining neural correlates of subjective value', Neuroimage **76**, 412–427.

Basu, R. (2009), 'High ambient temperature and mortality: a review of epidemiologic studies from 2001 to 2008', Environmental health **8**(1), 40.

Belongia, E. A., Kieke, B. A., Donahue, J. G., Greenlee, R. T., Balish, A., Foust, A., Lindstrom, S. and Shay, D. K. (2009), 'Effectiveness of inactivated influenza vaccines varied substantially with antigenic match from the 2004–2005 season to the 2006–2007 season', Journal of Infectious Diseases **199**(2), 159–167.

Bhaskaran, K., Gasparrini, A., Hajat, S., Smeeth, L. and Armstrong, B. (2013), 'Time

series regression studies in environmental epidemiology', International journal of epidemiology **42**(4), 1187–1195.

Bhaskaran, K., Hajat, S., Haines, A., Herrett, E., Wilkinson, P. and Smeeth, L. (2010), 'Short term effects of temperature on risk of myocardial infarction in england and wales: time series regression analysis of the myocardial ischaemia national audit project (minap) registry', Bmj **341**, c3823.

Blahd, W. (2015), 'Types of flu'.

URL: *http://www.webmd.com/cold-and-flu/flu-guide/advanced-reading-types-of-flu-viruses*

Bonassi, F. V., West, M. et al. (2015), 'Sequential monte carlo with adaptive weights for approximate bayesian computation', Bayesian Analysis **10**(1), 171–187.

Bowman, F. D., Guo, Y. and Derado, G. (2007), 'Statistical approaches to functional neuroimaging data', Neuroimaging Clinics of North America **17**(4), 441–458.

Braga, A., Zanobetti, A. and Schwartz, J. (2000), 'Do respiratory epidemics confound the association between air pollution and daily deaths?', European Respiratory Journal **16**(4), 723–728.

Cauchemez, S., Horby, P., Fox, A., Thai, P. Q., Hien, N. T., Ferguson, N. M. et al. (2012), 'Influenza infection rates, measurement errors and the interpretation of paired serology', PLoS pathogens **8**(12), e1003061.

Cauda, F., Cavanna, A. E., D'agata, F., Sacco, K., Duca, S. and Geminiani, G. C. (2011), 'Functional connectivity and coactivation of the nucleus accumbens: a combined functional connectivity and structure-based meta-analysis', Journal of cognitive neuroscience **23**(10), 2864–2877.

Centers for Disease Control and Prevention, National Center for Immunization and Respiratory Diseases (NCIRD) (2016), 'Types of influenza viruses'.
URL: *http://www.cdc.gov/flu/about/viruses/types.htm*

Cohen, C., Walaza, S., Treurnicht, F. K., McMorrow, M., Madhi, S. A., McAnerney, J. M. and Tempia, S. (2017), 'In-and out-of-hospital mortality associated with seasonal and pandemic influenza and respiratory syncytial virus in south africa, 2009–2013', Clinical Infectious Diseases **66**(1), 95–103.

Cox, R., Brokstad, K. and Ogra, P. (2004), 'Influenza virus: immunity and vaccination strategies. comparison of the immune response to inactivated and live, attenuated influenza vaccines', Scandinavian journal of immunology **59**(1), 1–15.

Cremers, H. R., Wager, T. D. and Yarkoni, T. (2017), 'The relation between statistical power and inference in fmri', PloS one **12**(11), e0184923.

DiazGranados, C. A., Dunning, A. J., Kimmel, M., Kirby, D., Treanor, J., Collins, A., Pollak, R., Christoff, J., Earl, J., Landolfi, V. et al. (2014), 'Efficacy of high-dose versus standard-dose influenza vaccine in older adults', New England Journal of Medicine **371**(7), 635–645.

Domínguez, A., Muñoz, P., Cardeñosa, N., Martínez, A. and Caylà, J. (2007), 'Time-series analysis of meningococcal disease in catalonia', Annals of epidemiology **17**(9), 654–662.

Dominici, F., McDermott, A. and Hastie, T. J. (2004), 'Improved semiparametric time series models of air pollution and mortality', Journal of the American Statistical Association **99**(468), 938–948.

Dushoff, J., Plotkin, J. B., Viboud, C., Earn, D. J. and Simonsen, L. (2006), 'Mortality due to influenza in the united statesan annualized regression approach using multiple-cause mortality data', American journal of epidemiology **163**(2), 181–187.

Efron, B. and Tibshirani, R. J. (1994), An introduction to the bootstrap, CRC press.

Feng, L., Shay, D. K., Jiang, Y., Zhou, H., Chen, X., Zheng, Y., Jiang, L., Zhang, Q., Lin, H., Wang, S. et al. (2012), 'Influenza-associated mortality in temperate and subtropical chinese cities, 2003-2008', Bulletin of the World Health Organization **90**(4), 279–288B.

Foppa, I. M., Cheng, P.-Y., Reynolds, S. B., Shay, D. K., Carias, C., Bresee, J. S., Kim, I. K., Gambhir, M. and Fry, A. M. (2015), 'Deaths averted by influenza vaccination in the us during the seasons 2005/06 through 2013/14', Vaccine **33**(26), 3003–3009.

Gelfand, A. E. and Smith, A. F. (1990), 'Sampling-based approaches to calculating marginal densities', Journal of the American statistical association **85**(410), 398–409.

Gilks, W. R. (1996), 'Full conditional distributions', Markov chain Monte Carlo in practice pp. 75–88.

Gilks, W. R., Best, N. and Tan, K. (1995), 'Adaptive rejection metropolis sampling within gibbs sampling', Applied Statistics pp. 455–472.

Gilks, W. R., Neal, R., Best, N. and Tan, K. (1997), 'Corrigendum: adaptive rejection metropolis sampling', Journal of the Royal Statistical Society: Series C (Applied Statistics) **46**(4), 541–542.

Goldstein, E., Viboud, C., Charu, V. and Lipsitch, M. (2012), 'Improving the estimation of influenza-related mortality over a seasonal baseline', Epidemiology (Cambridge, Mass.) **23**(6), 829.

Gran, J., Iversen, B., Hungnes, O. and Aalen, O. (2010), 'Estimating influenza-related

excess mortality and reproduction numbers for seasonal influenza in norway, 1975–2004', Epidemiology and infection **138**(11), 1559–1568.

Gran, J. M., Kacelnik, O., Grjibovski, A. M., Aavitsland, P. and Iversen, B. G. (2013), 'Counting pandemic deaths: comparing reported numbers of deaths from influenza a (h1n1) pdm09 with estimated excess mortality', Influenza and other respiratory viruses **7**(6), 1370–1379.

Guan, P., Huang, D.-S. and Zhou, B.-S. (2004), 'Forecasting model for the incidence of hepatitis a based on artificial neural network', World journal of gastroenterology: WJG **10**(24), 3579.

Hardelid, P., Pebody, R. and Andrews, N. (2013), 'Mortality caused by influenza and respiratory syncytial virus by age group in england and wales 1999–2010', Influenza and other respiratory viruses **7**(1), 35–45.

Heilbron, D. C. (1994), 'Zero-altered and other regression models for count data with added zeros', Biometrical Journal **36**(5), 531–547.

Hilbe, J. M. (2011), Negative binomial regression, Cambridge University Press.

Honey, C., Sporns, O., Cammoun, L., Gigandet, X., Thiran, J.-P., Meuli, R. and Hagmann, P. (2009), 'Predicting human resting-state functional connectivity from structural connectivity', Proceedings of the National Academy of Sciences **106**(6), 2035–2040.

Hu, M.-C., Pavlicova, M. and Nunes, E. V. (2011), 'Zero-inflated and hurdle models of count data with extra zeros: examples from an hiv-risk reduction intervention trial', The American journal of drug and alcohol abuse **37**(5), 367–375.

Iuliano, A. D., Roguski, K. M., Chang, H. H., Muscatello, D. J., Palekar, R., Tempia, S., Cohen, C., Gran, J. M., Schanzer, D., Cowling, B. J. et al. (2017), 'Estimates

of global seasonal influenza-associated respiratory mortality: a modelling study', The Lancet .

Izurieta, H. S., Thompson, W. W., Kramarz, P., Shay, D. K., Davis, R. L., DeStefano, F., Black, S., Shinefield, H. and Fukuda, K. (2000), 'Influenza and the rates of hospitalization for respiratory disease among infants and young children', New England Journal of Medicine **342**(4), 232–239.

Jackson, M. L. (2009), 'Confounding by season in ecologic studies of seasonal exposures and outcomes: examples from estimates of mortality due to influenza', Annals of Epidemiology **19**(10), 681–691.

Jiménez, E., Linares, C., Martínez, D. and Díaz, J. (2010), 'Role of saharan dust in the relationship between particulate matter and short-term daily mortality among the elderly in madrid (spain)', Science of the Total Environment **408**(23), 5729–5736.

Johnson, N. L., Kemp, A. W. and Kotz, S. (2005), Univariate Discrete Distributions, 3rd Edition, Wiley.

Kang, J., Johnson, T. D., Nichols, T. E. and Wager, T. D. (2011), 'Meta analysis of functional neuroimaging data via bayesian spatial point processes', Journal of the American Statistical Association **106**(493), 124–134.

Karlis, D. (2003), 'An em algorithm for multivariate poisson distribution and related models', Journal of Applied Statistics **30**(1), 63–77.

Kelly, H. and Valenciano, M. (2012), 'Estimating the effect of influenza vaccines', The Lancet infectious diseases **12**(1), 5–6.

Kerman, J. et al. (2011), 'Neutral noninformative and informative conjugate beta and gamma prior distributions', Electronic Journal of Statistics **5**, 1450–1470.

Kim, J. H. and Yeasmin, M. (2005), 'The size and power of the bias-corrected bootstrap test for regression models with autocorrelated errors', Computational Economics **25**(3), 255–267.

Kissling, E., Valenciano, M., Buchholz, U., Larrauri, A., Cohen, J., Nunes, B., Rogalska, J., Pitigoi, D., Paradowska-Stankiewicz, I., Reuss, J. et al. (2014), 'Influenza vaccine effectiveness estimates in europe in a season with three influenza type/-subtypes circulating: the i-move multicentre case-control study, influenza season 2012/13'.

Kober, H., Barrett, L. F., Joseph, J., Bliss-Moreau, E., Lindquist, K. and Wager, T. D. (2008), 'Functional grouping and cortical–subcortical interactions in emotion: A meta-analysis of neuroimaging studies', Neuroimage **42**(2), 998–1031.

Kostova, D., Reed, C., Finelli, L., Cheng, P.-Y., Gargiullo, P. M., Shay, D. K., Singleton, J. A., Meltzer, M. I., Lu, P.-j. and Bresee, J. S. (2013), 'Influenza illness and hospitalizations averted by influenza vaccination in the united states, 2005–2011', PloS one **8**(6), e66312.

Kuster, S. P., Shah, P. S., Coleman, B. L., Lam, P.-P., Tong, A., Wormsbecker, A. and McGeer, A. (2011), 'Incidence of influenza in healthy adults and healthcare workers: a systematic review and meta-analysis', PloS one **6**(10), e26239.

Lagarias, J. C., Reeds, J. A., Wright, M. H. and Wright, P. E. (1998), 'Convergence properties of the nelder–mead simplex method in low dimensions', SIAM Journal on optimization **9**(1), 112–147.

Larson, H. J. and Heymann, D. L. (2010), 'Public health response to influenza a (h1n1) as an opportunity to build public trust', Jama **303**(3), 271–272.

Lindquist, K. A., Satpute, A. B., Wager, T. D., Weber, J. and Barrett, L. F. (2015),

'The brain basis of positive and negative affect: evidence from a meta-analysis of the human neuroimaging literature', Cerebral Cortex **26**(5), 1910–1922.

Lindquist, M. A. et al. (2008), 'The statistical analysis of fmri data', Statistical Science **23**(4), 439–464.

Liu, X., Hairston, J., Schrier, M. and Fan, J. (2011), 'Common and distinct networks underlying reward valence and processing stages: a meta-analysis of functional neuroimaging studies', Neuroscience & Biobehavioral Reviews **35**(5), 1219–1236.

Lopman, B., Vennema, H., Kohli, E., Pothier, P., Sanchez, A., Negredo, A., Buesa, J., Schreier, E., Gray, J., Gallimore, C. et al. (2004), 'Increase in viral gastroenteritis outbreaks in europe and epidemic spread of new norovirus variant', The lancet **363**(9410), 682–688.

Lozano, R., Naghavi, M., Foreman, K., Lim, S., Shibuya, K., Aboyans, V., Abraham, J., Adair, T., Aggarwal, R., Ahn, S. Y. et al. (2013), 'Global and regional mortality from 235 causes of death for 20 age groups in 1990 and 2010: a systematic analysis for the global burden of disease study 2010', The Lancet **380**(9859), 2095–2128.

Lumley, T. and Heagerty, P. (1999), 'Weighted empirical adaptive variance estimators for correlated data regression', Journal of the Royal Statistical Society: Series B (Statistical Methodology) **61**(2), 459–477.

Mayo Clinic (2018), 'Brain lobes'.

URL: *https://www.mayoclinic.org/brain-lobes/img-20008887*

Mazziotta, J., Toga, A., Evans, A., Fox, P., Lancaster, J., Zilles, K., Woods, R., Paus, T., Simpson, G., Pike, B. et al. (2001), 'A probabilistic atlas and reference system for the human brain: International consortium for brain mapping (icbm)', Philosophical Transactions of the Royal Society B: Biological Sciences **356**(1412), 1293–1322.

McLean, H. Q., Thompson, M. G., Sundaram, M. E., Kieke, B. A., Gaglani, M., Murthy, K., Piedra, P. A., Zimmerman, R. K., Nowalk, M. P., Raviotta, J. M. et al. (2014), 'Influenza vaccine effectiveness in the united states during 2012–2013: variable protection by age and virus type', The Journal of infectious diseases **211**(10), 1529–1540.

Morbidity and Mortality Weekly Report (MMWR) (n.d.).
URL: *https://www.cdc.gov/mmwr/preview/mmwrhtml/mm5933a1.htm*

Morens, D. M. and Fauci, A. S. (2007), 'The 1918 influenza pandemic: insights for the 21st century', Journal of Infectious Diseases **195**(7), 1018–1028.

Moura, F. E. (2010), 'Influenza in the tropics', Current opinion in infectious diseases **23**(5), 415–420.

Mullahy, J. (1986), 'Specification and testing of some modified count data models', Journal of econometrics **33**(3), 341–365.

Muscatello, D. J., Newall, A. T., Dwyer, D. E. and MacIntyre, C. R. (2013), 'Mortality attributable to seasonal and pandemic influenza, australia, 2003 to 2009, using a novel time series smoothing approach', PloS one **8**(6), e64734.

Muscatello, D., Morton, P., Evans, I. and Gilmour, R. (2008), 'Prospective surveillance of excess mortality due to influenza in new south wales: feasibility and statistical approach', Communicable diseases intelligence quarterly report **32**(4), 435.

Nair, H., Brooks, W. A., Katz, M., Roca, A., Berkley, J. A., Madhi, S. A., Simmerman, J. M., Gordon, A., Sato, M., Howie, S. et al. (2011), 'Global burden of respiratory infections due to seasonal influenza in young children: a systematic review and meta-analysis', The Lancet **378**(9807), 1917–1930.

Neumann, J., Fox, P. T., Turner, R. and Lohmann, G. (2010), 'Learning partially directed functional networks from meta-analysis imaging data', Neuroimage **49**(2), 1372–1384.

Neuron (2016).

URL: *http://dictionary.reference.com/browse/neuron?s=t*

Newey, W. K. and West, K. D. (2017), 'A simple, positive semi-definite, heteroskedasticity and autocorrelation consistent covariance matrix', No1 (33) 2014 p. 125.

Nicoll, A., Ciancio, B., Lopez Chavarrias, V., Mølbak, K., Pebody, R., Pedzinski, B., Penttinen, P., van der Sande, M., Snacken, R. and Van Kerkhove, M. (2012), 'Influenza-related deaths-available methods for estimating numbers and detecting patterns for seasonal and pandemic influenza in europe', Euro Surveill **17**(January (18)).

Nielsen, F. Å., Hansen, L. K. and Balslev, D. (2004), 'Mining for associations between text and brain activation in a functional neuroimaging database', Neuroinformatics **2**(4), 369–379.

Nielsen, J., Mazick, A., Glismann, S. and Mølbak, K. (2011), 'Excess mortality related to seasonal influenza and extreme temperatures in denmark, 1994-2010', BMC infectious diseases **11**(1), 350.

Oehlert, G. W. (1992), 'A note on the delta method', The American Statistician **46**(1), 27–29.

Ohmit, S. E., Thompson, M. G., Petrie, J. G., Thaker, S. N., Jackson, M. L., Belongia, E. A., Zimmerman, R. K., Gaglani, M., Lamerato, L., Spencer, S. M. et al. (2014), 'Influenza vaccine effectiveness in the 2011–2012 season: protection against each circulating virus and the effect of prior vaccination on estimates', Clinical infectious diseases **58**(3), 319–327.

Omer, S. B., Goodman, D., Steinhoff, M. C., Rochat, R., Klugman, K. P., Stoll, B. J. and Ramakrishnan, U. (2011), 'Maternal influenza immunization and reduced likelihood of prematurity and small for gestational age births: a retrospective cohort study', PLoS medicine **8**(5), 683.

Osterholm, M. T., Kelley, N. S., Sommer, A. and Belongia, E. A. (2012), 'Efficacy and effectiveness of influenza vaccines: a systematic review and meta-analysis', The Lancet infectious diseases **12**(1), 36–44.

Park, H.-J. and Friston, K. (2013), 'Structural and functional brain networks: from connections to cognition', Science **342**(6158), 1238411.

Partonen, T., Haukka, J., Nevanlinna, H. and Lönnqvist, J. (2004), 'Analysis of the seasonal pattern in suicide', Journal of affective disorders **81**(2), 133–139.

Patel, R., Spreng, R. N. and Turner, G. R. (2013), 'Functional brain changes following cognitive and motor skills training a quantitative meta-analysis', Neurorehabilitation and neural repair **27**(3), 187–199.

Peng, R. D., Dominici, F. and Louis, T. A. (2006), 'Model choice in time series studies of air pollution and mortality', Journal of the Royal Statistical Society: Series A (Statistics in Society) **169**(2), 179–203.

Plummer, M. (2012), 'Jags: Just another gibbs sampler', Astrophysics Source Code Library .

Postuma, R. B. and Dagher, A. (2006), 'Basal ganglia functional connectivity based on a meta-analysis of 126 positron emission tomography and functional magnetic resonance imaging publications', Cerebral cortex **16**(10), 1508–1521.

R Core Team (2017), R: A Language and Environment for Statistical Computing, R

Foundation for Statistical Computing, Vienna, Austria.
URL: *https://www.R-project.org/*

R Core Team (n.d.), R: A Language and Environment for Statistical Computing, R Foundation for Statistical Computing, Vienna, Austria.
URL: *https://www.R-project.org*

Ramsay, T. O., Burnett, R. T. and Krewski, D. (2003), 'The effect of concurvity in generalized additive models linking mortality to ambient particulate matter', Epidemiology **14**(1), 18–23.

Reich, B. J., Hodges, J. S. and Zadnik, V. (2006), 'Effects of residual smoothing on the posterior of the fixed effects in disease-mapping models', Biometrics **62**(4), 1197–1206.

Ripley, B. D. (2007), Pattern recognition and neural networks, Cambridge university press.

Rizzo, C., Bella, A., Viboud, C., Simonsen, L., Miller, M. A., Rota, M. C., Salmaso, S. and Degli Atti, M. L. C. (2007), 'Trends for influenza-related deaths during pandemic and epidemic seasons, italy, 1969–2001', Emerging infectious diseases **13**(5), 694.

Robinson, J. L., Laird, A. R., Glahn, D. C., Blangero, J., Sanghera, M. K., Pessoa, L., Fox, P. M., Uecker, A., Friehs, G., Young, K. A. et al. (2012), 'The functional connectivity of the human caudate: an application of meta-analytic connectivity modeling with behavioral filtering', NeuroImage **60**(1), 117–129.

Samet, J. M., Zeger, S. L., Dominici, F., Curriero, F., Coursac, I., Dockery, D. W., Schwartz, J. and Zanobetti, A. (2000), 'The national morbidity, mortality, and air pollution study', Part II: morbidity and mortality from air pollution in the United States Res Rep Health Eff Inst **94**(pt 2), 5–79.

Satpute, A. B., Kang, J., Bickart, K. C., Yardley, H., Wager, T. D. and Barrett, L. F. (2015), 'Involvement of sensory regions in affective experience: a meta-analysis', Frontiers in psychology **6**, 1860.

Schwartz, J. (1994), 'Total suspended particulate matter and daily mortality in cincinnati, ohio.', Environmental Health Perspectives **102**(2), 186.

Serfling, R. E. (1963), 'Methods for current statistical analysis of excess pneumonia-influenza deaths', Public health reports **78**(6), 494.

Severini, T. A. (2005), Elements of distribution theory, Vol. 17, Cambridge University Press.

Shibata, R. (1976), 'Selection of the order of an autoregressive model by akaike's information criterion', Biometrika **63**(1), 117–126.

Simonsen, L., Clarke, M. J., Stroup, D. F., Williamson, G. D., Arden, N. H. and Cox, N. J. (1997), 'A method for timely assessment of influenza-associated mortality in the united states', Epidemiology pp. 390–395.

Simonsen, L., Clarke, M. J., Williamson, G. D., Stroup, D. F., Arden, N. H. and Schonberger, L. B. (1997), 'The impact of influenza epidemics on mortality: introducing a severity index.', American journal of public health **87**(12), 1944–1950.

Simonsen, L., Reichert, T. A., Viboud, C., Blackwelder, W. C., Taylor, R. J. and Miller, M. A. (2005), 'Impact of influenza vaccination on seasonal mortality in the us elderly population', Archives of internal medicine **165**(3), 265–272.

Simonsen, L., Spreeuwenberg, P., Lustig, R., Taylor, R. J., Fleming, D. M., Kroneman, M., Van Kerkhove, M. D., Mounts, A. W., Paget, W. J. et al. (2013), 'Global mortality estimates for the 2009 influenza pandemic from the glamor project: a modeling study'.

Skowronski, D. M., Chambers, C., Sabaiduc, S., De Serres, G., Winter, A.-L., Dickinson, J. A., Gubbay, J., Fonseca, K., Charest, H., Krajden, M. et al. (2015), 'Integrated sentinel surveillance linking genetic, antigenic and epidemiologic monitoring of influenza vaccine-virus relatedness and effectiveness, 2013-14 season', Journal of Infectious Diseases p. jiv177.

Sporns, O. (2013), 'Structure and function of complex brain networks', Dialogues in clinical neuroscience **15**(3), 247.

Sprenger, M., Van Naelten, M., Mulder, P. and Masurel, N. (1989), 'Influenza mortality and excess deaths in the elderly, 1967–82', Epidemiology & Infection **103**(3), 633–641.

Stroup, D. F., Thacker, S. B. and Herndon, J. L. (1988), 'Application of multiple time series analysis to the estimation of pneumonia and influenza mortality by age 1962–1983', Statistics in medicine **7**(10), 1045–1059.

Talairach, J. and Tournoux, P. (1988), 'Co-planar stereotaxic atlas of the human brain. 3-dimensional proportional system: an approach to cerebral imaging'.

Tempia, S., Walaza, S., Viboud, C., Cohen, A. L., Madhi, S. A., Venter, M., McAnerney, J. M. and Cohen, C. (2014), 'Mortality associated with seasonal and pandemic influenza and respiratory syncytial virus among children¡ 5 years of age in a high hiv prevalence settingsouth africa, 1998–2009', Clinical infectious diseases **58**(9), 1241–1249.

Thompson, W. W., Comanor, L. and Shay, D. K. (2006), 'Epidemiology of seasonal influenza: use of surveillance data and statistical models to estimate the burden of disease', Journal of Infectious Diseases **194**(Supplement 2), S82–S91.

Thompson, W. W., Shay, D. K., Weintraub, E., Brammer, L., Bridges, C. B., Cox,

N. J. and Fukuda, K. (2004), 'Influenza-associated hospitalizations in the united states', Jama **292**(11), 1333–1340.

Thompson, W. W., Shay, D. K., Weintraub, E., Brammer, L., Cox, N., Anderson, L. J. and Fukuda, K. (2003), 'Mortality associated with influenza and respiratory syncytial virus in the united states', Jama **289**(2), 179–186.

Thompson, W. W., Weintraub, E., Dhankhar, P., Cheng, P.-Y., Brammer, L., Meltzer, M. I., Bresee, J. S. and Shay, D. K. (2009), 'Estimates of us influenza-associated deaths made using four different methods', Influenza and other respiratory viruses **3**(1), 37–49.

Torta, D. and Cauda, F. (2011), 'Different functions in the cingulate cortex, a meta-analytic connectivity modeling study', Neuroimage **56**(4), 2157–2172.

Tzourio-Mazoyer, N., Landeau, B., Papathanassiou, D., Crivello, F., Etard, O., Delcroix, N., Mazoyer, B. and Joliot, M. (2002), 'Automated anatomical labeling of activations in spm using a macroscopic anatomical parcellation of the mni mri single-subject brain', Neuroimage **15**(1), 273–289.

Weinberg, G. A. and Szilagyi, P. G. (2010), 'Vaccine epidemiology: efficacy, effectiveness, and the translational research roadmap', Journal of Infectious Diseases **201**(11), 1607–1610.

Weinberger, D. M., Simonsen, L., Jordan, R., Steiner, C., Miller, M. and Viboud, C. (2012), 'Impact of the 2009 influenza pandemic on pneumococcal pneumonia hospitalizations in the united states', Journal of Infectious Diseases **205**(3), 458–465.

Wong, K., Cheng, P., Foppa, I., Jain, S., Fry, A. and Finelli, L. (2015), 'Estimated paediatric mortality associated with influenza virus infections, united states, 2003–2010', Epidemiology & Infection **143**(3), 640–647.

World Health Organization (2004), 'Influenza (seasonal)'.
URL: *http://www.who.int/mediacentre/factsheets/fs211/en/*

World Health Organization (2012), 'Vaccines against influenza who position paper–november 2012', Wkly Epidemiol Rec **87**(47), 461–76.

World Health Organization and others (2008), 'Generic protocol for monitoring impact of rotavirus vaccination on gastroenteritis disease burden and viral strains'.

Wu, P., Goldstein, E., Ho, L. M., Yang, L., Nishiura, H., Wu, J. T., Ip, D. K., Chuang, S.-K., Tsang, T. and Cowling, B. J. (2012), 'Excess mortality associated with influenza a and b virus in hong kong, 1998–2009', Journal of Infectious Diseases **206**(12), 1862–1871.

Xue, W., Kang, J., Bowman, F. D., Wager, T. D. and Guo, J. (2014a), 'Identifying functional co-activation patterns in neuroimaging studies via poisson graphical models', Biometrics **70**(4), 812–822.

Xue, W., Kang, J., Bowman, F. D., Wager, T. D. and Guo, J. (2014b), 'Identifying functional co-activation patterns in neuroimaging studies via poisson graphical models', Biometrics **70**(4), 812–822.

Yang, L., Chan, K., Cowling, B., Chiu, S., Chan, K., Peiris, J. and Wong, C. (2012), 'Excess mortality associated with the 2009 pandemic of influenza a (h1n1) in hong kong', Epidemiology & Infection **140**(9), 1542–1550.

Yang, L., Chen, P. Y., He, J. F., Chan, K. P., Ou, C. Q., Deng, A. P., Peiris, J. M. and Wong, C. M. (2011), 'Effect modification of environmental factors on influenza-associated mortality: a time-series study in two chinese cities', BMC infectious diseases **11**(1), 342.